



ISSN 2075-9746

Thi-Qar University Journal for

# Engineering Sciences

Refereed Scientific Journal  
Issued by:  
College of Engineering  
Thi-Qar University

# **Thi-Qar University Journal for Engineering Sciences**

ISSN 2075-9746

## **Editor- in-Chief**

**Assistant Professor Dr. Kadhim Karim Mohsen**

## **Managing Editor**

**Assistant Professor Dr. Mushtaq Ismael Hasan**

## **Editorial Board**

**Assistant Professor Dr. Hussain Kamel Chaiel**

**Assistant Professor Dr. Rasoul Raisan Shaker**

**Assistant Professor Dr. Rafid Mualek Hanon**

## **Advisory Board**



<b>Professor Dr. Nabil Kadim Abdul Sahib</b>	<b>University of Thi-Qar</b>
<b>Professor Dr. Ahmad Mahmoud Fakhry</b>	<b>University of Bradley</b>
<b>Professor Dr. Adnan A. A. Al-Samawi</b>	<b>University of Technology</b>
<b>Professor Dr. Saleh I. Najm</b>	<b>Basrah University</b>
<b>Professor Dr. Jalal M. Jalil</b>	<b>University of Technology</b>
<b>Professor Dr. R.S. Fyath</b>	<b>Nahrain University</b>
<b>Professor Dr. Qasim M. Doos</b>	<b>Baghdad University</b>
<b>Professor Dr. Turki Y. Abdalla</b>	<b>Basrah University</b>
<b>Professor Dr. Sabah Rasoul Dakhel</b>	<b>Karbala University</b>
<b>Professor Dr. Adel Abas Alwan</b>	<b>Babylon University</b>

## **Design and Type Setting**

**Mohammed Koshesh Mahdy**

## Instructions to Authors

Thi-Qar University Journal for Engineering Sciences is a refereed scientific journal accepts articles from inside and outside Iraq in different engineering sciences. These articles should not be submitted for publication in any scientific journal or conference proceedings. Following are guidelines to authors for writing the manuscripts sent to the journal:

1. Three copies of each manuscript should be submitted in either Arabic or English language together with an abstract and title in the other language printed on one side of A4 papers with a software copy on a CD using Microsoft Word.
2. The total number of pages should not exceed 15 pages.
3. The author has to submit a written request to the Editor-in-Chief asking for publication of his article. An application form should be attached to the request which includes an acknowledgment that the article should not previously submitted or published in any scientific journal or conference proceedings. The author should mention his address, affiliation, E-mail, and mobile number to facilitate communication with him.
4. The author is responsible for his article contents.
5. All manuscripts are subjected to scientific review by expert reviewers.
6. The author will be informed about the result of the article review.
7. The author who lives in Iraq has to pay to the journal accountant a nonreturnable (50000 ID) for lecturers and down and (75000 ID) for assistant professor and (100000 ID) for professor as review and publication fees according to the instructions of ministry of higher education and scientific research. Those who live outside Iraq have to pay \$100 for review and publication.
8. The original manuscripts will not be returned to authors.
9. A free copy of the journal will be sent to the author whose article is published in the journal.
10. Printing Instructions

### Manuscripts should be printed according to the following instructions:

- ❖ **Margins:** 2.5 cm from all sides.
- ❖ **Letter type:** Times New Roman.
- ❖ **Manuscript title:** Capital letters size 16 Bold.
- ❖ **Author(s) name(s):** Should be typed under the manuscript title size 14 Bold. Job title, scientific degree and Email should be written in the middle of page size 10 Bold.
- ❖ **Main titles:** Size 14 Bold attached to the right margin for Arabic manuscripts and to the left margin for English manuscripts.
- ❖ **Subtitles:** Size 14 Bold, the first letter of each word should be capital and attached to the right margin for Arabic manuscripts and to the left margin for English manuscripts. One empty line should be left before and after each subtitle.

- ❖ **Text: Size** 12 normal, small letters, spaced one and half times.
- ❖ **Equations:** Should be written by using Microsoft Equations Editor and numbered by brackets to the right. One empty line should be left before and after each equation. Reference to each equation must be written as follows: Equation(x) where x is the equation number.
- ❖ **Tables:** Should be numbered consecutively, and have a clear informative heading written on the top using size 12 Bold.
- ❖ **Figures:** Should be numbered consecutively, and have a clear informative heading written in the bottom using size 12 Bold, new drawing techniques have to be used.
- ❖ **References:** Are referred according to their appearance in the text with serial numbers in square brackets. References should be written as follows:
- ❖ **Articles:** Author's surname, space, first letter of the author's name. First letter of the author's father name. , Year, "Article Title", place of publication, Vol. and number, pages.
- ❖ **Books:** Author's surname, space, first letter of the author's name. First letter of the author's father name. , Year, "Book Title", Edition, place of publication.
- ❖ **Thesis and Dissertation:** Author's surname, space, first letter of the author's name. First letter of the author's father name. , Year, "Thesis / Dissertation Title", University, Country.

**Note:** The same sequence should be repeated in writing the names of coauthors.

- ✓ **Abstract:** Manuscript's text should be preceded by two abstracts of no more than 200 words each written in Arabic and English languages.
- ✓ **Keywords:** Five to ten keywords related to the article should be written after the abstract using size 12 Bold.
- ✓ **Symbols:** Should be ordered serially and placed after the References list.
- ✓ **Numbers:** Should be consistent with the text language.

## Correspondences:

**Thi-Qar University Journal for Engineering Sciences – College of Engineering –  
Thi-Qar University – Thi-Qar Governorate – Republic of Iraq.**

**E-mail: [thiqarej@gmail.com](mailto:thiqarej@gmail.com)**

# ***Thi-Qar University Journal for Engineering***

## ***Sciences***

ISSN 2075-9746

### *The English Section* Contents

Author	Title	Pages
Khalid M. Abdul-hassan Ramzy s. Ali Shahzanan Ali Kahdum	Simulation of Speed Control for Synchronous Reluctance Motor Based on Tuning Cascaded pid Controller with pso Algorithm	1-15
Ali Idham Alzaidi	Design and Implementation Backscatter Detector with Arduino System	16-28
Mohammed R.K.Alsheekh Ali A.Monem Emad Abdullah	Numerical and Experimental Study of the Indoor Environmental Conditions of a Large Athletic hall (Wrestling hall) using Ansys 15	29-45
Hassanen L. Jaber R. k. Salim, Ashraf S. Fahad	Effect of Heat Treatment Parameters on Microstructure and Mechanical Properties of (Aisi1005) Steel	46-55
Zainb Abd Alelah	Modeling of Short Duration Rainfall Intensity Duration Frequency(SDR-IDF) Equation for Basra City	56-68
Rafid Saeed Atea	Flexural Behavior of Reactive Powder Concrete with Hybrid Section T- Beams	69-89
Hashim A. Hussein	An Experimental Investigation for Water Flow Enhancement in Horizontal Pipes by Using Nanoparticles	90-103
Maryam Yousif Ghadhban	Dynamic Analysis of Absorption Column	104-119



# Modeling of Structural Human Dynamic

## Simulation of Speed Control for Synchronous Reluctance Motor Based on Tuning Cascaded PID Controller with PSO Algorithm

Shahzanan Ali Kahdum  
Electrical Engineering Department  
University of Basrah  
[Shah\\_aljourany@yahoo.com](mailto:Shah_aljourany@yahoo.com)

Khalid M. Abdul-Hassan  
Electrical Engineering Department  
University of Basrah  
[KhMh7447@gmail.com](mailto:KhMh7447@gmail.com)

Ramzy S. Ali  
Electrical Engineering Department/ University of Basrah  
[rsalwaily@gmail.com](mailto:rsalwaily@gmail.com)

### ABSTRACT

This paper presents simulation and control of synchronous reluctance motor (SynRM). The motor speed is controlled by using Traditional PID controller that have been used in cascaded form. The Particle Swarm Optimization (PSO) is used to find the optimal parameters of the PID controller. Lead-Lag controller introduce in the cascaded controller as a second stage of control. Space vector pulse width modulation (SVPWM) scheme proposed to control the motor by using variable input voltage. A comparison between the manually tuned and PSO tuned cascade controller shows that the PSO give amazing control characteristics for the motor speed and have advantage over the manually tuning controller.

**Key Words:** Synchronous Reluctance Motor, PID, Cascade Controller, PSO, SVPWM

المحاكاة والسيطرة على سرعة المحرك/التردد المتزامن بالاعتماد على ضبط ثوابت المتحكم المتعاقب  
PID و باستخدام خوارزمية PSO

### الخلاصة

هذا البحث يمثل محاكاة وسيطرة على محرك التردد المتزامن (SynRM). يتم التحكم في سرعة المحرك باستخدام وحدة التحكم التقليدية (PID) التي تم استخدامها في شكل متعاقب. استخدمت خوارزمية أسراب الطيور (PSO) للحصول على القيم المثلى لثوابت وحدة تحكم PID. تم استخدام وحدة تحكم المعوض المتقدم- المتأخر كمرحلة ثانية من السيطرة. تم اقتراح إستعمال تقنية العاكس ثلاثي الاطوار (VS-SVPWM) للسيطرة على المحرك عن طريق تغيير فولتية الادخال للمحرك. تمت المقارنة بين وحدة تحكم التي تم ضبطها يدويا والتي تم ضبطها باستخدام PSO وتبين أن PSO يعطي قيم الثوابت المثلى والتي تعطي خصائص سيطرة مدهشة لسرعة المحرك ولها ميزة على وحدة التحكم التي تم ضبطها يدويا.

## 1. INTRODUCTION

Syn RM is one of synchronous machine type with no magnetic material and winding in the rotor structure. As compared to other synchronous machine SynRM is very rugged and simple in structure. In the beginning the SynRM was inferior as compared to other type of motors such as induction motor (IM), brushless DC (BLDC) motor, switch reluctance motor

(SRM) and DC motor because of low average torque, larger torque pulsation and poor power factor. The stator winding of SynRM is same as IM but the rotor structure is differ from that. In recent years a major development have been made in the rotor structure to overcome these disadvantages to enable the SynRM to give a very stable performance. SynRM is a three phase motor with rotor made of steel axially laminated barriers to overcome the low torque and poor power factor characteristics. Optimization technique is used in rotor structure design to have high quadrature axis reluctance and low direct axis reluctance. Fig. 1 shows the rotor flux barrier of SynRM. Since SynRM does not need any winding or magnetic material on the rotor structure which make the motor rugged, simple in structure , lowest cost of manufacturing requirement, high torque per unit volume possibility and operating at very high speeds capability. The SynRM has neglected rotor windings loses there for result a simple control methods and the losses minimization make SynRM an attractive and famous choice for numerous industrial and automotive applications [1,2,3,4]. The SynRM have marvelous features make this motor perfect choice for many industrial application such as elevators, fans and lightly road electric vehicles ( EVs). The speed control is very important factor and play an important role in these application[3] .

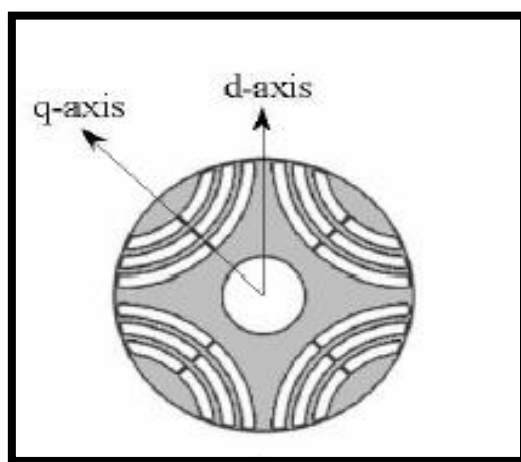


**Fig. 1 SynRM rotor flux barrier[4]**

The SynRMs does not have a starting torque so by using the new types of inverters, field orientation control (FOC) technology and the using of pulse width modulation (PWM) technique provide a very suitable technique for motor starting [5]. In recent years, the variable speed motor drive is casted over a fixed speed motor drive due to energy conservation, velocity or position control and improvement of transient response characteristics. These controllers are used to control the speed of the SynRM based on three phase VS-SVI technique and the stationary frame transformation. SynRm can be shown from it is d-q stationary axis equivalent circuits as in fig. 2. Depending on the closed loop speed control systems a fast response can be

obtained. In this paper the traditional PID in cascaded form with the lead-lag controller are proposed. PSO technique are used to find the optimal parameters of the controller parameters. A comparison been made between the manually tuning and the PSO tuning and the results are discussed briefly next.

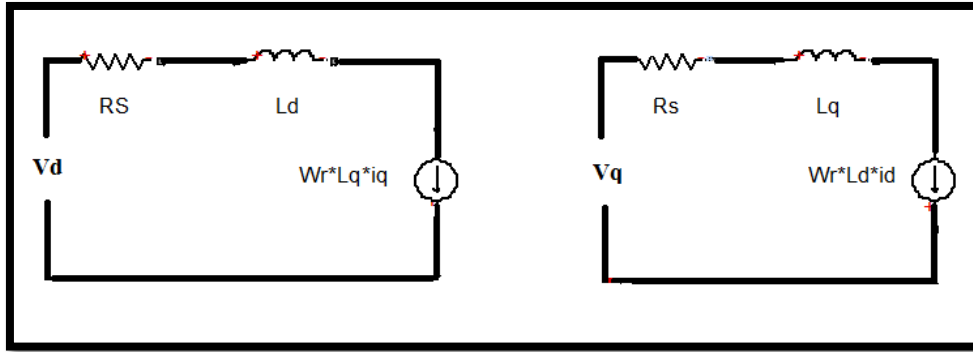


Fig. 2 SynRM d-q axis equivalent circuit

## 2. SynRM Mathematical Model

Three phase SynRM model is good for analyzing motor under different operation conditions, but for appropriate control action three phase analysis are rarely used. So the two axis SynRM model are mainly used for the control synthesis.

$$V_d = R_s I_d + \frac{d\lambda_d}{dt} - \omega_r \lambda_q \quad (1)$$

$$V_q = R_s I_q + \frac{d\lambda_q}{dt} + \omega_r \lambda_d \quad (2)$$

$$\lambda_d = L_d I_d \quad (3)$$

$$\lambda_q = L_q I_q \quad (4)$$

Where  $L_d$  and  $L_q$  are the direct and quadratic axis winding self-inductance and measured in henri (H),  $R_s$  represent the stator winding resistance in ohm ( $\Omega$ ) and  $\omega_r$  is the rotor angular speed in radian per second (rad/sec), the flux rate of change can be obtained as will be shown in equation (5) and (6) as follow.

$$\frac{d\lambda_d}{dt} = V_d - R_s I_d + \omega_r \lambda_q \quad (5)$$

$$\frac{d\lambda_q}{dt} = V_q - R_s I_q - \omega_r \lambda_d \quad (6)$$

and from equation (5) the rate of change of direct axis current can obtained in equation (7)

$$\frac{dI_d}{dt} = \frac{1}{L_d} (V_d - R_s I_d + \omega_r L_q I_q) \quad (7)$$

and from equation (6) the rate of change of quadratic axis current can obtained in equation (8).



$$\frac{dI_q}{dt} = \frac{1}{L_q} (V_q - R_s I_q + \omega_r L_d I_d) \quad (8)$$

The electromagnetic torque equation for SynRM can be obtained as follow in equation (9).

$$T_e = \frac{3}{4} \frac{P}{2} (L_d - L_q) I_d I_q \quad (9)$$

where  $T_e$  represent the electromagnetic torque of the SynRM in Newton meter (N.m). The total torque equation is given in equation (10).

$$T = \frac{3}{2} P (L_d - L_q) i_d i_q - \left( B \omega_r + J \frac{d\omega_r}{dt} \right) - T_L \quad (10)$$

where P the number of poles is pairs of the motor and load, J represent the moment of inertia coefficient of motor in kilogram square meter ( $K_g M^2$ ), and  $T_L$  is the load torque to the motor in newton meter (N.M) and B is the viscous friction coefficient of the motor N.m.s [1, 4]. All the motor parameters are shown in Table (A) in the appendix. The motor performance at nominal speed taken from ABB motors company manual data is shown in the appendix Table (B).

### 3. Mathematical Model of Voltage Source Space Vector Inverter (VS-SVI)

Inverters are a power electronic devices used to convert the DC voltage taken from a battery or any DC source into AC voltage. According to the inverter type the transformed voltage may be single phase, two-phase and three-phase, etc. An inverter that feeding synchronous motors are primarily used in variable voltage variable frequency for high-performance variable speed application. The most popular PWM technique is SVPWM technique which is used due to the larger DC bus voltage and less harmonic distortion. Three-phase voltage-source converter circuit consist of six switches and power supply as shown in Fig. 3. this scheme confines space vectors to be applied according to region where the output voltage vector is located. Fig. 4 shows the six sectors of the space vector and the space vector phase voltages. The mathematical modelling of space vector pulse width modulation (SVPWM) inverter are shown as follows [6,7].

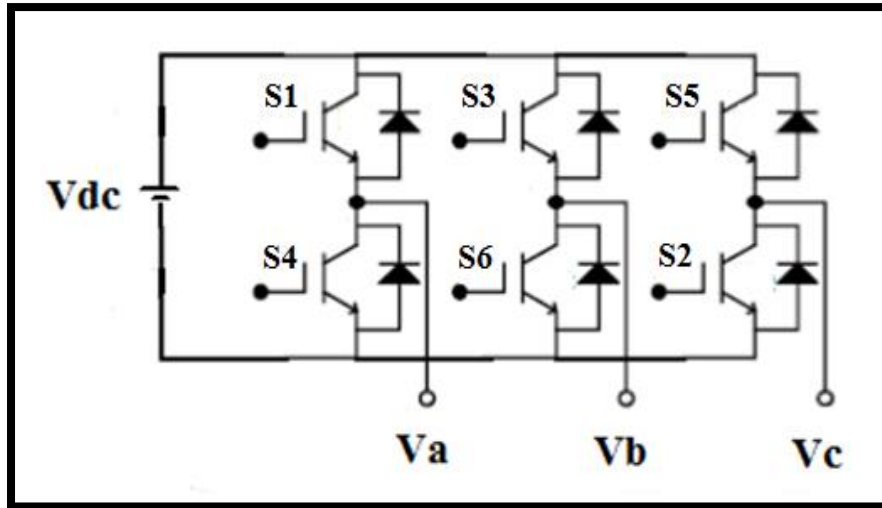


Fig. 3 Three-Phase VSI circuit connected to power supply [6]

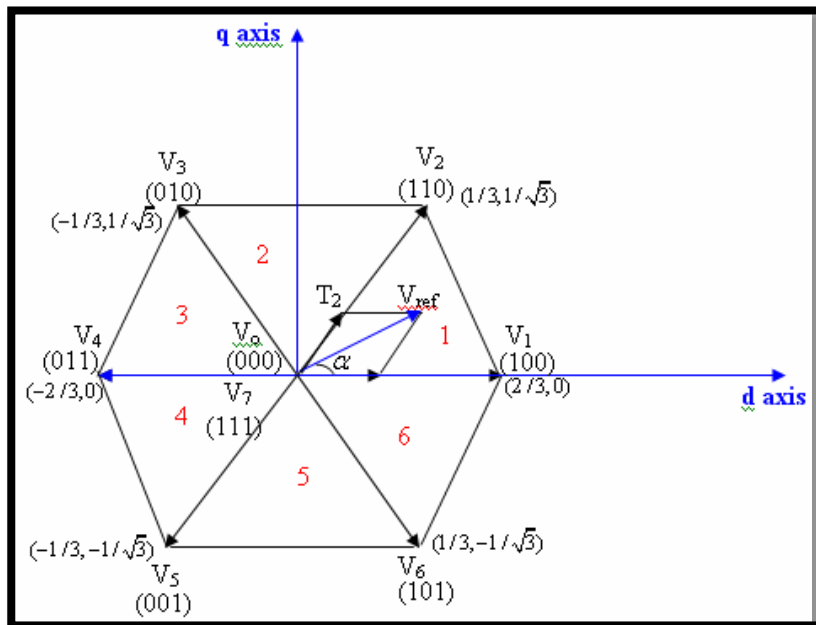


Fig. 4 Six sectors of SVPWM [7]

$$V_{ref} = \sqrt{V_d^2 + V_q^2} \quad (11)$$

$$\alpha = \tan^{-1}\left(\frac{V_d}{V_q}\right) = \omega_s t = 2\pi f_s t \quad (12)$$

$$V_{ref}T_s = (V_1T_a + V_2T_b + V_{0,7}T_o) \quad (13)$$

$$T_z = (T_a + T_b + T_o) \quad (14)$$

$$V_{ref} = V_{ref}e^{j\alpha} \quad (15)$$

$$V_1 = \frac{2}{3} V_d, V_{0,7} = 0, V_2 = \frac{2}{3} V_d e^{j\frac{\pi}{3}} \quad (16)$$

Where  $T_s$  represent the sampling period and calculated from  $(2*T_z)$  where  $T_z$  is the switching frequency and  $T_a, T_b$  and  $T_o$  represents the switching period that specified for  $V_1, V_2$  and  $V_{0,7}$  respectively. The reference space vector have been assumed to be constant during one switching cycle to get high switching frequency. The zero vectors represent the switching start of each switching period  $T_z$  or full null per vectors per  $T_s$ , each null have duration width of  $(T_o/2)$ , so the space vector equations can be written as follow.

$$\text{Re: } V_{ref} \cos \alpha T_z = \frac{2}{3} V_{dc} T_a + \frac{1}{3} V_{dc} T_b \quad (17)$$

$$\text{IM: } V_{ref} \sin \alpha T_z = \frac{1}{\sqrt{3}} V_{dc} T_b \quad (18)$$

$$T_a = \frac{\sqrt{3} T_z V_{ref}}{V_{dc}} \sin(\frac{\pi}{3} - \alpha) = T_z * m_a * \sin(\frac{\pi}{3} - \alpha) \quad (19)$$

$$T_b = \frac{\sqrt{3} T_z V_{ref}}{V_{dc}} \sin(\alpha) = T_z * m_a * \sin(\alpha) \quad (20)$$

$$T_o = (T_z - T_a - T_b) \quad (21)$$

$$m_a = \frac{\sqrt{3} V_{ref}}{V_{dc}} \quad (22)$$

$$T_a = \frac{\sqrt{3} T_z V_{ref}}{V_{dc}} (\sin(\frac{\pi}{3} - \alpha + \frac{n-1}{3} \pi)) = \frac{\sqrt{3} T_z V_{ref}}{V_{dc}} * (\sin(\frac{n\pi}{3} - \alpha)) \quad (23)$$

$$T_b = \frac{\sqrt{3} T_z V_{ref}}{V_{dc}} (\sin(\alpha - \frac{n-1}{3} \pi)) \quad (24)$$

Where  $\alpha$  is the voltage phase angle,  $m_a$  represent the modulation index of the SVPWM inverter and  $V_{dc}$  is the DC source voltage in volt[6,7].

#### 4. Simulink Model of SynRM Motor

The SynRM are represented by the direct and quadrature axis voltages. The motor voltages equations (1) and (2) are implemented in Matlab/Simulink environment in Fig.5. where the inputs of this block are direct and quadrature axis voltages and the output are the motor speed and torque.

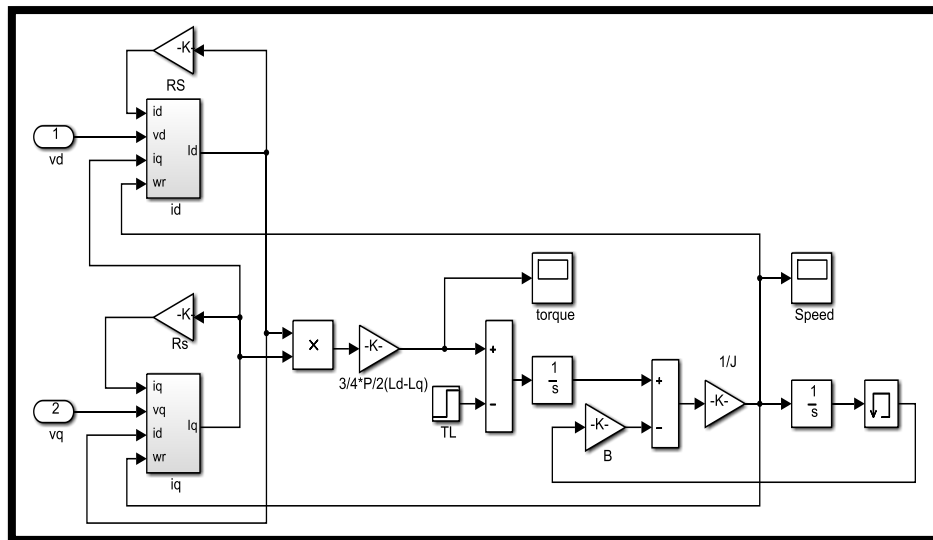


**Fig. 5. SynRM model block**

## 5. Speed Control of SynRM

Two tuning methods are applied to the cascade controller which are manually tuning with trial and error parameter estimation and PSO tuned cascade controller, each topology will be described as next.

### 5.1 Cascade Control System

The processes that have more than one variable at the output that should be controlled are well-known as multi-input, multi-output (MIMO) or multivariable processes. Interactions usually exist or sometimes not exist between the control loops of multivariable processes, which is famed by difficulties in control when compare it with the control of single-input, single output (SISO) processes. Lead-lag compensators are used to give a combines performance between both the lead and lag compensator and used as a second stage after PI and PID controllers which make the system have stabilized performance. PI controller have been used to control the direct axis current. This type of control process are shown in Fig. 6. The disadvantages of this type of control an exiguity of flexibility for interaction adjustment and when compare it with general multivariable control it have a few powerful tools for its design. SISO PID controller are tuned by control engineers , there is one simple way to tune a multi-loop PID controller by first tuning each individual loop one by one, and totally discarding the loop interactions and that is done by tune the (i) loop of cascade controller for the plant transfer. Then re-tuning all the loops together so that the overall system have stable performance and gives an acceptable load disturbance responses [8].

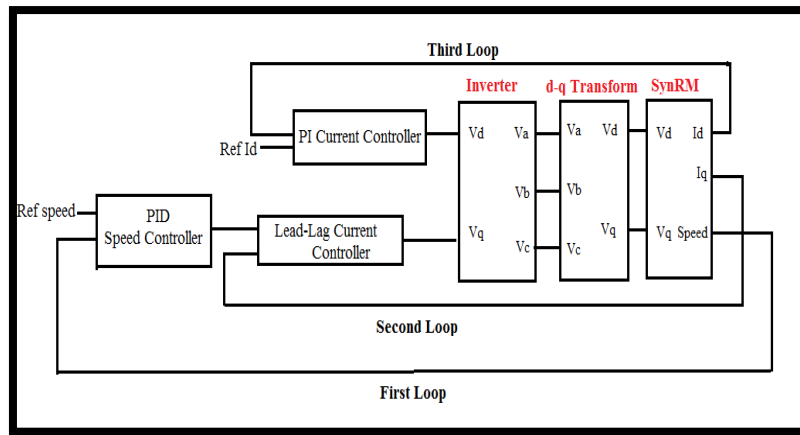


**Fig. 6. Cascade controller**

## 5.2 Particle Swarm Optimization Tuning PID Controller Parameter

Particle swarm optimization (PSO) is a population depend on computational schemes that the main concept came from the simulation of social behavior (social-psychological methods) fish schooling, bird flocking and swarm theory. PSO was firstly designed and evolved by Eberhart and Kennedy [9, 10]. This theory has been made to be powerful in solving problems exhibiting the non-linearity and the non-differentiability. The scheme is obtained from research on swarm such as bird flocking and fish schooling. Accommodation to the results of research for a flock of birds, find that birds food by flocking (not by each individual). The fitness function is casted to maximize the constrains domain or to minimize the preference constrains. The most commonly performance criteria that depend on the error criterion are Integrated Absolute Error (IAE), Integrated of Time weight Square Error (ITSE) and Integrated of Square Error (ISE) that can be calculated analytically in frequency domain. The criteria selection is depend on the system and the controller[11, 12]. In this paper the fitness functions are used depend on the Integral of Squared Error (ISE) criterion and overshoot ( $M_p$ ) criterion as follow:

$$\text{Fitness function} = \min(\text{ISE}) + \min(M_p) \quad (25)$$

Where

$$\text{ISE} = \int e^2(t)dt \quad (26)$$

$$M_p = \max(n) - (n_{\text{ref}}) \quad (27)$$

$$e(i) = D(i) - y(i) \quad (28)$$

where  $y(i)$  is the model output, and  $D(i)$  is the wanted output. While  $n$  is the actual speed, and  $n_{\text{ref}}$  is the reference speed. The velocity  $v_i(t)$  and the current position  $x_i(t)$  updating for each particle in the swarm are done in equations (30, 31). The velocity of each agent can be updated by the following equation.

$$v_i^{k+1} = w * v_i^k + c_1 * R_1 * (lbest_i - x_i^k) + c_2 * R_2 * (gbest_i - x_i^k) \quad (29)$$

and, the current position can be updated by the following equation:

$$x_i^{k+1} = x_i^k + v_i^{k+1} \quad (30)$$

where  $x_i^k$  is the current position of particle  $i$  at iteration  $k$ ,  $v_i^k$  is the velocity of particle  $i$  at iteration  $k$ ,  $w$  is the inertia weight which can be shown in Eq. (36),  $c_1$ ,  $c_2$  represent positive acceleration constants and  $R_1$ ,  $R_2$  are random variables distributed uniformly in the range  $[0; 1]$ .

$$w = w_{\max} - \frac{(w_{\max} - w_{\min})}{\text{iter}_{\max}} \quad (31)$$

where,  $w_{\min}$  is the initial weight,  $w_{\max}$  is the final weight  $\text{iter}_{\max}$  is the maximum iteration number. Fig.7 shows a general flowchart form for PSO algorithm.

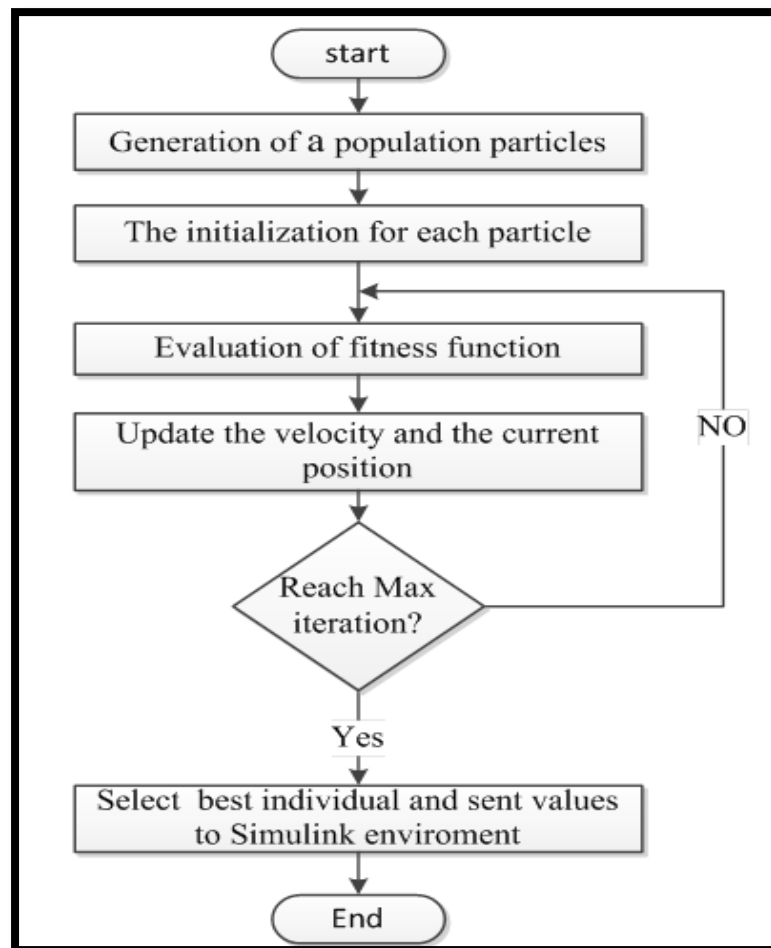


Fig. 7: Flow chart of PSO algorithm [11]



## 6. System Simulation and Results

This section presents simulation and results for the SynRM drive. The motor drive system with vector control method has been simulated using Matlab/Simulink environment packages. The drive system and the controller system are shown in Fig.8. The cascaded controller is shown in Fig.9. The cascade controller have a parameters shown in Table (1) which are found by trial and error. Table (2) shows the PSO algorithm parameters. Table (3) the parameters of cascade controller that been found depending on PSO algorithm. Figures (10, 11 and 12) represent the speed and torque response due to step load change at 0.8 sec time to and value of 25 N.m load applied to the motor with traditional and optimized parameters. Figures (13, 14 and 15) show the speed and torque response due to step reference speed due a step speed respond torque response. The results shows that the traditional controller with manually tuning parameters need more time to back to reference speed value when applying load to the motor in the other hand the PSO tuning parameters controller shows a major enhancement in the speed response and almost the load effect has not effect on the speed response which clarified in Table (4) . When applying step speed reference the speed is much better when using the PSO parameters and that shown in Fig.13. As a result the PSO algorithm gives a major improvement in the speed and torque response of the motor when operated at different operation conditions.

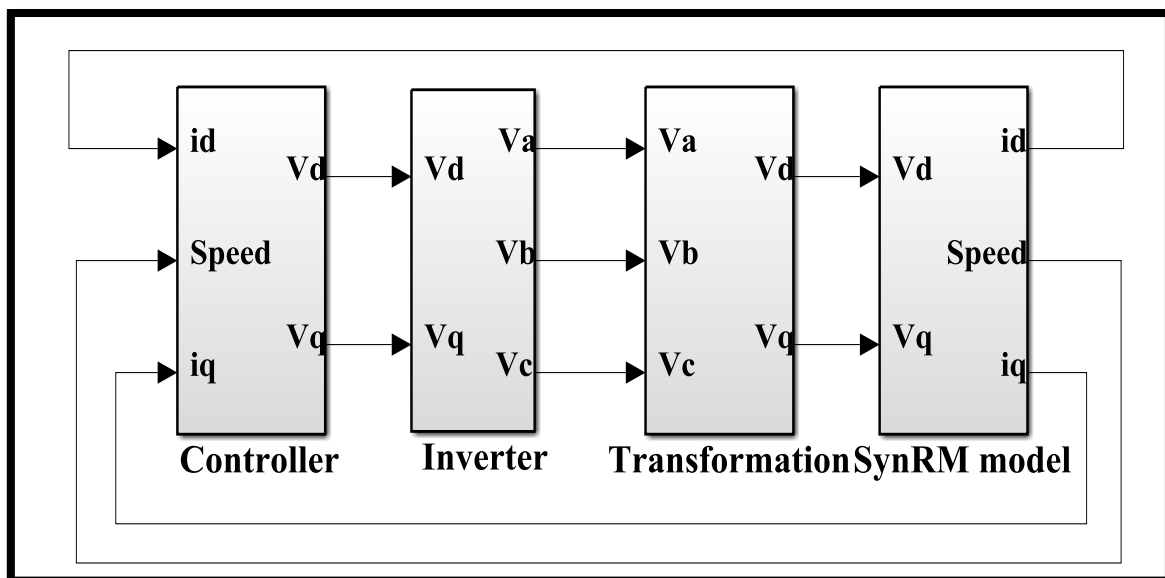


Fig.8 Motor drive system and controller

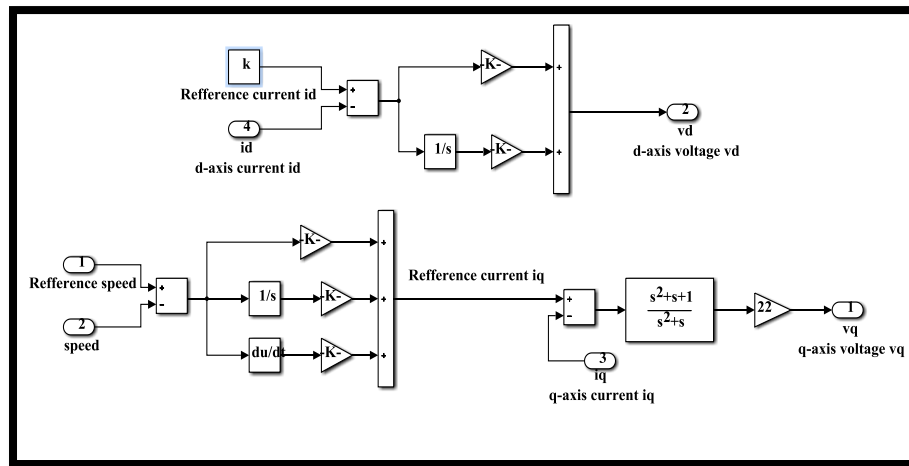


Fig. 9 Cascade controller block

TABLE 1: PID PARAMETERS

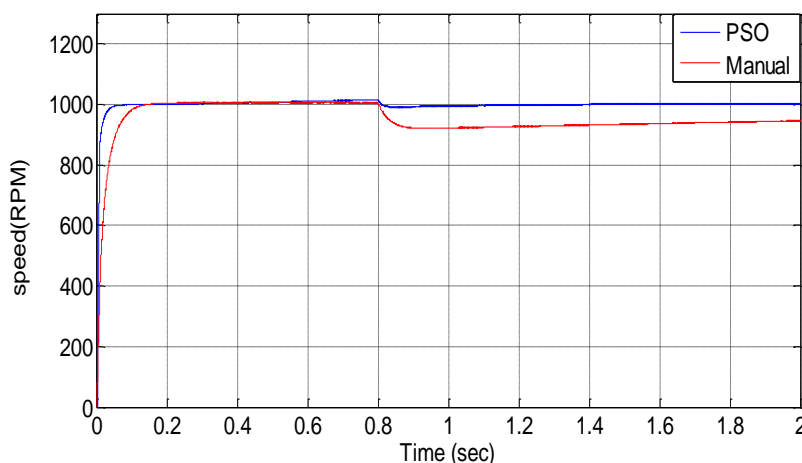
Controller type	Speed Controller Parameters			q-axis Current Controller Parameters	d axis Current Controller Parameters	
Parametrs	$K_P$	$K_I$	$K_d$	$K_3$	$K_P$	$K_I$
Values	40	10	1	22	1200	10

TABLE 2: THE VALUES OF PSO ALGORITHM PARAMETERS

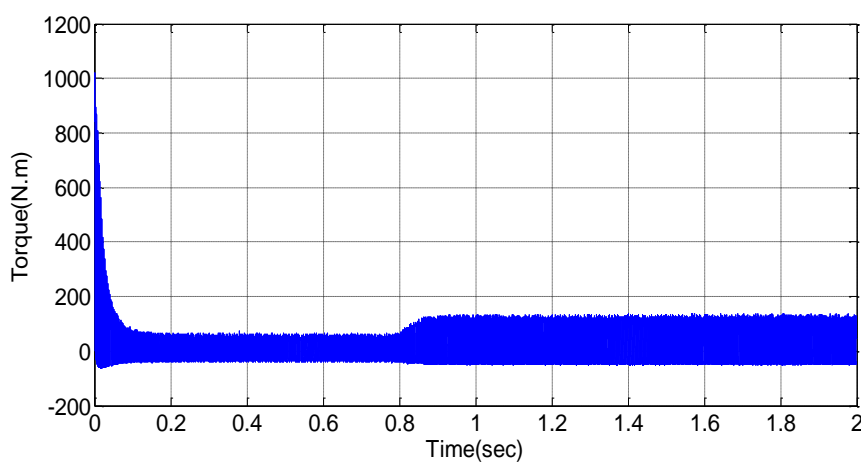
PSO_Parameters	Value
Maximum iteration number	50
Size of the swarm " no of birds "	50
Dimension	20
PSO parameter $c_1$	1.2
PSO parameter $c_2$	1.2
Wmax	0.9
Wmin	0.2

TABLE 3: PID PARAMETERS TUNED USING PSO

Controller type	Speed Controller Parameters			q-axis Current Controller Parameter	d- axis Current Controller Parameter	
Parametrs	$K_P$	$K_I$	$K_d$	$K_3$	$K_P$	$K_I$
Values	200	8.8	0.749	20.879	2130	9.8



**Fig. 10 Motor torque due 1000 RPM reffrence and 25 N load at 0.8sec applied to PSO and PID controllers**



**Fig. 11 Motor torque due 1000 RPM reffrence and 25 N load at 0.8 sec applied to traditional controllers**

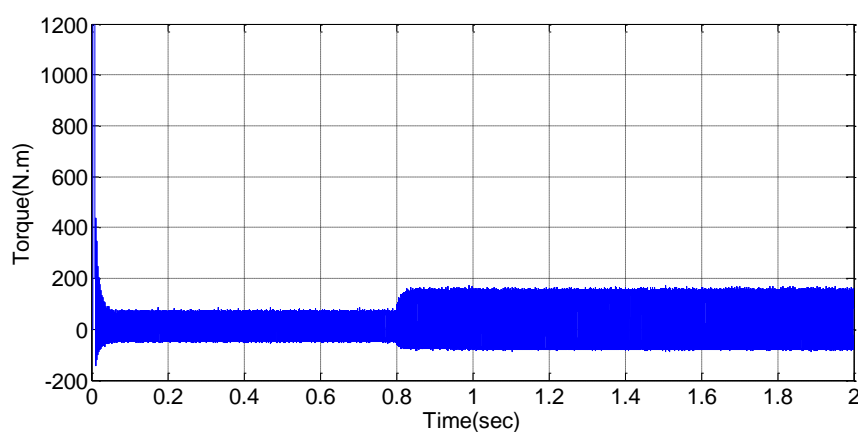


**Fig. 12 Motor torque due 1000 RPM reffrence and 25 N load at 0.8 sec applied to PSO tuned controllers**

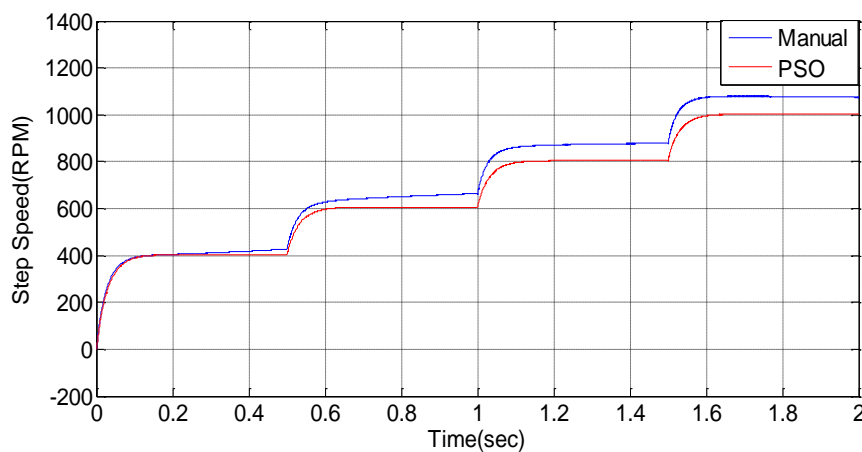


**Fig. 13 Motor speed due step reference speed applied to PSO and traditional controllers**

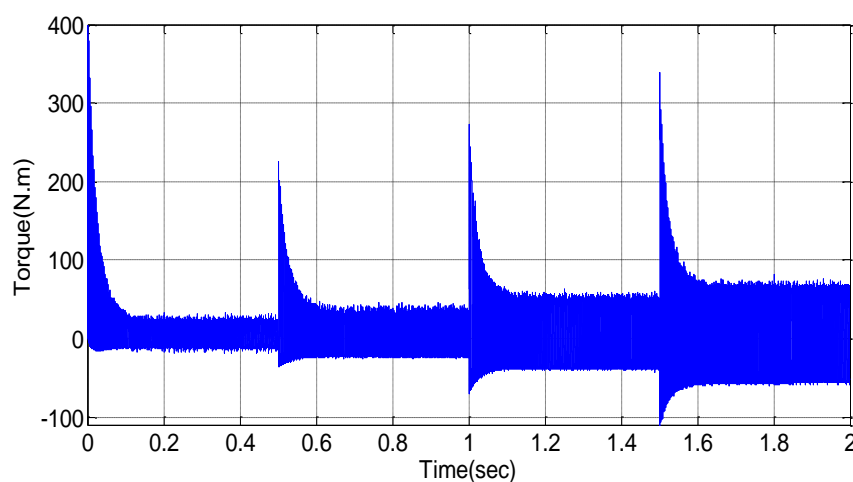


**Fig. 14 Motor torque due step reference speed applied to traditional controllers**

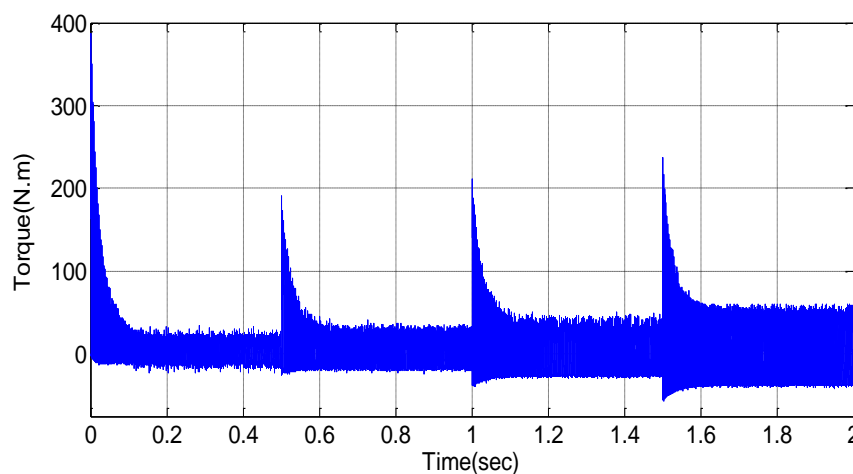


**Fig. 15 Motor torque due step reference speed applied to PSO tuned controllers**

**TABLE 4: COMPARISON BETWEEN THE MANUALLY AND PSO TUNED CONTROLLER PERFORMANCE**

System Performance	Manually Tuned Controller	PSO Tuned Controller
Over Shoot	1.3979 %	Approximately 0%
Steady State Error	$3 \times 10^{-3} \%$	$2 \times 10^{-3} \%$
Settling Time	1.2589	0.0350
Rise Time	0.0407	0.0079

## 7. CONCLUSION

This paper has concerned the simulation and control of the synchronous reluctance machine drive systems using Matlab/Simulink environment. The main motivation was due to the large number of SynRM advantages. In this paper the vector control by depending on space vector pulse width modulation is used to control motor speed. The inverter stage represent the open loop control to the motor. The cascade controller is very difficult to tune manually so the trail and error may parameters give a good control performance but not the optimal performance so the loop intersection is the main cause of that difficulty of the tuning process. Particle swarm optimization is very suitable algorithm to tune this controller parameters. According to the PSO parameters the system performance is improved. Both the motor speed and torque response of motor are improved and any desired speed in the range of the motor characteristics the controller make the motor run at that speed.

## 8. APPENDIX

**Table (A): SynRM parameters**

Parameter	Parameter Value	Units
<b>Ld</b>	<b>6.0641</b>	<b>mH</b>
<b>Lq</b>	<b>0.9099</b>	<b>mH</b>
<b>Rs</b>	<b>0.0265</b>	<b>Ohm</b>
<b>J</b>	<b>0.245</b>	<b><math>Kgm^2</math></b>
<b>B</b>	<b>0.0000009</b>	<b>N.m.s</b>
<b>P</b>	<b>2</b>	<b>poles</b>

**Table (B): Performance at nominal speed From ABB motors company manual data**

Output power	45	Kw
Speed	3000	RPM
Operation frequency	100	Hz
Efficiency at full load	94.6%	-
Current	103	A
Torque	143	N.m
Torque Ratio	1.5	-

## 9. REFERENCES

- [1] Fellani, M. A. , Daw. and Abaid E., " Modeling and Simulation of Reluctance motor using digital computer", International Journal of Computer Science and Electronics Engineering, IJCSEE, VOL. 1, 2013, PP.148-152.
- [2] Consoll, A., Russo, F., Scarcella, G., Testa, A., " Low-and Zero Sensorless Control Of Synchronous Reluctance Motor", IEEE Transection on Industrial Electronics, Vol.35, No. 5, PP. 1050-1057, September/ Ooctober(1999).
- [3] Fratta, A., Vagati, A., "A Reluctance Motor Drive for High Dynamic Performance Applications ", IEEE Transection on Industrial Electronics, Vol.28, No. 4, PP. 1050-1057, July/August (1992).
- [4] Fellani, M. A., Daw., and Abaid E., " Matlab/Simulink-Based Transient Stability Analysis of A Sensorless Synchronous Reluctance Motor", International Scholarly and Scientific Research & Innovation Vol. 4, No. 8, (2010).
- [5] Soltani, J., and Zarchi, H. A., "Robust Optimal Speed Tracking Control of A Current Sensorless Synchronous Reluctance Motor Drive Using A New Sliding Mode Controller", IJE Transactions B: Applications, Vol. 17, No. 2, pp. 155-170, (2004).
- [6] Gupta, A., and Kumar, S., "Analysis of Three Phase Space Vector PWM Voltage Source Inverter for ASD's", International Journal of Emerging Technology and Advanced Engineering, Vol. 2, No. 10, pp. 163-168, (2012).
- [7] Kumar, K. V., Michael, P. A., John, J. P., and Kumar, S. S., "Simulation and Comparison of SPWM and SVPWM Control for Three Phase Inverter", ARPN Journal of Engineering and Applied Sciences, Vol. 5, No. 7, pp. 61-74, (2010).
- [8] Golten, J. and Verwer, A. "Control System Design And Simulation", London, 1991, PP.154-157
- [9] Effatnejad R., Bagheri S., Farsijani M., Talebi R., "Econmic Dispatch With Particle Swarm Optimization and Optimal Power Flow", International Journal on "Technical and Physical Problems of Engineering" (IJTPE), Vol. 5, March 2013, PP. 9-16.
- [10] Rambabu CH, Y. P. Obulesh, C. H. Saibabu, "Multi-Objective Optimization using Evolutionary Computation Techniques", International Journal of Computer Applications, Vol. 27, Aug. 2011, PP. 19-25.
- [11] Yogendra K. Soni1 and Rajesh B., "BF-PSO Optimized PID Controller design using ISE, IAE, IATE and MSE Error Criteria", International Journal of Advanced Research in Computer Engineering & Technology (IJARCET), Vol.2, July 2013, PP. 2333-2336.
- [12] Mohammad S. Rahimian and Kaamran R., "Optimal PID Controller Design for AVR System Using Particle Swarm Optimization Algorithm", IEEE, 24th Canadian Conference on Electrical and Computer Engineering (CCECE), May 2011, PP. 337-340.



# Design and implemetation Backscatter Detector with Arduino System

Ali Idham Alzaidi

Southern Technical University /Shatrah Technical institute

Thiqar /Shatrah – Iraq

[aalzaidi@bridgeport.edu](mailto:aalzaidi@bridgeport.edu) , [engali78@yahoo.com](mailto:engali78@yahoo.com)

**ABSTRACT:-** Backscatter X-beam is used to obtain on X-beam imaging innovation. Conventional X-ray machines recognize hard and delicate materials by the variety in transmission through the objective. Conversely, backscatter X-beam identifies the radiation that reflects from the objective. It has potential applications where less-dangerous examination is required, and can be utilized if stand outside of the objective is accessible for examination. The innovation is one of two sorts of entire body imaging advancements that have been utilized to perform full-body sweeps of carrier travelers to recognize shrouded weapons, apparatuses, fluids, opiates, money, and other stash. A contending innovation is millimeter wave scanner. These application can be very useful by detecting system specially in security system Purpose . At the point when The X-beams pass through the human body or whatever other Materials The item under X-beam will be absorb , penetrate or Scattered the X-beams bar. These beams which are scattered or launched out from the subject's body are detected by detector placed close to object . The sign delivered by this scattered X-beam detector then used to balance a picture show gadget to create a picture of the subject and any covered Objects conveyed by the subject The indicator get together is built in a setup to consequently and consistently improve the picture edges low nuclear number (low Z) hid articles to encourage their identification. A capacity means is given by which beforehand procured pictures can be contrasted and the present picture for dissecting fluctuations in similitudes with the present picture, and gives intends to making a nonexclusive representation of the body being inspected while stifling anatomical components of the subject to minimize intrusion of the subject's protection-beam imaging systems in view of Compton backscatter license review and screening of ocean compartments, a wide assortment of vehicles, baggage, and even individuals.. Potential applications in the paper will design the X-ray detector machine relay on new technique for image processing by using Arduino as control system with less dangerous assessment on the human body and Contrasts in the sort of data showed by backscatter pictures will be highlighted, between backscatter picture quality furthermore, interpretability, output speed, successful infiltration.

**Keywords-;** Scatter ; X-ray beam, Photo Multiplier Tube ,Image processing , Arduino

**الخلاصة :-**

يستخدم الأشعة السينية المرتدة من الاجسام التي تتعرض اليها للحصول على صورته ذات طبيعة محدده حسب الغرض من التصوير . علما ان أجهزة الأشعة السينية التقليدية تواجه صعوبة كبيرة لتعرف على المواد الصلبة او الحساسة. على العكس من ذلك فان الأشعة السينية المرتدة من الاجسام يمكن ان يحدد نوع الجسم ونوع المادة التي مر من خلالها . لذلك فان التطبيقات المحتملة لهذا النوع من الأجهزة تكون أقل خطورة، ويمكن أن تستخدم من موقع خارج الجسم المطلوب الوصول اليه او الفحص .ان هذا الابتكار يقدم نوعين من التقدم الحاصل في تصوير الجسم و التي استخدمت تقنيات حديثة لتنفيذ عمليات تمشيط كامل الجسم في العديد من الاماكن مثل تعرض المسافرين لهذا النوع من اجهزه الفحص وذلك للتعرف على أسلحة والأجهزة والسوائل، والمواد الأفيون، والمال، وغيرها التي ممن الممكن ان تكون مخبأ . أن تكون هذه تطبيق مفيد للغاية في الكشف والتحقق وخصوصا في الأنظمة الأمنية. يعتمد عمل الجهاز من خلال تعرض الجسم الي الأشعة السينية عندما تصل إلى النقطة تمرير-أشعة X من خلال جسم الإنسان أو أي مواد أخرى فان الشعاع السيني سيكون اما امتصاص ، اختراق أو ارتداد. نقوم بالكشف عن هذه الأشعة المرتدة و التي تنتشر أو أطلقت خارج من الجسم هذا الموضوع من خلال الكاشف عن وضعها بالقرب من الجسم . حيث ان تصميم كاشف اللاقط للأشعة المرتدة من الاجسام المسلط عليها الاشعاع وبالتالي تحليل هذا الاشعاع للحصول على صورته رقميه تبين لنا محتويات والمواد الرئيسية للجسم المرتد منه الاشعاع علما ان سقوط الاشعاع على الجسم يؤدي الى اما امتصاص الاشعاع من قبل الجسم او نفاذيته او ارتداد او انعكاس هذا الاشعاع . ان اللاقط او الكاشف المصمم له القدرة على التقاط الأشعة المرتدة من الجسم وتحويلها الى اشارات كهربائية باستخدام الكثر وده الضوئية PHOTO MULTIPLIER TUBE PMT التي بدورها تحول الاشعاع المرتد الى اشارات تتناسب مع طبيعة الجسم ثم تحول هذه الاشارات الى اشارات رقميه من خلال Analogue to digital converter والتي تقوم بحفظها على شكل مصفوفات داخل الذاكرة الكي يتعامل معها فيما بعد وتحويلها الى صور قابله للمعالجة والتعديل من خلال برنامج الماتلاب والمعالج الرئيسي هو اريدينو Arduino .

**I. Introduction**

This paper will introduce new method to develop an X-ray detector system less dangerous on the human body or any object . Detectors with integrated phosphor scintillation , conductive, or metallic fiber can have a good conductivity for X-rays Photon and transmitted to Photo multiplier tube[3] . Highly conductive Phosphor scintillation have been proposed in the past to pick up the signal which reflected and scatter from the human body to Photomultiplier tube (PMT). Photomultiplier tubes (photomultipliers or PMTs for short), one of type the [vacuum tubes](#), and more consider sensitive materials used as detectors of light in the [ultraviolet](#), [visible](#), and [near-infrared](#) ranges of the [electromagnetic spectrum](#) [ 4 ]. These devices can amplify current when the incident light pass on the PMT can be amplify more than 100 million times ,During the amplify stages, enabling [photons need](#) to be detected when the incident light is very low[4.5 ] .



**Fig(1) Backscatter X-ray system with Arduino**

As Show in Fig(2) The Photomultiplier tube has large area of collection , high [gain](#), low interference [noise](#), high bandwidth frequency response, and has maintained photomultipliers an essential medical [diagnostics](#) such as [blood tests](#), [medical imaging](#), [telecine](#), [radar jamming](#), and high-end image scanners known as [drum scanners](#)[ 3 ]. Photomultipliers can be used in different application such as to detect light high-sensitivity detection of light that is imperfectly [collimated](#) [1]. Connected the PMT to Arduino . Arduino is an open-source PC equipment and programming organization, undertaking and client group that plans and produces microcontroller-based packs for building computerized gadgets and intuitive articles that can sense and control objects in the physical world[ 4 ].the task depends on microcontroller board plans, fabricated by a few merchants, utilizing different microcontrollers. These frameworks give sets of advanced and simple I/O sticks that can be interfaced to different extension sheets ("shields") and different circuits. the Arduino gives an improvement environment in the image Processing, which incorporates support for the C and C++ programming dialects. Now day using the Arduino in our application to enhancements and collect all the data from detectors . The benefits of Detectors - construct movement sensors in light of x-beam photon are their high affectability and trademark and the likelihood of coordination in Microcontroller framework, for example, Arduino[ 3 ]. X-beam backscatter finds cathodes to quantify and recognize parameters, for example, distinctive metals , show awesome guarantee because of the simplicity of coordination of identifiers ,Arduino , and conductive. Arduino framework and weaving is generally used to acknowledge picture . Inaccessibility of x-beam picture handling innovation and confinement in the quality components plan posture challenges in creating X-beams picture framework based indicators. In this segment we will exhibit the convention to build up our recognizing framework to get

the sign and changed over to picture for long time without creating any sort of meddling. In this section we will present the protocol to develop our detecting system to pick up the signal and converted to image for long time without causing any kind of interfering , in addition to As shown in Fig(1) the Backscatter X-ray Imaging System Produce beam of X-rays to the Object which can be person , Vehicle, bags being examined. In the preferred embodiment, an X-ray generator 1, X-ray tube 2 connect to produce an X-ray beam source as is known in the art for scanning the pencil beam in a horizontal motion across the body, illustrated in Fig(1). X-rays that are scattered or reflected from the body are detected by X-ray sensitive detectors will be fixed on the same direction of scatter ray. The electronic sign created from the indicators and synchronization signals from the X-beam source are steered into Memory then will be move in by bass to control unit to generates an image display on a monitor at each point in the display corresponds to the relative intensity of the detected scattered X-rays. The detectors are mounted on two vertical shafts which are thus mounted on a base to control the movement of the locators as they are moved in a vertical bearing. The X-beam pencil shaft source is mounted on a carriage, which thus in upheld by two turn joints as show in fig (1).one associated with the finder, and the other to a vertical backing. As the locators show above are moved in a vertical heading, the X-beam pencil shaft is moved in a circular segment, such that it generally goes through the opening in the detectors[5] .

## **(II) Arduino System**

Arduino is an open-source prototyping stage taking under consideration simple to-utilize instrumentation and programming As show in Fig(2)[13]. Arduino will scan all input in detector, you'll be able to check your board what to try to do and find out of directions to the microcontroller on the board[12]. The Arduino used the programming idiom (in lightweight of Wiring), and therefore the Arduino code (IDE)[13]. visible of process. Throughout the years Arduino has been the neural structure of a large variety of tasks, from regular articles to advanced experimental instruments. associate degree overall cluster of producers - understudies, specialists, craftsmen, developers, and consultants - has assembled around this open source , their commitments have import unbelievable} live of obtainable info which will be of incredible facilitate to beginners and specialists[9].

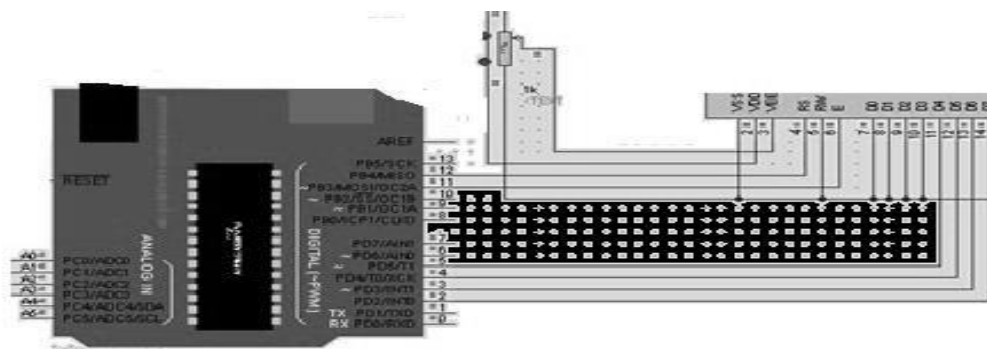


**Fig (2) Arduino System** <sup>[13]</sup>

The Arduino board will ever-changing to adapt to new wants and challenges, differentiating its supply from easy 8-bit boards to product for Io T applications, wearable, 3D printing, and embedded environments[9]. the item detection rule has been developed on MATLAB platform by the mixture of many image process algorithms. victimization the speculation of Image Acquisition and Fundamentals of Digital Image process, the item has been detected in real time. varied options of associate degree object like the form, size and color is wont to sight and track the item. The variation in vertical and horizontal axis of detected object is tempered by serial communication port and victimization serial information communications, the state of Arduino board pin has been controlled[9]. MATLAB programming develops a laptop vision system within the real time for object detection and pursuit victimization camera as a picture acquisition hardware. Arduino programming provides associate degree interfacing of a hardware model with management signals generated by real time object detection and tracking[12]. Arduino programming provides associate degree interfacing of a hardware model with management signals generated by real time object detection and pursuit. The revolutionized computers open up the probabilities of victimization pictures associate degreed video frames as an input signals of the signal process. Such signal process is known as as image process. Image process transforms varied sets of characteristics of image parameters into output as management signals[13]. The constant revolution within the field of digital image process release a large number of application in varied areas, during which innovative technologies may are developed. the most effective platform on that several image process algorithms are developed to date is MATLAB. Major advantage of victimization MATLAB as a picture process rule development surroundings is its in-built image process functions and its compatibility with hardware like cameras [9].

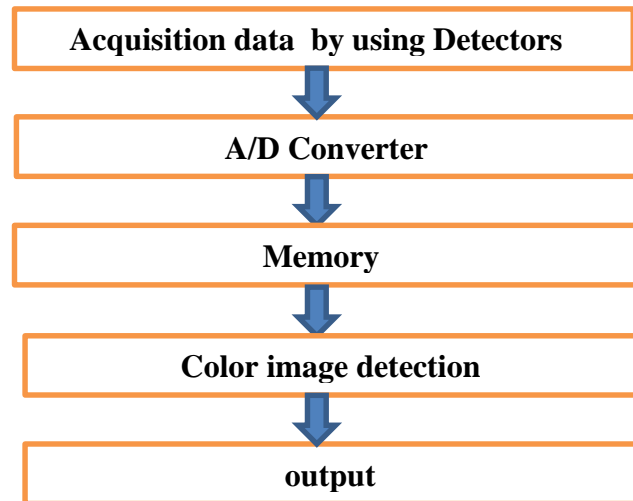


**Fig (3) Flowchart of proposed prototype system**

Software includes MATLAB and Arduino software whereas hardware includes Detectors ,Camera, Arduino board with Converter Adapter.The goal of this work is to visually detect and track an object in a region and send the data to the Arduino board to glow LEDs connected with the microcontroller's digital output port. The most challenging issue raised while developing the object detection algorithm is that of selecting the feature to use for segmenting the object[10]. Here, using approach based on object's shape is very difficult and less efficient with the system in real time constraints. So, rather using the segmentation by shape, the color of an object has been taken into consideration. The color of an object is a subject of its lightning condition. Working of the proposed prototype system can be understood by the above flowchart.

### **(III) Detector collection area**

To design new detector which able to detect X-ray from known source with range from 50 kv to 170 kv as in fig (4) which represents the principle of the X-ray backscatter system As Show below consist of the following :-

- 1- X- Ray Generator
- 2- Detectors
- 3- A/D Converter
- 4- Memory
- 5- Control Unit (Arduino )
- 6- Display system

Each part was explained separately and The present system consists of an electronic detector can be built by adding a [photomultiplier](#). These kind of detector scintillation or "[scintillation](#)



[counters](#)". The main advantage of using we can get on required image with low energy and an area sensitive to X-rays and pyramid shape with the total size are 45 cm width , 50 cm height and 55 Cm length As show in Fig (4) below . X-ray detectors are equipment used to detect the [spectrum](#) or the properties of [X-rays](#) .there are two main purpose of detectors for imaging and dose measurement. in this study we focus on use the Imaging detectors for X-ray backscatter devices were originally [imaging plates](#) and photographic but most of them replaced by different kind of computerized methods such as [image plates](#) or [flat panel detectors](#). Usually detector place between the body and X-ray generator which as show Fig(3):

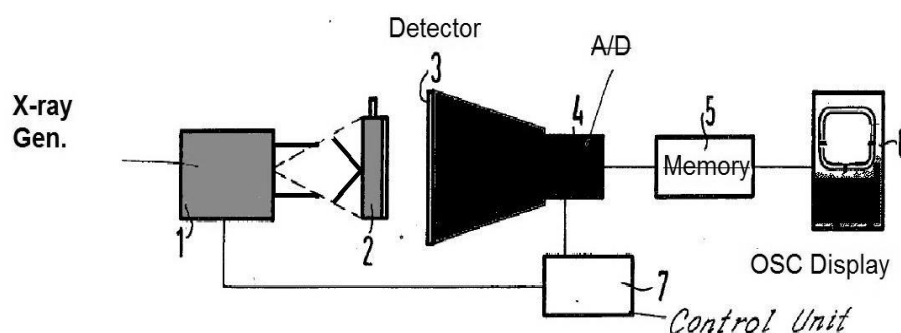


**Fig (4) Basic Principle of image of X-ray system <sup>[7]</sup>**

can be placed at the same distance from the subject. In the backscatter detectors will be pick up backscattered radiation when start a scan. We can determine the effective detection area at any given point in the scan is can be the same scan Detector , i.e., one-half the total detector area of the stationary detector configuration[5]. During our experiments we can notice the measurements show that the shape and located of detector receiving about more than fifty percent (50%) of X-rays as backscatter[6]. As indicated above, this is can be more than the transmission method. our detector consists of an active area 1 inch by 24 inches, or a total X-ray collection area of 24 square inches. This is a factor of approximately 40 lower than the 952 square inches of X-ray sensitive area provided in the present invention[3]. The increased collection area of the present invention is increased number of scattered X-rays allowing for reduction in dose compared with the backscatter system of the prior art.

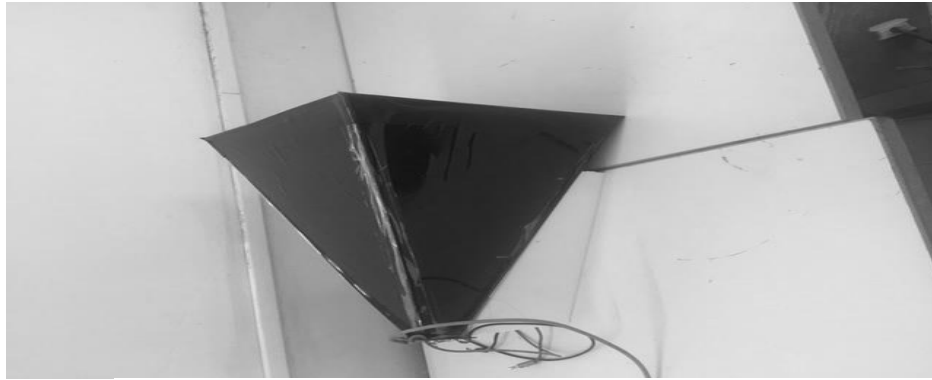


**Fig (5) Design detector with Photo multiplier tube**

Through our experiments and measurement that the detector must consist of an active area in the range of 150 to 1500 square inches and placed in the range of 9 to 20 inches from the person being searched so that at least 2% of the scattered radiation is detected. When system start work ,we got digital image of the subject. Our detection will concentrate on the part of photons scattered back towards the x-ray source[7]. This can be done with scintillators made out of materials such as sodium iodide. These materials which made up the Scintillators can "convert" an X-ray backscatter to a visible light; In order to gain energy spectrum information, we used A/D to separate the different photons.. These signals are amplified and then converted to digital signal for processing, as seen below [8].X-ray backscatter imaging can be used to see through objects. This can be done by subtracting a lower energy scan from a higher energy scan. The results of this can be seen in our simulation below when we upload in Matlab. This image is then processed by the digital computer to identify key features in the image. This library of human images is used to identify common anatomical features in the present subject so those anatomical features can be suppressed[2]. The library may also contain within its images certain common benign objects which can also be suppressed to permit more accurate detection of dangerous or illegal concealed objects. The location of detected features can be referenced to the absolute location in the image, or in relation to the body of the person being examined[10]. The latter method has the advantage of being insensitive to subject positioning within the imaging window and differing subject size.

## **(VI) Simulation by Using Matlab**

The entire algorithm for object detection and tracking is a base on image processing. The proposed system uses MATLAB as a platform on which image processing algorithm has been developed and tested. As an image acquisition device , camera is used[8]. A camera can be an built in camera of laptop or it can be a USB camera as well. To get the detail of the hardware device interfaced with the computer, *imqhwinfo* command of MATLAB is used. Entire

MATLAB programme for this algorithm can be divided in parts as follows. A. *Image Acquisition*: The first task in image processing algorithm is to get the live video feed from the camera connected[9]. This live video feed has further been converted into sequence of frames and these frames are used in order to apply further image processing algorithm. For that *get snapshot* command of MATLAB is used, which converts video feed into image array. Conditionally, ROI (Region of Interest) can also be defined for capturing specified area of the frame. Image acquisition toolbox of MATLAB can also be used for image acquisition purpose. To perform the image, which is p\_3\_2.jpg, negative transformation, first we have to read the image p\_3\_2.jpg that shows the MRI of the brain by using command `imread`, let us name our image (brain). After we read the image, we use the command `Size` to determine the image's size (size of array). Using command `double` will help us to convert to double precision. I use command `zeros` to make a matrix that is N-by-N zeros. Next steps, I used the expression `s=L-1-r` that are given with question to perform the negative of the image, which is gray levels, with the range `[0, L-1]`. Then, I closed with the commands `end` and `end`. To be able to compare the original image with the image after perform, I used command `imshow (brain)` for original image; after that I used command `figure` to be able to see the image after performing negative transformation and `imshow (f, [0 255])`. We see that from two images. In the original image, around the brain image is the black level and the brain in the image with gray level. In the image after transformation, the brain has less gray level than the original and around the brain is more white level.

*The program on MATLAB should be as the following:*

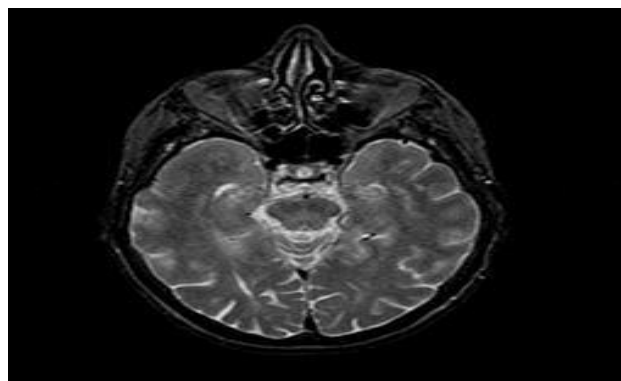
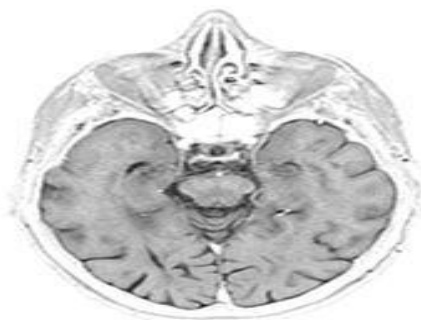


Fig (6)The original image of brain



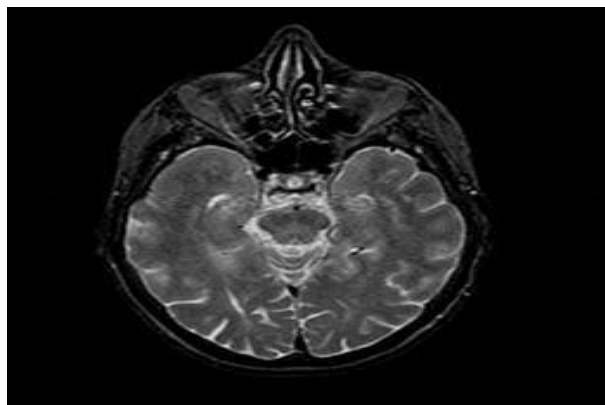
Fig(7) The image of the brain after negative transformation

In part B question 1, log transformation to the brain image. Part B in question 1 is close to part A. The difference will be in the expression. First we have to read the image p\_3\_2.jpg that shows the MRI of the brain by using command `imread`, the name of the image will be (brain). After we read the image, we use the command `Size` to determine the image's size (size of array). Using command `double` will help us to convert to double precision. I use command `zeros` to make a matrix that is N-by-N zeros. In the part B, I have to use a log transformation. The general form of the log transformation, which is given in the question, is:

$$S = c \log (1+r) \quad \text{-----}( 1)$$

The constant of  $c = 100$   $r$  is the original pixel value ; and  $s$  is the new pixel value ;

***The program should be as the following:***



Fig(8)The original image of the brain



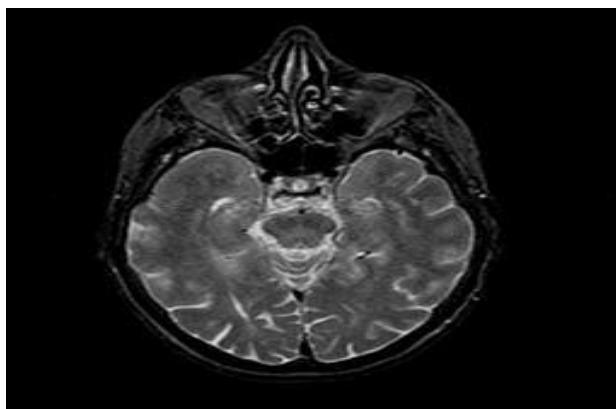
Fig(9) The image after the log transformation

The difference between two images is in the original image shows the brain image and the area around with different gray levels. In the image after log transformation, the image shows brain white and the area around the brain is black. In the part C, we have to do the power law transformation to the brain image. First we have to read the image p\_3\_2.jpg that shows the MRI of the brain by using command `imread`, let us name our image (brain) too in this transformation. After we read the image, we use the command `Size` to determine the image's size (size of array). Using command `double` will help us to convert to double precision. I use command `zeros` to make a matrix that is N-by-N zeros. The basic form of the power law transformation is:

$$S = cr^y \quad \text{-----} (2)$$

Where  $C=1$  and  $y=0.6, 0.3$ .

***The program on MATLAB should be as the following:***



Fig(10)The original image of the brain

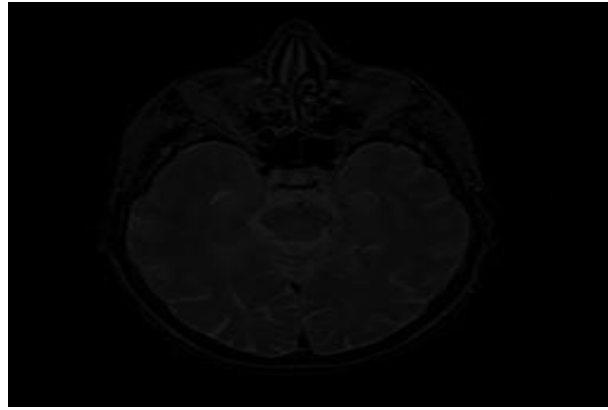


Fig (12) The image after power law transformation with 0.6



Fig(13) The image after power law transformation with 0.3

Three images have got after program, the first image is an original image of brain. The second image is the image of brain after the power law transformation; we can see in the second image that brain in the image is darker (we still able to see it) than original image due to 0.6 is considered a small number. In the third image, it shows the dark image (it is hard to see brain in the image) because of 0.3 which is really small number. So, the image is a dark (black) image.

## (V) Conclusion

Now day there is increased concerns about security everywhere after all the relevant events , Image Using backscatter x-ray Detectors can used widely to implementation in around the world . These devices use Compton scattered x-rays to make the new connection to computerized to detect and recognize any explosives or weapons they might be carrying. However, there are concerns over the detector's abilities to always detect hidden explosives[4]. Also, There are concerns about Health effect by X-rays radiation when human body exposure for long time. The imaging impact is much the same as taking a photo of the compartment substance through the optically murky mass of the holder with picture shine exceptionally



corresponded with the normal nuclear number of the segments of the picture. Besides, these pictures can be taken at relative framework versus target object rates of 10 km/hour and that's only the tip of the iceberg. Such frameworks can be outlined with an extensive variety of tradeoffs between determination, check speed, and field-of-perspective and offer one of a kind uneven imaging abilities that are impractical with straightforward transmission X-beam frameworks. On the other hand, if fancied, transmission imaging ability can be included onto any backscatter framework. Various perspectives are likewise conceivable with appropriate framework plan, so that cargoes may be imaged from a few distinct bearings.

## REFERENCES

- [1] Marmier, P. and Sheldon, E., Physics of Nuclei and Particles, Academic Press: New York and London, 1969, 103-111
- [2] " Kravets, David (2013-01-18). "TSA Pulls Plug on Airport Nude Body Scanners".Jump up ^ Rapiscan backscatter contract (World wide Web log), TSA, Jan 2013.
- [3] David ,M."TSA pulls ALL X-ray body scanners from airports over privacy concerns... but claims they were never a health risk to fliers". UK. Daily Mail. 2013-05-30.
- [4]Phillip , N. "Imaging Technology". Transportation Security Administration. Archived from the original on 6 January 2010.
- [5]. Aji Joy, Ajith P Somaraj, Amal Joe, Muhammed Shafi, Nidheesh T M, "Ball Tracking Robot Using Image Processing and Range Detection", IJIRCCE, Vol. 2, Issue 3, March 2014, ISSN:2320-9801
- [6] Steven W. Smith, Poway, Calif, X-RAY BACKSCATTER DETECTION Primary Examiner-Constantine Hannaher SYSTEM ,
- [7] Joseph Callerame , X-RAY BACKSCATTER IMAGING:PHOTOGRAPHY THROUGH BARRIERS, JCPDS-International Centre for Diffraction Data 2006 .
- [8] Marmier, P. and Sheldon, E., Physics of Nuclei and Particles, Academic Press: New York and London, 1969, 103-111
- [9]. Raquib Buksh, Soumyajit Routh, Parthib Mitra, Subhajit Banik,Abhishek Mallik, Sauvik Das Gupta, "Implementation of MATLAB based object detection technique on Arduino Board and iROBOT CREATE", IJSRP, Vol. 4, Issue 1, Jan 2014.
- [10]. Nikhil Sawake, "Intelligent Robotic Arm", Submitted to Innovation Cell, IIT- Bombay, July 2013
- [11]. V. Subburaman and S. Marcel. Fast Bounding Box estimation based face detection in „Workshop on Face Detection of the European Conference on Computer Vision (ECCV)“, 2010.
- [12]. <http://www.mathworks.in/help/images/ref/regionprops.html>
- [13]. <http://arduino.cc/en/Tutorial/HomePage>

## Numerical and Experimental study of the indoor environmental Conditions of a large Athletic hall (wrestling hall) using ansys 15

Mohammed R.K.Alsheekh\* Ali A.Monem Emad Abdullah

\*M.Sc. student

E-mail: [miemrk@yahoo.com](mailto:miemrk@yahoo.com)

Department of Mechanical Engineering, Engineering College, University of Basrah, Basrah -Iraq

### Abstract

This study investigates numerically and experimentally the environmental conditions prevailing in a large mechanically ventilated athletic hall, with the aid of the computational fluid dynamics by ANSYS 15 program. The indoor space of the building was simulated in the ANSYS 15 program environment and the model results were validated against experimental data collected during a 7-day campaign in the hall. The measurements included airflow characteristics at different locations of the indoor space, as well as surface temperatures of the indoor materials. Having obtained good agreement between experimental and numerical results, different scenarios were applied in the model to investigate the environmental conditions prevailing in the hall under different ventilation and occupational conditions. These regard air-conditioning and cooling modes, as well as empty and full hall during an athletic event. The velocity, temperature and relative humidity were studied and results revealed dynamic behavior of the fields, significantly altering with the different considered cases.

**Keyword:** Large Enclosure, Athletic Hall, CFD model, IAQ.

### الخلاصة

هذه الدراسة تتحرى بشكل عددي و تجريبي الشروط البيئية التي تسود في قاعة رياضية كبيرة و مكيفة ميكانيكيا ، وتتم هذه الدراسة بواسطة ديناميك السوائل الحسابية ( CFD ) ضمن برنامج ( ANSYS 15 ) الهندسي ، الفضاء الداخلي للبنية تم بنائه بواسطة برنامج ( ANSYS 15 ) و ان النتائج العددية النموذجية في البرنامج تم مطابقتها و تصديقها مع البيانات التجريبية التي جمعت اثناء حملة سبعة أيام في القاعة الرياضية ، تضمنت المقاييس خصائص التيار الهوائي في المواقع المختلفة من الفضاء الداخلي بالإضافة الى درجات الحرارة السطحية من المواد الداخلية وقد حصل التوافق الجيد بين النتائج التجريبية و العددية ، المخططات المختلفة طبقت في النموذج لتحري الشروط البيئية التي تسود في القاعة تحت التهوية المختلفة و الشروط المهنية ، التي تتعلق بأنماط التبريد المختلفة بالإضافة الى القاعة الفارغة والكاملة اثناء الحدث الرياضي ، تم دراسة سرعة التيار الهوائي و درجة الحرارة والرطوبة النسبية بشكل ملحوظ في الحالات المدروسة المختلفة .

## **(1)Introduction**

The Computational fluid dynamics (CFD) codes have become an important tool in the research field of air quality, in both the indoor and outdoor environments.

They are currently applied for investigations of indoor airflow fields for building design and optimum ventilation purposes and for pollutants dispersion in working areas for health and safety reasons. However, few studies combine theoretical and experimental methods to investigate air quality in stadiums and athletic halls, where a large number of people are present during events and athletes train and compete. Proper ventilation and supply of fresh air play a significant role in the control of indoor air quality and thermal comfort given that metabolism is intense due to the overcrowding of people. [1]

The last decade has been characterized by a significant increase of worldwide scientific database in indoor environments. People recognize that indoor air quality may be more important than outdoor air quality because they spend over 70% of their time indoors. Applications of heating, ventilation and air conditioning system are known to modify the indoor air quality by means of filtration, humidification, dilution and cooling the outdoor air entering the occupied space. For instances, adequate filtration of outdoor air intake of air-conditioning system through a well-maintained filter can be effective in preventing outdoor microbial contamination associated with outdoor sources of environmental microbes in air-conditioning buildings. Air-conditioning system has also been shown to contribute to the rising fungal contamination in indoor air from various components in the system. [5]

Therefore, this study investigates numerically and experimentally the environmental conditions prevailing in a large indoor (wrestling hall) under different mechanical ventilation schemes and occupation conditions.

## **(2) Methodology**

### **(2.1) Experimental Procedure**

A 7-day experimental campaign in the frame of a research project is accomplished in an indoor wrestling hall within the athletic Education College, University of Basrah. This hall is surrounded with the close vicinity includes heavy-traffic roads at about 1 km and the sea at about 2 km to the southwest. The height of the indoor space is 8 m, the area is 265 m<sup>2</sup>, and the capacity of the hall is (35-50) people. The windows are normally closed and the heating–

ventilating–air conditioning (HVAC) system operates according to the needs. Measurements were taken at different locations in the hall with and without the HVAC system is in operation.

The instrument used is (Data logging / Printing Anemometer + Psychrometer) [8] this device simultaneously measures and displays air velocity, temperature, humidity, wet bulb temperature, and air Volume (CFM / CMM). Surface temperatures of indoor materials were measured with an infrared thermometer. This can be seen in Figures (6and7).

## **(2.2)Theoretical Model—Initial and Boundary Conditions**

The ANSYS 15 (CFD) code [7] solves the time-averaged conservation equations of mass, momentum, energy, and chemical species in steady three-dimensional flows:

$$\frac{\partial(\rho\phi)}{\partial t} + \text{div}(\rho\phi v) = \text{div}(\Gamma \text{grad}\phi) + S_\phi \text{-----} (1)$$

Rate of increase Of $\phi$ of fluid Element	+   Net rate of flow of $\phi$ out of fluid element	=   Rate of increase of $\phi$ due to diffusion	+   Rate of increase of $\phi$ due to sources
---	---	---	---

Where;  $\rho$ ,  $v$ ,  $\Gamma$  and  $S_\phi$  are density, velocity vector, effective exchange coefficient of  $\phi$ , and source rate per Unit volume, respectively, for a solved for variable  $\phi$ . [2]

The discretization of the domain is followed by the reduction of the previous equations to their finite domain form using the hybrid formulation of the coefficients and the solution technique employs the SIMPLEST algorithm (an improved version of the well-known SIMPLE algorithm). The standard turbulence model is applied, while buoyancy effects are considered. To improve convergence, under relaxation was used.

As seen in (Fig.1) the dimensions of the objects are real, the geometry is as detailed as possible according to the plans of the building and the blueprints of the mechanical ventilation system, always taking into account computational efficiency. The domain size is (16m x16m x 8m), and it includes 3 rows of spectators' seats, and 5 inlet air fans of split unit devices. It should be noted that the model configurations were set so that the best balance is achieved among convergence, grid independency, and runtime saving, due to the high complexity of the domain geometry as can be shown in Figures (2and3).

### **(2.3) Validation of CFD Program**

A commercial CFD program was used for the computations. By default, the code uses the finite-volume method and the upwind-difference-scheme for the convection term. The convergence criterion was set such that the respective sum of the absolute residuals must be less than  $10^{-3}$ . [6]

The CFD program was validated by comparing the flow patterns, vertical profiles of temperature, velocity, relative humidity and turbulence intensity of the measured data and computed results for a Large Athletic Hall (Wrestling Hall). This can be seen in (Fig. 4).

**Basic case:** It corresponds to a selected day from the experimental campaign. The hall is empty and the HVAC system operates in the air-conditioning mode, Without cooling.

**Cooling case:** This is a hypothetical case; the hall is assumed to be empty and the HVAC system operates in the cooling mode.

**Event case:** The hall is half-full with 20 spectators attending an athletic event and ventilation conditions are the same as in the basic case.

Model configurations concerning boundary and initial conditions, as well as settings information of the cases studied, are given below: Fresh air comes in the hall via split unit fans (air inlets of Figs. 1 and 5), the dimensions of inlet are 0.3m x 0.5m, with mean axial z-velocity of 4m/s and turbulence intensity of 5%, respectively, according to the experimental measurements in all cases. The boundary condition and the temperature locations, can be shown in table (1).

### **(3) Design and performance of thermal comfort.**

There are several factors that can account for the design and performance of thermal comfort, one of them:

Air Diffusion Performance Index (ADPI), can be calculated from the following general relationships: [9]

$$EDT(\theta) = (T_x - T_{av}) - 8 * (V_x - 0.15) \text{ ----- (2)}$$

Where: ( $\theta$ ) Effective draft temperature (K), ( $T_x$ ) Local air stream dry-bulb temperature (°C), ( $T_{av}$ ) Average (set-point) room dry-bulb temperature (°C), ( $V_x$ ) Local airstream centerline velocity (m/s), must be ( $V_x < 0.36$  m/s).

$$ADPI = \frac{N_{\theta}}{N} * 100\% \text{ ----- (3)}$$

Where: ( $N_{\theta}$ ) Number of points measured in the occupied space that falls within ( $-1.5 < \theta < +1$ K), (N) Total number of point measured in the occupied space

The performance of an air distribution system within a room/zone can be rated in terms of ADPI (the Air Diffusion Performance Index). Among the several evaluation methods used to design air distribution systems based on flow rate, sound data, isovels and comfort criteria, the ADPI selection method is quite commonly used. The selection process takes advantage of ADPI's correlation with the ratio of isothermal throw of the diffuser and the characteristic length of the system in the room. This paper clarifies what ADPI is and is not, what is involved in the selection process and how it fares against the industry standards and benchmarks in ventilation and thermal comfort. Several factors that may potentially cause any deviation to the predicted value of ADPI during the design stage are discussed. The post-installation ADPI that reflects the actual ADPI rating for a space has to be assessed and verified on-site. This on-site measurement should be conducted in accordance with a set of guidelines given in the ASHRAE Standard 113. A detailed CFD analysis can also provide an alternative solution to verify the actual "as built" ADPI rating. [9]





**Fig. 1 Domain of the athletic hall**

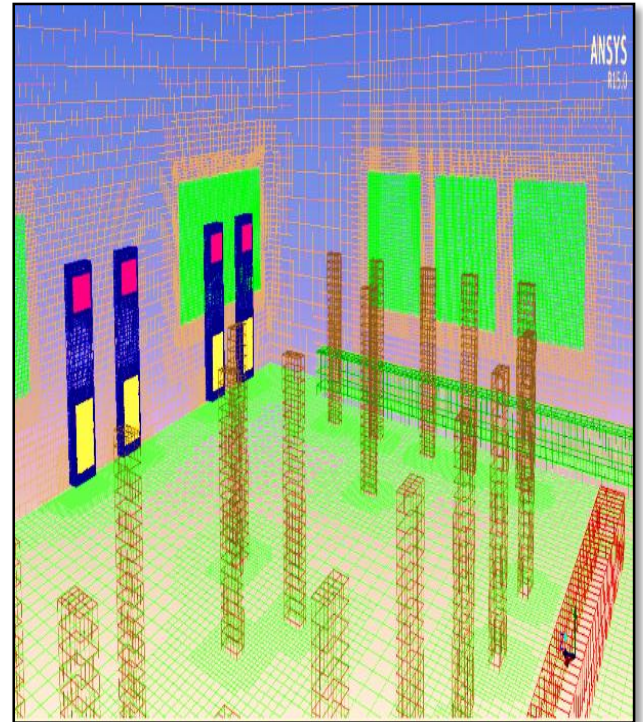


**Fig. 3 Plane view of the geometrical grid for the Event Case.**



**Fig. 2 Plane view of the geometrical grid For the Basic Case.**

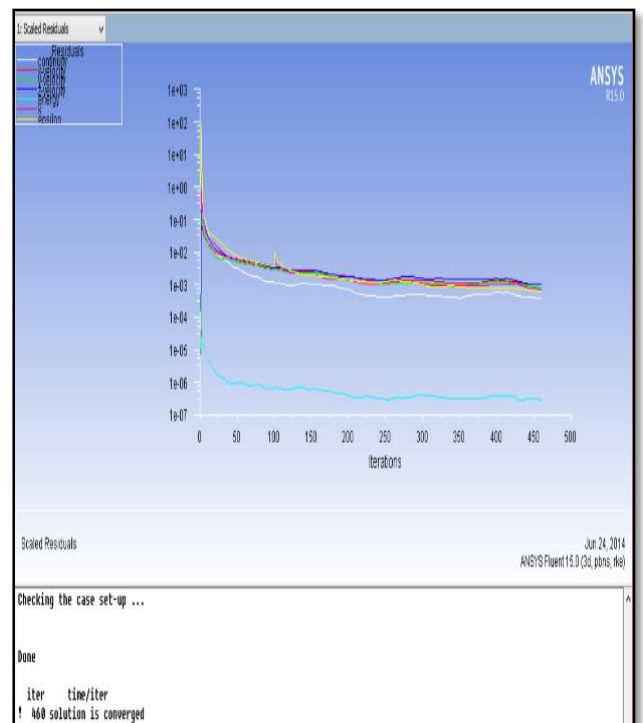


**Fig.4 Validation of the Basic Case.**

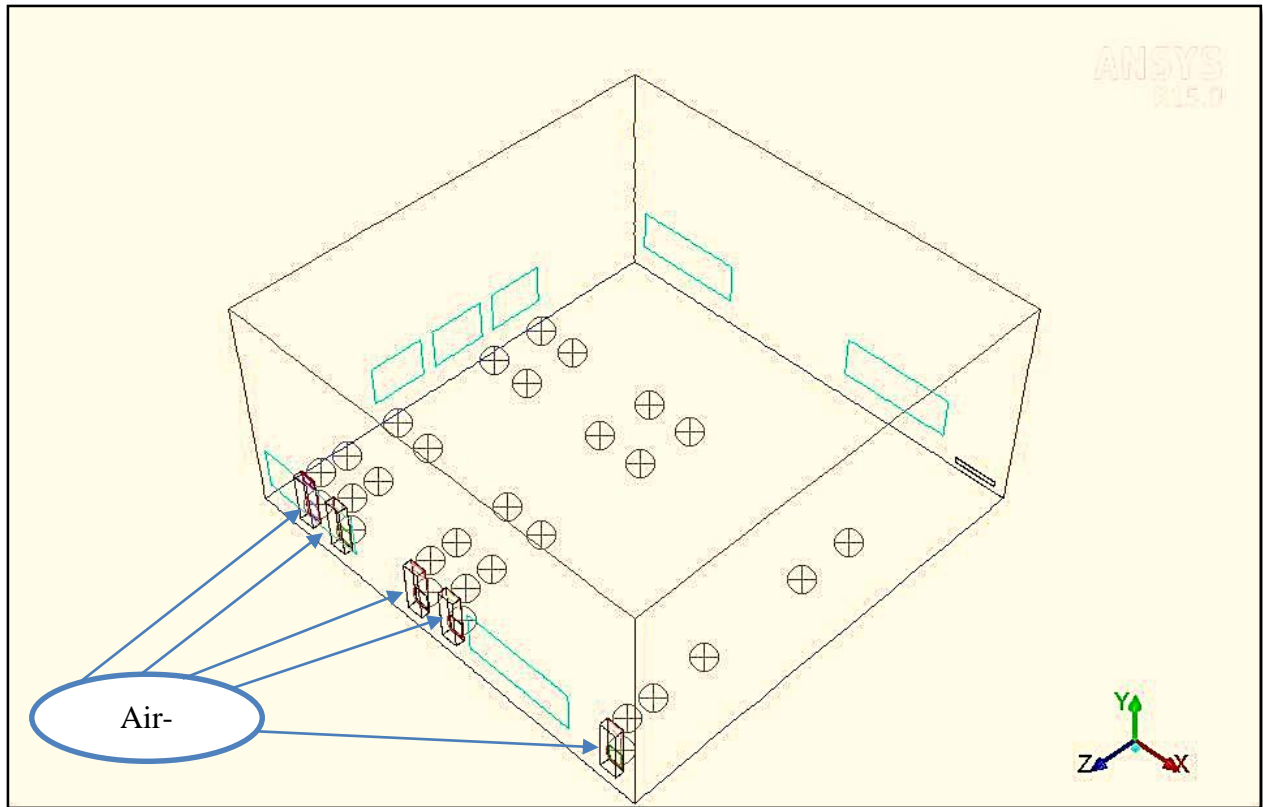


**Fig. 5 Plane view of some points for Basic Case**

**Table 1: Information and input model data of the studied cases.**

Data	Basic case	Cooling case	Event case
Inlet air temp. (°C) of split unit 1	39.6	18.1	18
Inlet air temp. (°C) of split unit 2	39.8	18	18
Inlet air temp. (°C) of split unit 3	40	18.2	18.1
Inlet air temp. (°C) of split unit 4	39.9	18.3	18.1
Inlet air temp. (°C) of split unit 5	39.5	18	18
Ceiling surface temp. (°C)	43-44	42	41
Floor surface temp. (°C)	40-40.5	39	38.4
East wall surface temp. (°C)	41-41.5	41	40
North wall surface temp. (°C)	41-41.5	41	40
Windows temp.(°C)	45	43.5	42
Surface temp. of 1st seat level (°C)	40	38.4	37.3
Surface temp. of 2nd seat level (°C)	40.5	38	37.2
Surface temp. of 3rd seat level (°C)	40	38.1	37



**Table 2: Measured and simulated air velocities and temperatures and relative humidity at measured points and CFD points of the domain for the basic case.**

Point No.	Locations			$V_{exp}$ m/s	$V_{th}$ m/s	$T_{exp}$ k	$T_{Nu}$ k	$RH_{exp}$ %	$RH_{Nu}$ %
	X(m)	Y(m)	Z(m)						
points average of outlet 1				2.195	2.2624276	313.8	313.90848	20.6	21.063747
points average of outlet 2				2.221	2.2513804	314	313.90964	21	21.062483
points average of outlet 3				2.151	2.2722647	313.5	313.86801	21	21.110161
points average of outlet 4				2.131	2.2648635	313.9	314.00629	21	20.957156
points average of outlet 5				2.211	2.3529201	314	313.84778	21	21.132594
1	1.75	1.75	15	3.981	4.0036712	313.2	312.60104	21.6	22.584687
2	1.75	1.75	14	3.506	3.7488418	313	312.68161	21.8	22.487541
3	1.75	1.75	12	1.677	1.8409307	313.5	313.26901	21.1	21.793309
4	1.75	1.75	8	0.788	0.9938601	312.9	313.50818	21.7	21.51766
5	1.75	1.75	6	0.759	0.8949071	312.9	313.52466	20.8	21.498837
6	3.25	1.75	15	4.004	4.0030689	314	312.80087	21.6	22.344561
7	3.25	1.75	14	3.513	3.7641978	313	312.86511	21.9	22.268002
8	3.25	1.75	12	1.234	1.3831714	312.9	313.46289	21.2	21.569553
9	3.25	1.75	8	0.611	0.7159041	313.4	313.6492	20.9	21.356991
10	3.25	1.75	6	0.598	0.7013043	313.7	313.63037	21.7	21.378379
11	6.75	1.75	15	3.881	4.003036	313.5	313.00079	21.8	22.107236
12	6.75	1.75	14	3.588	3.7865133	313.6	313.04742	21	22.052343
13	6.75	1.75	12	1.001	1.1597604	313.4	313.63239	21	21.376073
14	6.75	1.75	8	1.087	1.160279	313.5	313.65195	21	21.353878
15	6.75	1.75	6	0.789	0.955303	313.7	313.65424	21.2	21.35129
16	8.25	1.75	15	3.793	4.0056858	313	312.90091	21.8	22.225451
17	8.25	1.75	14	3.511	3.7837541	313.1	312.96408	21.4	22.150633
18	8.25	1.75	12	1.281	1.5217694	313.5	313.60651	21	21.405497
19	8.25	1.75	8	0.586	0.7325229	313.9	313.68277	20.6	21.318963
20	8.25	1.75	6	0.409	0.3737494	314	313.63708	21	21.370752
21	14.75	1.75	15	3.901	4.0043802	313	312.50131	21.9	22.705635
22	14.75	1.75	14	3.501	3.1413331	313	312.77518	21.6	22.375293
23	14.75	1.75	12	0.701	0.8661697	313.2	313.39767	21.5	21.64454
24	14.75	1.75	8	0.461	0.2566139	313.6	313.61172	21	21.399586
25	14.75	1.75	6	0.401	0.2766746	313.7	313.69684	20.7	21.303037
26	1.75	0.5	15	0.712	0.8897354	314	313.84055	20.5	21.141085
27	3.25	0.5	15	0.698	0.8444201	314.1	313.83344	21	21.149071
28	6.75	0.5	15	0.801	0.8614534	313.8	313.84171	20.7	21.139804
29	8.25	0.5	15	0.842	0.9377113	313.6	313.97055	21	20.995869
30	14.75	0.5	15	0.803	0.8408837	314	313.83591	20.1	21.146329

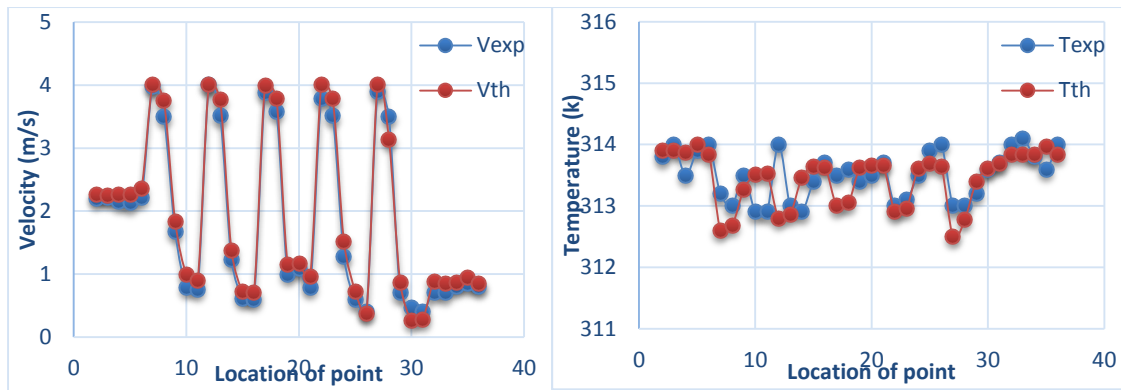
Chart .1 compare between  $V_{exp}$  &  $V_{Nu}$ .Chart .2 compare between  $T_{exp}$  &  $T_{Nu}$ .

Table 3: simulated air velocities and temperatures and relative humidity at CFD points of the domain for the Event Case.

Point No.	location			$V_{Nu}$ m/s	$T_{Nu}$ k	$RH_{Nu}$ %	EDT
	X(m)	Y(m)	Z(m)				
1	0.5	0.5	2	0.089656	304.909	17.34213	3.087579
2	0.5	0.5	13	0.094675	304.1983	18.05705	1.52993
3	4	0.5	3	0.181778	305.7208	16.56523	2.355539
4	4	0.5	13	0.265107	302.7708	19.596	-1.26108
5	11	0.5	12	0.305292	302.8033	19.56509	-1.55006
6	10	0.5	12	0.297353	302.741	19.63384	-1.54886
7	12	0.5	14	0.266446	302.9426	19.40763	-1.09997
8	13	0.5	13	0.229425	302.79	19.57939	-0.95636
9	14	0.5	1	0.304621	303.7619	18.51944	-0.58606
10	14	0.5	14	0.195231	303.0063	19.33685	-0.46659
11	0.5	0.9	1	0.267156	304.1579	18.09824	0.109619
12	0.5	0.9	13	0.068662	302.8181	19.54171	0.35778
13	2	0.9	2	0.251388	302.8158	19.54447	-1.10633
14	4	0.9	13	0.224906	302.1224	20.34169	-1.58781
15	10	0.9	9	0.276736	302.5956	19.8009	-1.52928
16	10	0.9	12	0.215363	302.5822	19.81407	-1.05166
17	12	0.9	14	0.246176	302.7581	19.61475	-1.12231
18	13	0.9	13	0.209616	302.6156	19.7773	-0.97229
19	14	0.9	1	0.330056	303.2569	19.0624	-1.29458
20	14	0.9	14	0.172172	302.776	19.59464	-0.51241
21	2	3	11	0.31187	301.1882	21.47488	-3.21779
22	0.5	3	13	0.231973	302.1484	20.31214	-1.61838
23	4	3	8	0.306338	301.5724	21.00202	-2.78931
24	4	3	13	0.154633	302.1992	20.25328	-0.94884
25	10	3	9	0.20424	302.1953	20.26194	-1.34961
26	10	3	12	0.174403	302.3608	20.06841	-0.94538
27	12	3	14	0.330681	302.5616	19.83786	-1.9949
28	13	3	13	0.315739	302.4944	19.91566	-1.94253
29	14	3	3	0.314467	302.1726	20.28889	-2.25418
30	14	3	12	0.259413	302.3684	20.06179	-1.61792

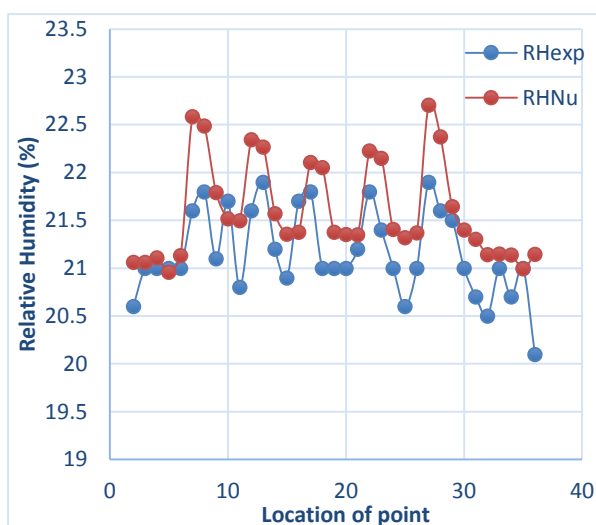
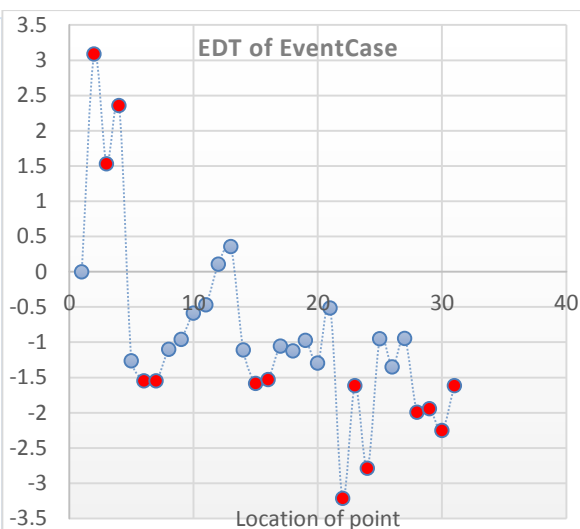
Chart .3 compare between  $RH_{exp}$  &  $RH_{Nu}$ .

Chart .4 (EDT) for Event Case.

## **(4) Results and Discussion**

### **(4.1) Basic Case**

In this case the hall to be studied was empty and the HVAC system operates in the air-conditioning mode without cooling, i.e., only the fan is operated. The experimental measurements are accomplished, comprising, air velocity temperature and relative humidity, inside the hall at a certain air velocity of the fan. The numerical values of the same air properties using the (ANSYS 15) program are also accomplished corresponding to the same inlet air velocity used in the previous experiment test. Two inlet air velocities of the HVAC fan, are studied. These velocities supply are (4 m /s) and (5 m/s), but in this case chosen only (4 m/s). The comparison experimental data and numerical result, seems a good agreement as given by the table (2), which includes the experimental and numerical results for several points and for the points at the arena, for the two studied inlet velocities, Comfort of human feeling. It was observed that the temperature differences are between (1-2°C) in large halls as shown in figures (11 and 12). The result of the studied hall are compared with graphical figures (8 and 9) of velocity contour only because the flow in the large space is isothermal and the variances are shown in the chart (1 and 2). The comparison with the published data reveals a good agreement.

### **(4.2) Cooling Case**

A typical summer day is considered in this case, with an outdoor temperature of 47°C and an initial indoor temperature of 41°C. The velocity in the hall is standard velocities are (4m/s and 5m/s ) for the type split unit to better indoor air mixing. has been taking the experimental

results and the theoretical to this case , as in the basic case, for the purpose of validation of result , and then took the points of the program (ANSYS15, CFD, Fluent15) on levels ( $y=0.5, y=0.9, y=3$ ) velocity of less than ( $0.36 \text{ m/s}$ ) for the purpose of calculating (ADPI) as in the event case and the value when velocity supply ( $5 \text{ m/s}$ ) is (ADPI=53), which indicates the presence of errors in the design of the cooling system of the sports hall, which needs to raise the velocity of the air to ( $7.5 \text{ m/s}$  standard velocity for large hall according to ASHRAE standards [4]) or redistributed air conditioning split unit according to an engineering manner for get thermal comfort . This can be seen in fig.14, 15 and 16.

### **(4.3) Event Case**

The hall is half-full with 20 spectators attending an athletic event. The ventilation conditions are tested when the HVAC system operates in the air – conditioning mode with and without cooling. The (ANSYS15) program, CFD, and Fluent 15 are applied for the selected points in the numerical study at the levels ( $y=0.5\text{m}, y=0.9\text{m}, y=3\text{m}$ ). Chosen velocity less than ( $0.36\text{m/s}$ ) for the purpose of obtaining (ADPI) according to the requirement to calculate (EDT). The value was (ADPI=53%). The result of this case is shown in table (3). In this case, it is observed that ,when the hall is semi or fully loaded with people the thermal comfort factor (ADPI) is decreased ,even if the inlet air velocity is increased the (ADPI) will not enhanced . This indicates that there is lock in the air-conditioning load of the tested hall, and the air distribution system applied is not favourable. See the chart (4) and figures (17, 18 and 19) which are related to this case.

### **(5) Conclusions**

From the results obtained in this study, the following conclusions can be made:

- 1- The engineering (ANSYS 15) program can be used to redesign the air conditioning system of a large athletic hall and to select a new air distribution system. So that the (ADPI) is improved, with saving time, cost and effort.
- 2- In this study, and by using the (ANSYS15) program it is found that the air conditioning system and the air distribution system of the wrestling hall of the faculty of physical Education of Basrah University have some problems. By a little improvement in these two systems, it is found that the (ADPI) is improved from (53%) to more (80%).
- 3- It is recommended for this college ,that ,if the air conditioning split unit are redistributed according to an engineering manner ,and may be add some other units to the hall the human comfort will be enhanced more and more and this will increase the air diffusion performance factor to its maximum value .

## **References**

- [1] O. I. Stathopoulou & V. D. Assimakopoulos, (2007) "Numerical Study of the Indoor Environmental Conditions of a Large Athletic Hall Using the CFD Code PHOENICS Published online: 8 June 2007.
- [2] H. K. Versteeg and W. Malalasekera, (2007) "An introduction to computational fluid dynamics-the finite volume method", Longman, 2nd Edition.
- [3] Hazim B. Awbi, (2005) "Ventilation of Buildings", Second edition, the Taylor & Francis e-Library.
- [4] ASHRAE. ANSI/ASHRAE Standard 62.1, (2004) "Ventilation for acceptable air quality" Atlanta: American Society of Heating, Refrigerating and Air-Conditioning Engineers, Inc.
- [5] K. Ponsoni and M. S. G. Raddi, (2010) "Indoor Air Quality Related to Occupancy at an Air conditioned Public Building", Araraquara – SP Brazil.
- [6] Q. Chen and L. Glicksman, (1999) "Performance Evaluation and Development of Design Guidelines for Displacement Ventilation" Final Report to ASHRAE.
- [7] ANSYS, Inc. (2013), Users Guide, 15 version.
- [8] User's Guide for Extech Instruments Model 451181 Data logging / Printing Anemometer+Psychrometer.
- [9] E. Rusly and M. AIRAH, (2014) "The truth about the Air Diffusion Performance Index (ADPI)", TROX Australia.

## **Nomenclature:**

(CFD)	<u>C</u> omputational <u>F</u> luid <u>D</u> ynamics.
(HVAC)	<u>H</u> eating <u>V</u> entilating <u>A</u> ir <u>C</u> onditioning.
(IAQ)	<u>I</u> ndoor <u>A</u> ir <u>Q</u> uality.
( $\rho$ )	Density. (Kg/m <sup>3</sup> )
(V)	Velocity vector. (m/s)
( $\Gamma$ )	Effective exchange coefficient of $\emptyset$ .
( $S_{\emptyset}$ )	source rate per Unit volume.

(CFM)  $\text{ft}^3/\text{min}$

(CMM)  $\text{m}^3/\text{min}$

(ADPI) Air Diffusion Performance Index.

(EDT) Effective Draft Temperature.

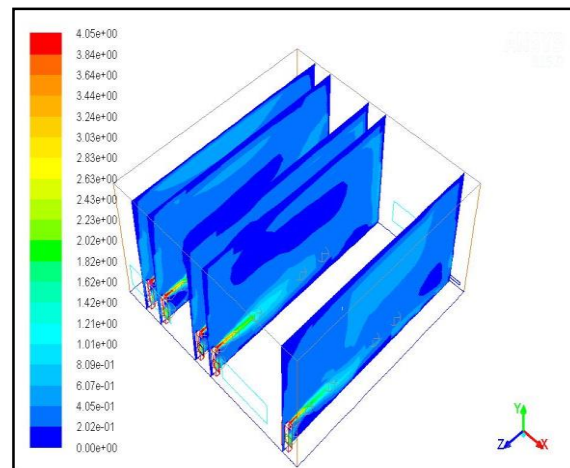
(exp) experimental; (Nu) numerical.



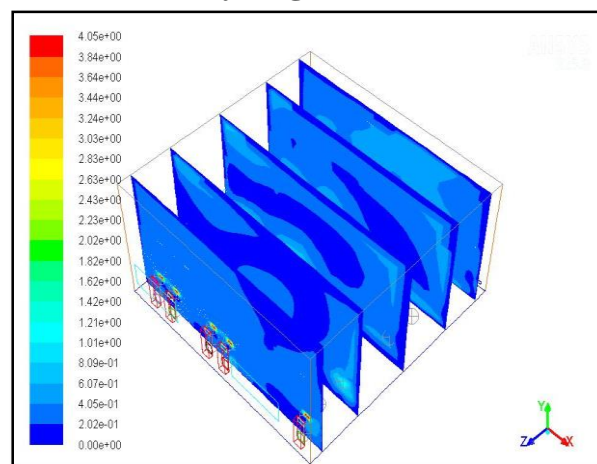
Fig.6 infrared thermometer



Fig. 7 Anemometer + Psychrometer



**Fig.8: contours of velocity magnitude for Basic Case at x-plane.**



**Fig.9: contours of velocity magnitude for Basic Case at z-plane.**

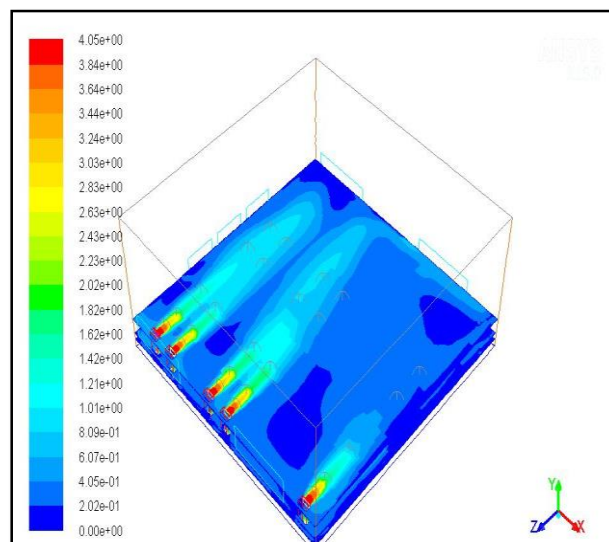


**Fig.10: contours of velocity magnitude for Basic Case at y-plane.**



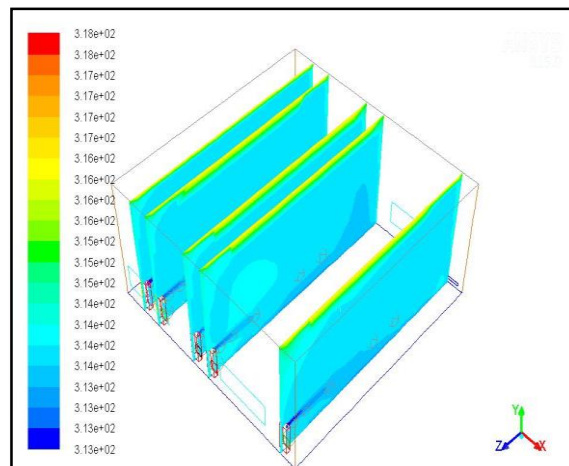
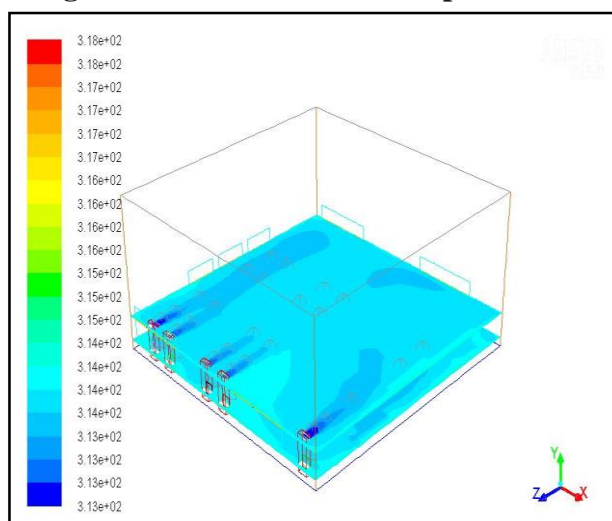


**Fig.11: contours of static Temperature for**



**Basic Case at x-plane. Fig.12: contours of static Temperature for Basic Case at y-plane.**

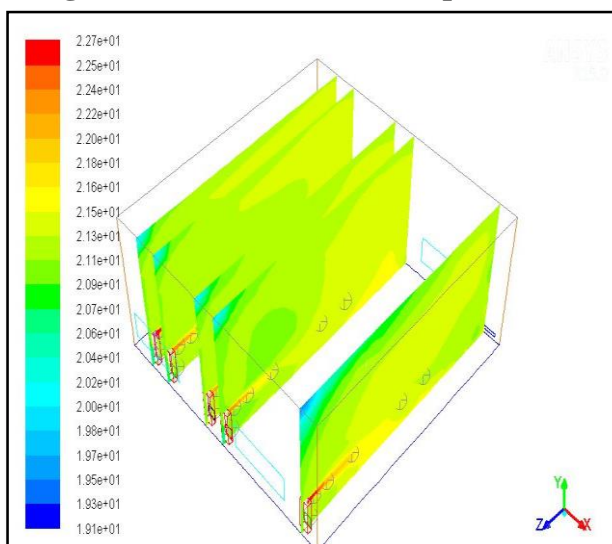


**Fig.13: contours of Relative Humidity for Basic Case.**



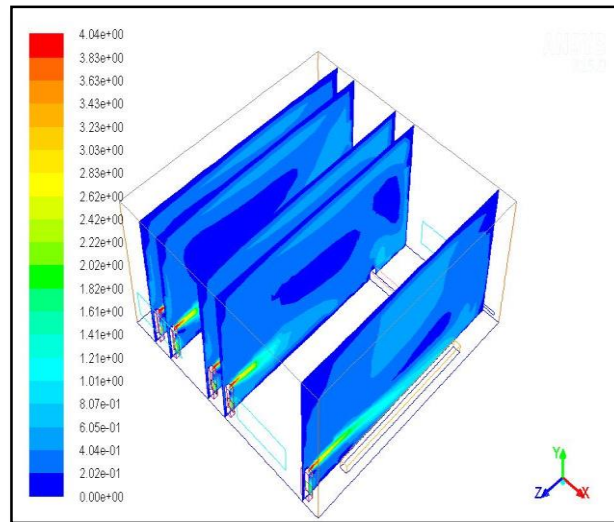


**Fig.14: contours of velocity magnitude for Cooling Case.**

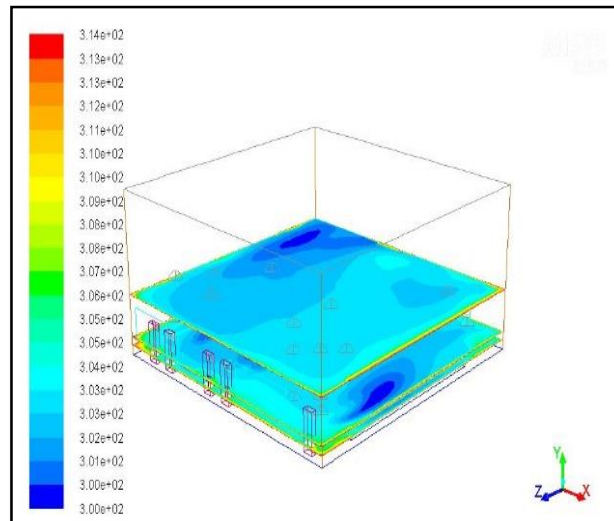


**Fig.15: contours of static Temperature for Cooling Case.**

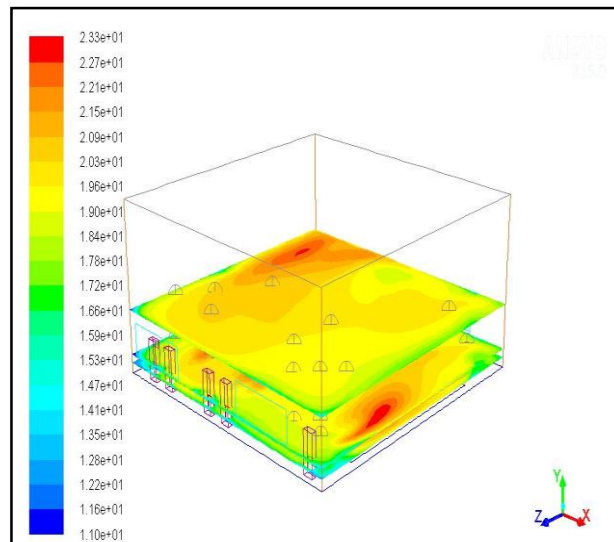


**Fig.16: contours of Relative Humidity for Cooling Case.**

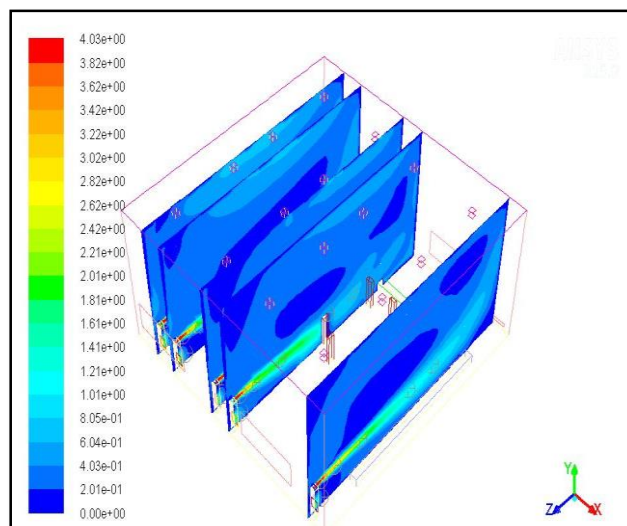


**Fig.17: contours of velocity magnitude for Event Case.**

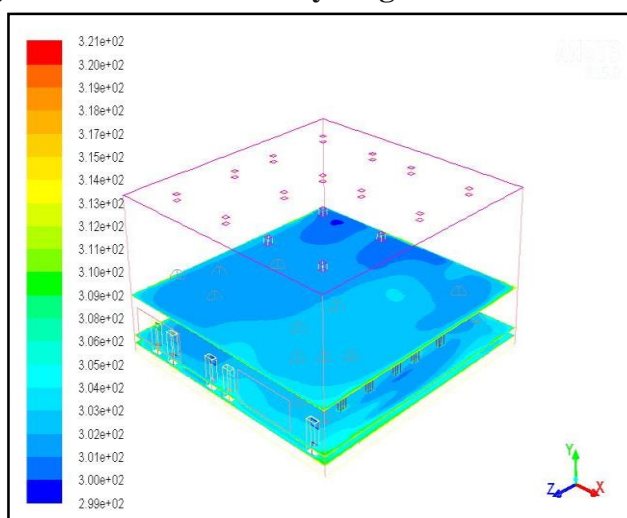


**Fig.18: contours of static Temperature for Event Case.**

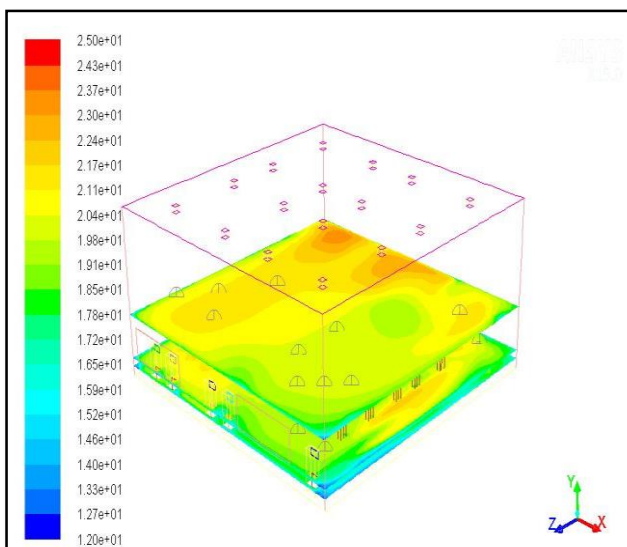


**Fig.19: contours of Relative Humidity for Event Case.**

# Effect of Heat Treatment Parameters on Microstructure and Mechanical Properties of (AISI1005) Steel

Hassanen L. Jaber, R. K. Salim, Ashraf s. fahad

## Abstract

This study aims to investigate tensile properties and work hardening behavior of dual phase (DP) steels. A series of DP steels containing ferrite and martensite with different volume fractions of martensite ( $V_m$ ) were produced by intercritical heat treatment. Microstructural investigations, hardness test, and tensile test were carried out. The experimental results showed that dual phase steels at 760°C and 10s have excellent mechanical properties in terms of tensile strength, ductility and fracture energy. A further increase in  $V_m$  was found to increase tensile strengths and ductility. The increasing and then decreasing trend in tensile strength is in contrast to the law of mixture. These unusual behaviors are discussed and explained. Work hardening behavior was analyzed in terms of Holloman analysis.

**Keywords** Dual phase steel, heat treatment, mechanical properties.

## 1. Introduction

### 1-1 Advanced High-Strength Steel (AHSS)

AHSS: A series of high-strength steels containing microstructural phases other than ferrite and pearlite, these other phases include martensite, bainite, and/or retained austenite in quantities sufficient to produce unique mechanical properties. Most AHSS have a multi-phase microstructure [1]. AHSS can be classified according to the microstructure including dual phase (DP), transformation induced plasticity (TRIP) assisted, complex phase (CP) and martensitic (MS) steels.

Fig (1) compares the tensile strength and total elongation of lower strength steels [interstitial free and mild steel], conventional high strength steels (carbon–manganese, bake hardenable and high strength low alloy steels) and AHSS [2,3].

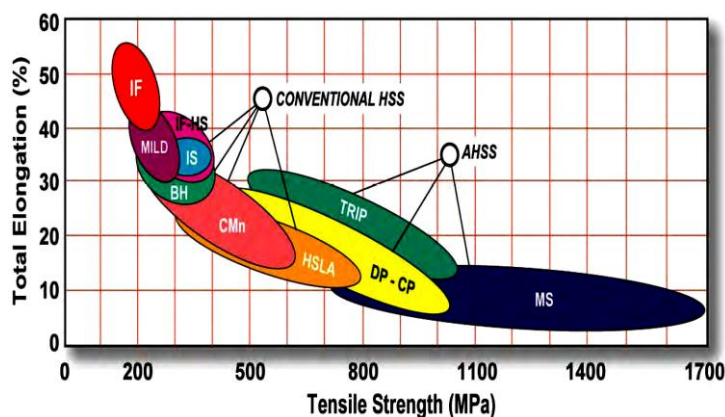


Fig. 1 - Relationship between ultimate tensile strength and total elongation (50.8 mm gauge length) for various types of steel [1].

## 1-2 Dual Phase Steel

Ferrite–martensite dual phase (DP) steel is one of the most common Advance High Strength Steels (AHSS) which is currently used in automotive industry [4]. Usually ferrite–martensite DP steels are produced by intercritical annealing followed by rapid cooling. During the intercritical annealing small pools of austenite are formed in the ferrite matrix, which subsequently transform into martensite upon rapid cooling. Intercritical heat treatment is the simplest way to enhance low alloys (carbon content less than 0.2%) steels to dual phase microstructure with superior strength–ductility combination [3].

In this combination of two phases, martensite contributes with high strength and ferrite matrix provides good elongation that can produce a good combination of strength and ductility for applications which required good formability. This unique composite microstructure offers other interesting mechanical properties such as continuous yielding, low yield stress to tensile strength ratios and high initial work-hardening rate [2, 5].

## 1-3 Application of Dual Phase Steel

Fig. 2 shows the use of modern multiphase steels for structural components, taking the example of a new auto body [6]. Honda and BMW as shown in Fig. 3, two car manufacturers that most quickly and warmly welcomed DP grades into their portfolios, have each become known for their forward-thinking use of materials [7]. The wheels in the ULSAB-AVC are made of 1.2 mm DP 350/600 steel and the inner portion is made of 1.8 mm HSLA 490/600, resulting in an optimized, lightweight steel wheel design. The disc is made of 2.1 mm DP 500/800 as shown in Fig. 4. [8].

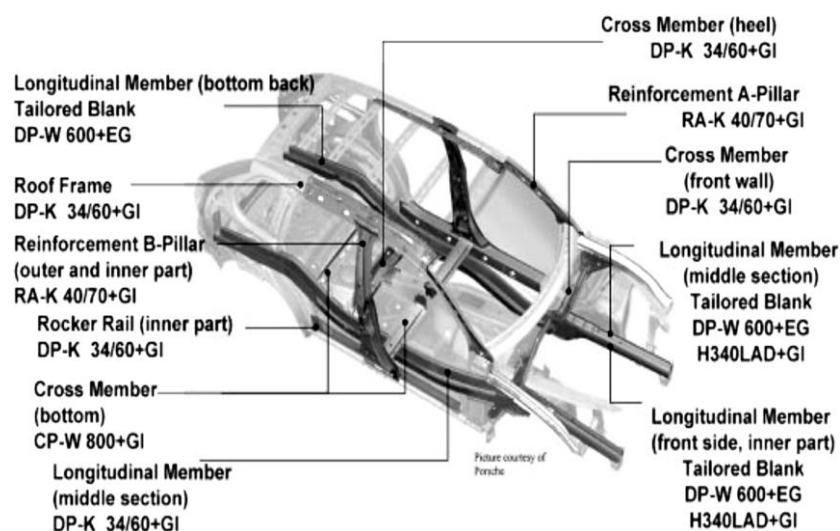


Fig. 2: Application of multiphase steels to the body structures of VW Touareg and Porsche Cayenne [6].

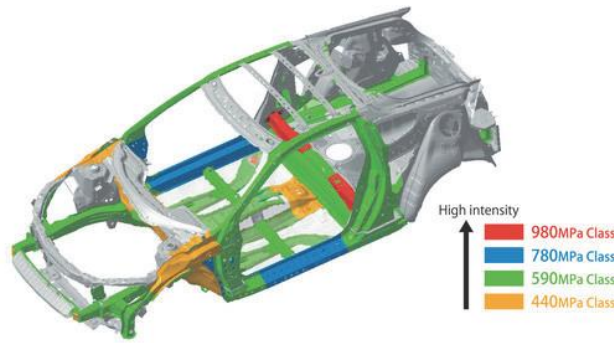


Fig 3: DP in the 2011 Honda CR-Z [7]

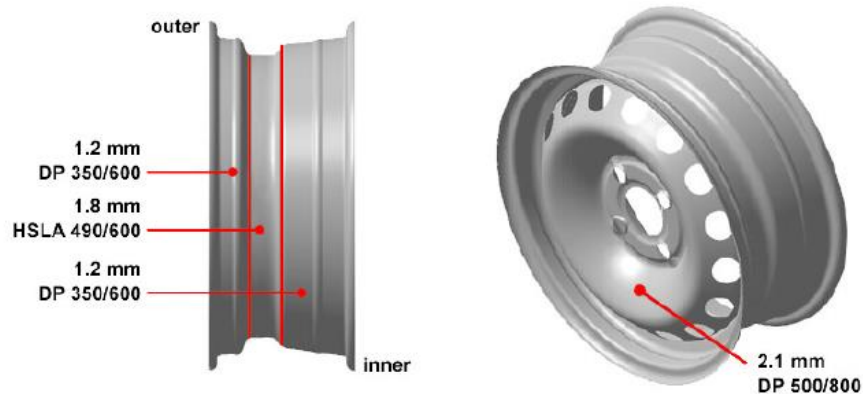


Fig 4: DP steel on wheels [8]

## 2. Experimental procedure

The steel used in the present investigation was 2-mm in thickness AISI 1005 sheet steel whose chemical composition is given in Table 1. Fig. 5 shows the engineering stress–strain curve and Fig. 6 shows the microstructure of base metal. The microstructure of the base metal sample consists of mainly ferrite with small amount of pearlite.

Table 1: Chemical composition of the investigated steel (weight %).

Element %	C	Mn	P	S	Si	Cr
AISI1005	0.048	0.58	0.03	0.02	0.028	0.02

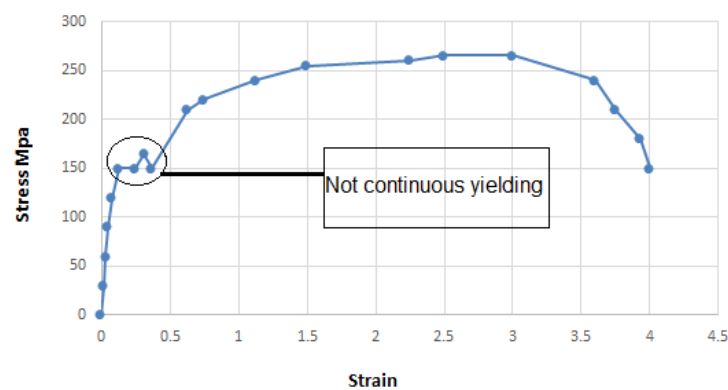


Fig. 5: Engineering stress–strain curve of base metal





Fig. 6: microstructure of base metal sample [80X].

For this study, the  $AC_1$  and  $AC_3$  temperatures were calculated to be 735 and 856 °C, respectively by Eqs. (1) And (2) [9].

$$AC_1 (°C) = 751 - 16.3C - 27.5Mn - 5.5Cu - 5.9Ni + 34.9Si + 12.7Cr + 3.4Mo \quad (1)$$

$$AC_3 (°C) = 881 - 206C - 15Mn - 26.5Cu - 20.1Ni - 0.7Cr + 53.1Si + 41.7V \quad (2)$$

The heat treatment which is used in this work is shown in Fig. 7. All of the specimens were heated in intercritical temperature range (between  $AC_1$  and  $AC_3$ ). All the specimens were held between (5-20) min in (CARBOLITE) furnace as shown in Fig (8) and followed by water quenching (WQ). The heat-treated samples are designated by capital letter, as shown in Fig (7). Metallographic specimens were prepared according to the standard procedure from the base metal and heat-treated samples and etched with 2% nital solution. Microscopic examinations were carried out by an optical microscope.

The tensile test was conducted on base metal and heat-treated specimens with 50mm gage length, 200mm overall length, 20mm width of grip section and 12.5mm width of reduced section using an (QUASAR 25) testing machine as shown in Fig (9) with strain rate of 10mm/min at room temperature in accordance to ASTM E8M [10].

Key parameters obtained from stress–strain curves include yield strength ( $\sigma_{YS}$ ), ultimate tensile strength (UTS), uniform elongation (UEL), total elongation (TEL) and tensile fracture energy. The amount of energy absorption was digitally calculated by measuring the area under the stress–strain curve up to the final fracture point using the concept of Riemann Sums Eq. (3) [11].

$$\int_0^{L_{max}} F dx = \sum_{n=1}^N F(n) \cdot [L(n) - L(n-1)] \quad \text{-----(3)}$$

Where  $F$  is the load,  $x$  the displacement,  $L_{max}$  the displacement at the peak load,  $n$  the sampled data and  $N$  the peak load.

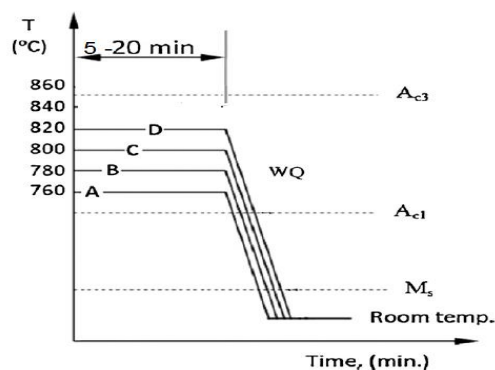


Fig. 7. Schematic illustration of the heat treatment cycle used in this study.



Fig.(8) : Muffle furnace



Fig. (9): QUASAR 25 Testing machine

### 3. Results and discussion

#### 3.1. Microstructural investigation

The microstructures of the heat-treated samples (A, B and C) are shown in Fig. 10. Increasing  $V_m$  is clearly observed in Fig. 10a–c. This complies with lever rule in the ferrite–austenite dual phase region. According to the lever rule, increasing the temperature increases the austenite volume fraction, which then will transform to martensite upon quenching in the water. It worth noticing that by increasing the temperature,  $V_m$  increases at higher rate.

Fig. 11 shows variations hardness of the heat-treated samples with increasing heat treatment temperature. Hardness of base metal steel is (134) HV. Hardness of the heat-treated samples

are higher than the hardness of the specimen in the as-received condition. The higher hardness of the dual phase steels due to the presence of the martensite phase.

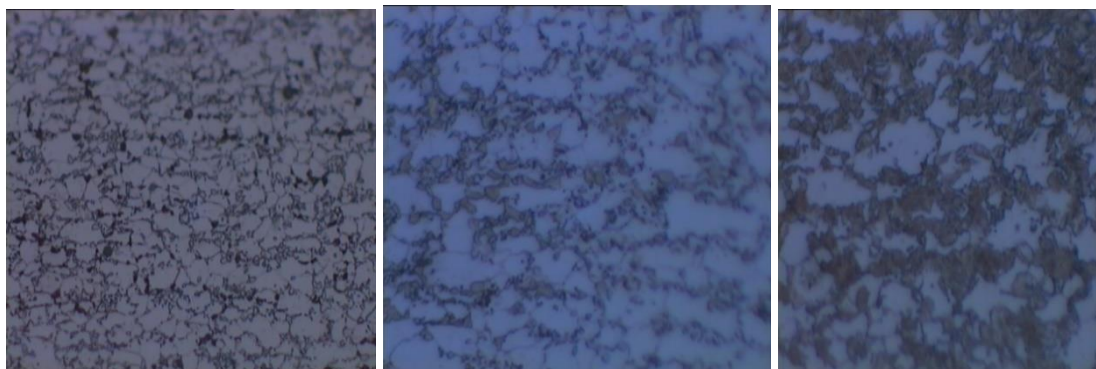


Fig. 10. The microstructures of the heat-treated samples at various intercritical temperatures of (a) 760 °C (b) 800 °C and (c) 820 °C . [80X]

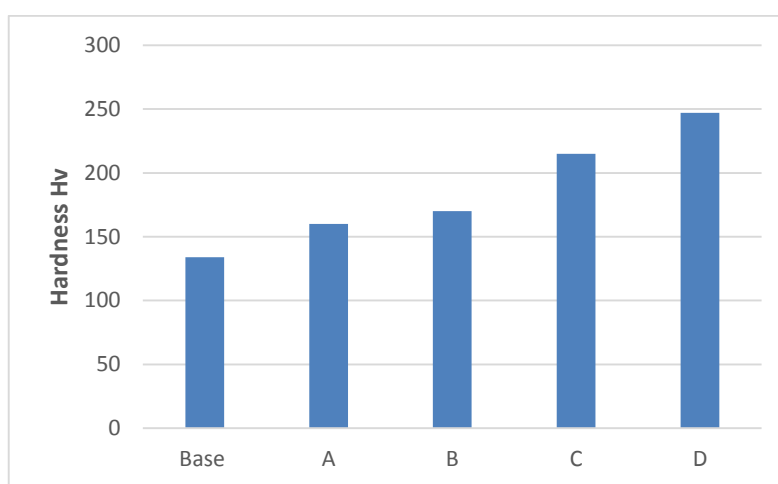


Fig. 11. Hardness for heat-treated samples (A, B, C, D) and Base metal.

### 3.2. Tensile properties

#### 3.2.1. Continues yielding behavior

The stress–strain curve of the base metal sample has yield point elongation and exhibit well-defined yield point (see Fig. 6). In low carbon steels, this behavior has been attributed to the effect of interstitial solute atoms (carbon), called the Cottrell atmosphere, on locking-in the dislocation. When stress is applied to such steel in a tensile test, it must exceed a certain critical value to unlock the dislocations. The stress necessary to move the dislocations is less than the stress required to unlock them; hence the phenomenon of a sharp yield drop and the appearance of an upper and lower yield point in the tensile stress–strain curve [12].

The yield point has come to be accepted as a general phenomenon, since it has been observed in a number of other metals and alloys. Three factors which control sharp yield point in materials are as follows [13,14]:

- 1) Low density of mobile dislocation in initial stage of deformation,
- 2) Rapid dislocation multiplication during plastic deformation and,
- 3) Low stress dependence of dislocation velocity.



However, this phenomenon is not observed for dual phase steels. As can be seen from Fig. 12 the stress–strain curves of dual phase steels exhibit continuous yielding behavior. The Continuous yielding of the ferrite–martensite dual phase has been related to the following [15–16]:

- 1) Presence of unpinned dislocations which are created in a ferrite matrix via plastic deformation during the austenite to martensite transformation.
- 2) These unpinned dislocations, located at the ferrite–martensite boundaries are assumed to be mobile in the early stage of plastic deformation.

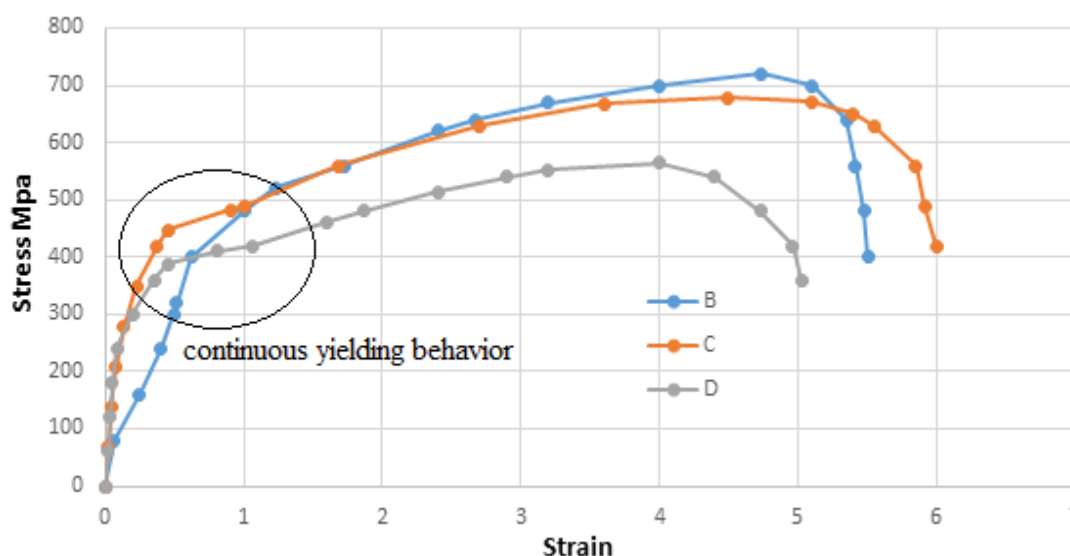


Fig. 12. Engineering stress–strain curves for heat-treated samples (A, D, E).

### 3.3. Work hardening

The flow behavior of the most metals and alloys can be described by Hollomon Eq. (4) [17]:

$$\sigma = K\varepsilon^n \quad \text{----- (4)}$$

Where ‘K’ and ‘n’ are constants which are normally called: the strength coefficient and strain hardening exponent, respectively. Drawing the stress–strain data in logarithmic scale and fitting a line to these data, determines the values of these coefficients for the under investigation metal. Strain hardening exponent (n) is the slope of this line and its cross section with  $\varepsilon = 1$  ( $\log \varepsilon = 0$ ), gives the strength coefficient (K).

Strain hardening exponent (n) is a good indicator for work hardenability of the material.

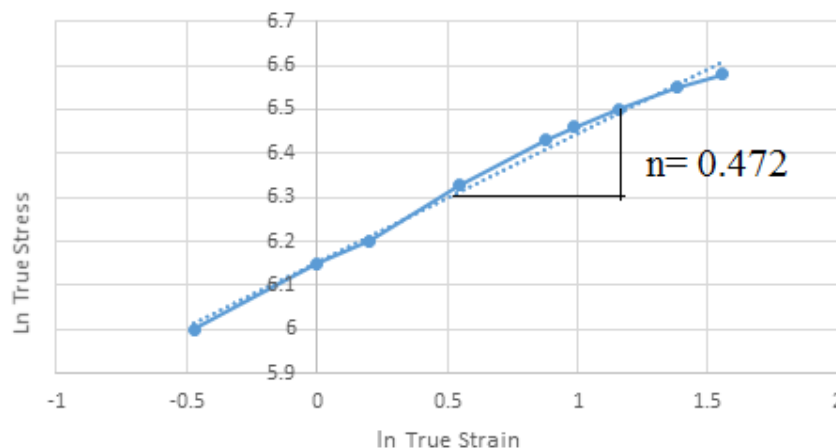


Fig. 13.  $\ln \sigma - \ln \epsilon$  plot of true stress vs. true strain for investigated steel

### 3.4 Fracture energy

Fig. 14 shows the effect of temperature of heat treatment on the fracture energy of DP steels. In the automotive industry, the energy absorption capability is an important parameter in vehicle crashworthiness. Variation of fracture energy follows a similar trend for variation of elongation with  $V_m$ . The failure energy increases and maximum failure energy in stage (B). Fracture is understood in terms of the nucleation (either by particle cracking or interfacial decohesion), growth, and coalescence of damage [19]. As the martensite volume fraction increases, its flow stress decreases, resulting in an increase in the potential for martensite to co-deform with the ferrite matrix. In these cases, the nucleation of voids is much more difficult, with the final result being that the fracture strain and fracture energy are increased [19]. It is also interesting to note that 4% volume expansion accompanies the transformation of austenite to martensite. This volume expansion creates a compression stress in the ferrite/martensite interface which impedes the crack growth even if it is nucleated [20]. This can contribute to the increasing energy absorption capability. With further increase in  $V_m$ , the matrix structure changes from ferrite to martensite and coherency of the ferrite matrix is also damaged by high amount of martensite phase, thus the DP structure becomes brittle and the failure energy is reduced.

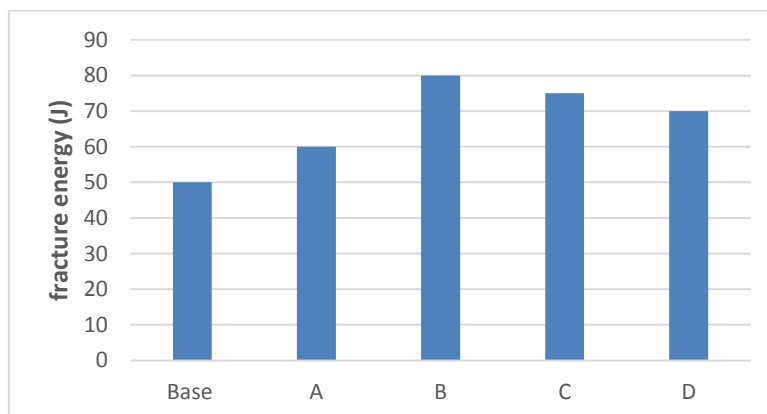


Fig. 14: The variation of the fracture energy with temperature of heat treatment

#### 4. Conclusions

- 1 – A different samples of dual phase steels containing ferrite and martensite with different volume fractions of martensite ( $V_m$ ) was produced by intercritical heat treatment.
- 2 - It was found that martensite volume fraction increases by increasing the intercritical heat treatment temperature.
- 3 - Generally, dual phase steels in stage A (780 C, Time 10 S) exhibit the optimum mechanical properties in terms of tensile strength, ductility and fracture energy.
- 4 - The variations of ultimate tensile strength, ductility and fracture energy with volume fraction of martensite exhibit unusual behavior.
- 5 - Work hardening behavior was analyzed in terms of Holloman analysis. In this analysis, the work hardening behavior of the samples is single stage.

#### References

- 1- American Iron and Steel Institute, "Advanced High Strength Steel (AHSS) Application Guidelines", Washington, Version 4.1, June 2009, Page 1.
- 2- J. Galán, L. Samek, P. Verleysen, K. Verbeken and Y. Houbaert, "Advanced High Strength Steels for Automotive Industry<sup>(c)</sup>" *rEviSTa DE METalUrGia*, Vol 48, No2, P. 118-131, 2012.
- 3- R. Kuziak, R. Kawalla, S. Waengler, "Advanced High Strength Steels for Automotive Industry" *Archives of Civil And Mechanical Engineering*, Vol VIII, No. 2, p. 103-117, 2008.
- 4- X. Sun, E. Stephens and M. Khaleel, "Effects of Fusion Zone Size on Failure Modes and Performance of Advanced High Strength Steel Spot Welds ", SAE, paper series 2006-01-0531.
- 5- M. Delince, Y. Brechet, JD. Embury, MGD. Geers, PJ. Jacques, T. Pardoen, [Separation of size-dependent strengthening contributions in fine-grained Dual Phase steels by nanoindentatio](#), *Acta. Mater.* 55 (2007) 2337-2350.
- 6- H. Hofmann, D. Mattissen, T. W. Schaumann, "Advanced cold rolled steels for automotive applications", *Mat.-wiss. u. Werkstofftech*, Vol 37, No. 9, P. 716-723, 2006.
- 7- Ultra Light Steel Auto Body Consortium, overview report, Wiley, January 2002
- 8- The Evolving Use of Advanced High-Strength Steels for Automotive Applications, Steel Market Development Institute 2000 Town Center, Suite 320 Southfield, Michigan
- 9- F. Hayat, "Comparing Properties of Adhesive Bonding Resistance Spot Welding and Adhesive Weld Bonding of Coated and Uncoated DP 600 Steel ", *Journal Of Iron And Steel. Research, International*. Vol 18, No 9: P. 70-78, 2011.

- 10- Standard Methods of Tension Testing of Metallic Materials, E 8. Annual book of ASTM standards, vol. 03.01. ASTM, Philadelphia; 2004. p. 130–150.
- 11- H. Zhang and J. Senkara: "Resistance Welding: Fundamentals and Applications", CRC Group, London, New York, 2006.
- 12- M.A. Meyers, K.K. Chawla, W.F. Hosford, Mechanical Behavior of Materials, second ed., Cambridge University Press, 2008.
- 13- G.E. Dieter, Mechanical Metallurgy, second ed., Published by McGraw-Hill, 1976.
- 14- R.W. Hertzberg, Deformation and Fracture Mechanics of Engineering Materials, John Wiley & Sons, 1996.
- 15- M.A. Maleque, Y.M. Poon, H.H. Masjuki, [The effect of intercritical heat treatment on the mechanical properties of AISI 3115 steel](#), Journal of Materials Processing Technology, Volumes 153-154, 10 November 2004, Pages 482-487.
- 16- Jinxing Jiang, Huibin Wu, Jinming Liang, Di Tang, Microstructural characterization and impact toughness of a jackup rig rack steel treated by intercritical heat treatment. Materials Science and Engineering: A, Volume 587, 10 December 2013, Pages 359-364
- 17- J.H. Hollomon, Trans. AIME 162 (1945) 268.
- 18- Mohammad Reza Akbarpour, A. Ekrami, [Effect of temperature on flow and work hardening behavior of high bainite dual phase \(HBDP\) steels](#), Materials Science and Engineering: A, Volume 475, Issues 1–2, 25 February 2008, Pages 293-298
- 19- G. Rosenberg, I. Sinaiová, L. Juhar Effect of microstructure on mechanical properties of dual phase steels in the presence of stress concentrators. Materials Science and Engineering: A, Volume 582, 10 October 2013, Pages 347-358
- 20- H. Saghafian, Sh. Kheirandish [Correlating microstructural features with wear resistance of dual phase steel](#) Materials Letters, Volume 61, Issues 14–15, June 2007, Pages 3059-3063

## Modeling of Short Duration Rainfall Intensity Duration Frequency(SDR-IDF) Equation for Basrah City

Zainb Abd Alelah

Department of Civil Engineering, College of Engineering, University of Basrah, Iraq.

### Abstract:

The Rainfall Intensity-Duration-Frequency (IDF) relationship is one of the most commonly used tools in water resources engineering, either for planning, designing and operating of water resource projects or for various engineering projects against floods. The objective of this study is to develop an empirical formula to estimate rainfall intensity for any duration and any return period with minimum effort. Daily rainfall data for years 1980-2010 from Iraqi Metrological Organization and Seismology was used in this study. Hershfeild's method was used to estimate the short duration rainfall intensity from daily rainfall data. Various distribution functions were used for analysis and Chi-Square goodness to fit test were used to identify the best statistical distribution among them. Study showed that Log Pearson type III is the best probability distribution and the best (IDF) empirical formula was in the form  $[i=a/(b+td)]$ .

**Keyword:** Chi-Square tests, Probability Distribution Function, Return Period, Short Duration rainfall.

تمثيل معادلة الشدة المطرية – التكرار – الاستدامة القصيرة لمدينة البصرة

زينب عبد الإله عبد اللطيف

جامعة البصرة / كلية الهندسة- قسم الهندسة المدنية

### الخلاصة:

العلاقة بين الشدة المطرية وتكرار الشدة المطرية والاستدامة هي إحدى أكثر الأدوات المستعملة في هندسة مصادر المياه، سواء في التخطيط أو في تشغيل مصادر المياه أو في مختلف المشاريع الهندسية لمقاومة الفيضانات. الهدف من هذه الدراسة هو تمثيل معادلة تجريبية لتخمين الشدة المطرية لأي تكرار وأي استدامة بجهد قليل. استخدمت في هذه الدراسة معلومات مطرية لـ 31 سنة كما استخدمت طريقة هيرشفيلد لإيجاد الاستدامة القصيرة للشدة المطرية. استخدمت مختلف الدوال التوزيعية الإحصائية لتحليل المعلومات واستخدمت طريقة الـ Chi-Square كاختبار لتشخيص التوزيع الإحصائي المناسب. ولقد بينت الدراسة أن Chi-Square هي الأفضل وأن أفضل معادلة للشدة المطرية هي بالشكل-Log Pearson type III  $[i=a/b+td]$

## **Introduction:**

The design of storm water drainage system is a critical issue in urban areas since it depends on estimation of rainfall intensity which varies with time and location. The fall in estimating the rainfall intensity can cause flood of these areas. The rainfall intensity is usually estimated based on rainfall duration and return period. The formula that represents the mathematical relationship between rainfall intensity, duration and return period is called Intensity Duration Frequency (IDF) formula.

In order to formulate IDF relationship for specific site, like Basrah city in south of Iraq, historical series of the maximum rainfall intensity data at a higher time resolution (in order of minutes) is required. Due to instrumental limitation short duration rainfall data in Basrah city are not available. The aim of this study is to put an empirical formula for IDF relationship in Basrah city.

Many sets of IDF relationships have been constructed for several parts of the globe: Hershfield (1961) developed various rainfall contour maps to provide the design rain depths for various return periods and durations. Bell (1969) proposed a generalized IDF formula using the one hour, 10 years rainfall depths;  $P_1^{10}$ , as an index. Chen (1983) further developed a generalized IDF formula for any location in the USA using three base rainfall depths;  $P_1^{10}$ ,  $P_{24}^{10}$ ,  $P_1^{100}$ , which describe the geographical variation of rainfall. Kouthyari and Garde (1992) presented a relationship between rainfall intensity and  $P_{24}^2$  for India.

## **Estimation of Short Duration Rainfall**

Daily rainfall data for the study area ( Basrah city) were available for a period of 30 years. From this database, the maximum values were extracted for each year and were converted into shorter duration values (5, 10, 15, 30, 60, and 1440min) using Hershfield's method, this method gives the relationship as ratios as follows (Brian, 2009):

- The ratio of 60- minutes maximum rainfall to 24-hour maximum rainfall is 0.6.
- The ratio of 30- minutes maximum rainfall to 1-hour maximum rainfall is 0.79.
- The ratio of 15- minutes maximum rainfall to 1-hour maximum rainfall is 0.57.
- The ratio of 10- minutes maximum rainfall to 1-hour maximum rainfall is 0.45.
- The ratio of 5- minutes maximum rainfall to 1-hour maximum rainfall is 0.29.

## **Empirical IDF Equation**

IDF is a mathematical relationship between the rainfall intensity (i), the duration (td) and the return period (T) (Burlando 1996, Koutsoyiannis 1998). Equations (1)-(2) are the forms of IDF empirical equation which were used in this study.

$$i = [a / (b + td)] \text{ -----(1)}$$

$$i = x.(td)^{-y} \text{ -----(2)}$$

where, i is the rainfall intensity in mm/hr, td is the rainfall duration in min. and a, b, x, and y are the fitting parameter.

These empirical equations are widely used in various hydrological applications. These equations indicate that for a given return period the rainfall intensity decrease with the increase in rainfall duration. Least- square method was applied to find the parameter a, b, x, and y for the IDF empirical formula. Correlation coefficient (R) was estimated to find the best fit for IDF empirical equation. For a specific return period the equation that gives R value nearer to 1 have the best fit.

## **Generalized IDF Formula**

To put a formula for IDF, rainfall data for at least 25 years is required. The first step of constructing the IDF curve for Basrah city is to assess the local rainfall data and determine the maximum rainfall depth associated with each year. Then, statistical analysis for each duration is run. The mean and standard deviation are determined as functions of duration. Two arrays were obtained: one for the mean depth of rainfall ( $\mu$ ) as a function of rainfall duration and the other one is for the standard deviation of the rainfall depth ( $\sigma$ ).

The second step is to fit a Probability Distribution function (PDF) or a Cumulative Distribution Function(CDF) to each group comprised of the data values for a specific duration. It is possible to relate the maximum rainfall intensity for each time interval with the corresponding return period from the cumulative distribution function. Given a return period (T), its corresponding cumulative frequency (F) will be:

$$F = 1-(1/T) \text{ or } T = (1/1-F) \text{ ----- (3)}$$

Once a cumulative frequency is known, the maximum rainfall intensity is determined using chosen theoretical distribution function (e.g. Normal, Gumbel, Pearson type III distributions).

Before explaining the third step, frequency analysis using frequency factors will be explained. The magnitude  $X_T$  of a hydrologic event may be represented as the mean  $\mu$  plus the departure  $\Delta X_T$  of the variate from the mean:

$$X_T = \Delta X_T + \mu \text{ -----(4)}$$

The departure may be taken as equal to the product of the standard deviation  $\sigma$  and a frequency factor  $K_T$ ; that is,  $\Delta X_T = K_T \sigma$ . The departure  $\Delta X_T$  and the frequency factor  $K_T$  are functions of the return period and the type of probability distribution to be used in the analysis. Equation (4) may therefore be expressed as,

$$X_T = K_T \sigma + \mu \text{ -----(5)}$$

### **Probability Distribution:**

In this study the maximum rainfall intensity for various return periods were estimated using different theoretical distribution functions. Normal (Hazen 1914), Two Parameter Log Normal, Three Parameter Log Normal (Kite, 1977), Gamma Distribution Two Parameter, Pearson Type III, Log Pearson Type III, and Extreme Value Type I (Gumbel) (Chow, 1964; Yevjevich, 1972). were used for probability distribution of the daily rainfall data.

**Normal Distribution:** If  $X$  is the sum of  $n$  independent and identically distributed random variables with finite variance, then with increasing  $n$  the distribution of  $X$  becomes normal regardless of the distribution of random variables the Probability Distribution function PDF for normal distribution is.

$$f_X(x) = \frac{1}{\sigma\sqrt{2\pi}} e^{-\frac{1}{2}\left(\frac{x-\mu}{\sigma}\right)^2} \text{ -----(6)}$$

Where  $\mu$  is the mean and  $\sigma$  is the standard deviation. A standard normal distribution is a normal distribution with mean ( $\mu$ ) = 0 and standard deviation ( $\sigma$ ) = 1. Normal distribution is transformed to standard normal distribution by using the following formula:

$$z = \frac{X - \mu}{\sigma} \text{ -----(7)}$$

Where  $z$  is called the standard normal variable.

**Two Parameter Log Normal:** If the PDF of  $X$  is skewed, it's not normally distributed. If the PDF of  $Y = \log(X)$  is normally distributed, then  $X$  is said to be log normally distributed.

$$f(x) = \frac{1}{x\sigma\sqrt{2\pi}} \exp\left(-\frac{(y-\mu_y)^2}{2\sigma_y^2}\right) \quad x > 0, \text{ and } y = \log x \text{ -----(8)}$$



**Three Parameter Log Normal:** A combination of the normal distribution and the modified logarithmic transformation results in the three parameter log normal distribution. This distribution has an additional parameter is the location parameter  $\zeta$ , which is the lower limit of the variable.

$$Y = \ln(x - \zeta) \leftrightarrow x = \zeta + e^y \quad \text{-----}(9)$$

$$f(x) = \frac{1}{x\sigma\sqrt{2\pi}} \exp\left(-\frac{(y - \mu_y)^2}{2\sigma_y^2}\right) \quad x > 0, \text{ and } y = \log x \quad \text{-----}(10)$$

**Gamma Distribution:** In hydrology, the interarrival time (time between stochastic hydrologic events) is described by exponential distribution,

$$f(x) = \lambda e^{-\lambda x} \quad x \geq 0; \lambda = \frac{1}{x} \quad \text{-----}(11)$$

Gamma distribution – a distribution of sum of  $\beta$  independent and identical exponentially distributed random variables.

$$f(x) = \frac{\lambda^\beta x^{\beta-1} e^{-\lambda x}}{\Gamma(\beta)} \quad x \geq 0; \Gamma = \text{gamma function} \quad \text{-----}(12)$$

**Pearson Type III :** Named after the statistician Pearson, it is also called three-parameter gamma distribution. A lower bound is introduced through the third parameter ( $\varepsilon$ ).

$$f(x) = \frac{\lambda^\beta (x - \varepsilon)^{\beta-1} e^{-\lambda(x-\varepsilon)}}{\Gamma(\beta)} \quad x \geq \varepsilon; \Gamma = \text{gamma function} \quad \text{---}(13)$$

**Log-Pearson Type III:** If  $\log X$  follows a Person Type III distribution, then  $X$  is said to have a log-Pearson Type III distribution.

$$f(x) = \frac{\lambda^\beta (y - \varepsilon)^{\beta-1} e^{-\lambda(y-\varepsilon)}}{\Gamma(\beta)} \quad y = \log x \geq \varepsilon \quad \text{-----}(14)$$

**Extreme value Type I (Gumbel) distribution:** If  $M_1, M_2, \dots, M_n$  be a set of daily rainfall or stream flow, and let  $X = \max(M_i)$  be the maximum for the year.

If  $M_i$  are independent and identically distributed, then for large  $n$ ,  $X$  has an extreme value type I or Gumbel distribution.

$$f(x) = \frac{1}{\alpha} \exp \left[ -\frac{x-u}{\alpha} - \exp \left( -\frac{x-u}{\alpha} \right) \right]$$

$$\alpha = \frac{\sqrt{6}s_x}{\pi} \quad u = \bar{x} - 0.5772\alpha \quad \text{-----}(15)$$

### **Frequency Analysis for Extreme Events:**

#### **ExtreamVlue type(I) PDF and CDF**

$$f(x) = \frac{1}{\alpha} \exp \left[ -\frac{x-u}{\alpha} - \exp \left( -\frac{x-u}{\alpha} \right) \right]$$

$$\alpha = \frac{\sqrt{6}s_x}{\pi} \quad u = \bar{x} - 0.5772\alpha \quad \text{-----}(15)$$

$$F(x) = \exp \left[ -\exp \left( -\frac{x-u}{\alpha} \right) \right] \quad \text{-----}(16)$$

Define a reduced variable  $y$

$$y = \frac{x-u}{\alpha}$$

$$F(x) = \exp[-\exp(-y)]$$

$$y = -\ln[-\ln(F(x))] = -\ln[-\ln(1-p)] \quad \text{where } p = P(x \geq x_T)$$

$$y_T = -\ln \left[ -\ln \left( 1 - \frac{1}{T} \right) \right]$$

If you know  $T$ , you can find  $y_T$ , and once  $y_T$  is know,  $x_T$  can be computed by

$$x_T = u + \alpha y_T$$

### **Chi-Square Test:**

To identify a specific theoretical distribution for the available data it is important to do a test. The aim of the test is to find how a good fit is between the observed and the prediction data. Chi –square test is one of the most widely used tests to find the best fit theoretical distribution of any specific data set which is represented by equation(17).

$$X^2 = \sum_{i=1}^n (O_i - E_i) / E_i \text{ -----(17)}$$

Where,  $O_i$  and  $E_i$  represent the observed and expected frequencies respectively. If the observed frequencies are close to the corresponding expected frequencies, the  $X^2$  value will be small, indicating a good fit; otherwise it will be a poor fit.

### **Results and Discussions:**

In order to put an empirical formula for intensity- duration- frequency relationship in Basrah city, the available data required from the General Iraqi Meteorological Authority and Seismology includes 24-hour rainfall data from 1980 – 2010 for Basrah city were considered as presented in Table (1).

Various short duration rainfalls like (5, 10, 15, 30, 60, and 1440 min.) were estimated from annual maximum 24 hours rainfall data using Hershfield's method as shown in Table (2). These estimated short duration rainfall data were used in various probability distribution methods to determine the rainfall and their corresponding return period. Table (3) shows the  $X^2$  values of different probability distribution for 5, 10, 15, 30, 60, and 1440minutes duration rainfall.

**Table (1): Maximum Daily Rainfall Recorded in Basrah City  
During the period 1980-2010.**

Year	Daily Rainfall (mm)	Year	Daily Rainfall (mm)
1980	28.1	1996	29.4
1981	21.3	1997	30.8
1982	15.1	1998	22.1
1983	18.3	1999	73.6
1984	45.4	2000	33.0
1985	73.2	2001	26.6
1986	58.5	2002	15.7
1987	9.60	2003	17.5
1988	M	2004	17.0
1989	17.5	2005	26.0
1990	11.6	2006	27.5
1991	57.0	2007	37.0
1992	21.9	2008	18.0
1993	22.9	2009	20.0
1994	28.5	2010	6.5
1995	21.0		

It was found in the study that  $X^2$  value of all probability function was increasing with increasing the rainfall duration. The study shows that Log-Pearson Type III probability distribution function gives the best estimation of the distributed predicted rainfall data as it has the smallest value of  $X^2$ , 0.0372, as compared to other distribution functions. Rainfall intensity values (in mm / hr) for various short durations and return periods in Basrah city were estimated using Log- Pearson Type III probability distribution function and they are presented in Table (4). Table (4) showed that maximum intensities occur at short duration with large variations with return period, while with long duration there is no much difference in intensities with return period and the maximum intensity occur at return period 100 years with duration of 5 minutes and minimum intensity occur at return period 2 years with duration of 1440 minute.

**Table (2): Annual Time Series of Maximum Rainfall Amount in Basrah City**

Year	Maximum rainfall amount in mm during indicated durations				
	5min.	10min.	15min.	30min.	60min.
1980	4.89	7.59	9.61	13.32	16.86
1981	3.71	5.75	7.29	10.10	12.78
1982	2.63	4.08	5.17	7.16	9.06
1983	3.18	4.94	6.26	8.68	10.98
1984	7.90	12.26	15.53	21.52	27.24
1985	12.74	19.76	25.04	34.7	43.92
1986	10.18	15.80	20.01	27.73	35.1
1987	1.67	2.59	3.28	4.55	5.76
1988	-	-	-	-	-
1989	3.05	4.73	5.99	8.30	10.5
1990	2.02	3.13	3.97	5.5	6.96
1991	9.92	15.39	19.50	27.02	34.2
1992	3.81	5.91	7.49	10.38	13.14
1993	3.99	6.18	7.83	10.86	13.74
1994	4.96	7.7	9.75	13.51	17.1
1995	3.65	5.67	7.18	9.95	12.6
1996	5.12	7.94	10.10	13.94	17.64
1997	5.36	8.32	10.54	14.60	18.48
1998	3.85	5.97	7.56	10.48	13.26
1999	12.81	19.87	25.17	34.89	44.16
2000	5.74	8.91	11.29	15.64	19.8
2001	4.63	7.18	9.10	12.61	15.96
2002	2.73	4.24	5.37	7.44	9.42
2003	3.05	4.73	5.99	8.3	10.5
2004	2.96	4.59	5.82	8.06	10.2
2005	4.53	7.02	8.89	12.32	15.6
2006	4.79	7.43	9.41	13.04	16.5
2007	6.44	9.99	12.65	17.54	22.2
2008	3.13	4.86	6.16	8.48	10.8
2009	3.48	5.4	6.84	9.48	12
2010	1.13	1.76	2.22	3.08	3.9

Mean ( $\mu$ )	4.935	7.656	9.7	13.441	17.012
Standard deviation ( $\sigma$ )	2.75	4.43	5.67	7.91	10.05
Coeff. of variation ( $C_v$ )	0.56	0.58	0.585	0.589	0.591
Coeff. of skewness ( $C_s$ )	1.12	1.16	1.17	1.18	1.18

**Table(3):Chi-Square value of various probability distribution functions for different rainfall duration.**

Rainfall duration (min.)	X <sup>2</sup> for different probability distribution functions						
	Normal	Log-Normal two parameter	Log-Normal-three parameter	Gamma distribution two parameter	Pearson Type III	Log-Pearson Type III	Gumbel
5	0.105	0.0197	0.0152	0.0185	0.0185	0.016	0.0149
10	0.020	0.033	0.023	0.031	0.031	0.027	0.0215
15	0.023	0.039	0.031	0.043	0.043	0.031	0.0278
30	0.030	0.058	0.045	0.062	0.062	0.048	0.0466
60	0.037	0.069	0.082	0.083	0.083	0.05	0.055
1440	0.061	0.114	0.097	0.142	0.142	0.051	0.0932
Average value of X <sup>2</sup>	0.0461	0.0555	0.0488	0.0632	0.0632	0.0372	0.0432

**Table(4):Rainfall intensity at different rainfall durations and return periods in Basrah city.**

Rainfall duration (min.)	Rainfall intensity in mm / hr at indicated return periods					
	2 years	5years	10years	25years	50years	100years
5	48.72	79.8	106.68	148.92	184.92	228.48
10	37.8	61.92	82.62	115.2	143.04	176.58
15	31.68	52	69.4	96.88	120.36	148.68
30	22.06	36.1	48.16	67.18	83.38	102.92
60	13.87	22.76	30.39	42.42	52.7	65.1
1440	.963	1.579	2.11	2.94	3.65	4.513

After estimating the rainfall intensity a plot of rainfall duration versus rainfall intensity for different return period was done. Figure (1) represents the rainfall (IDF) curve of Basrah for different return period.

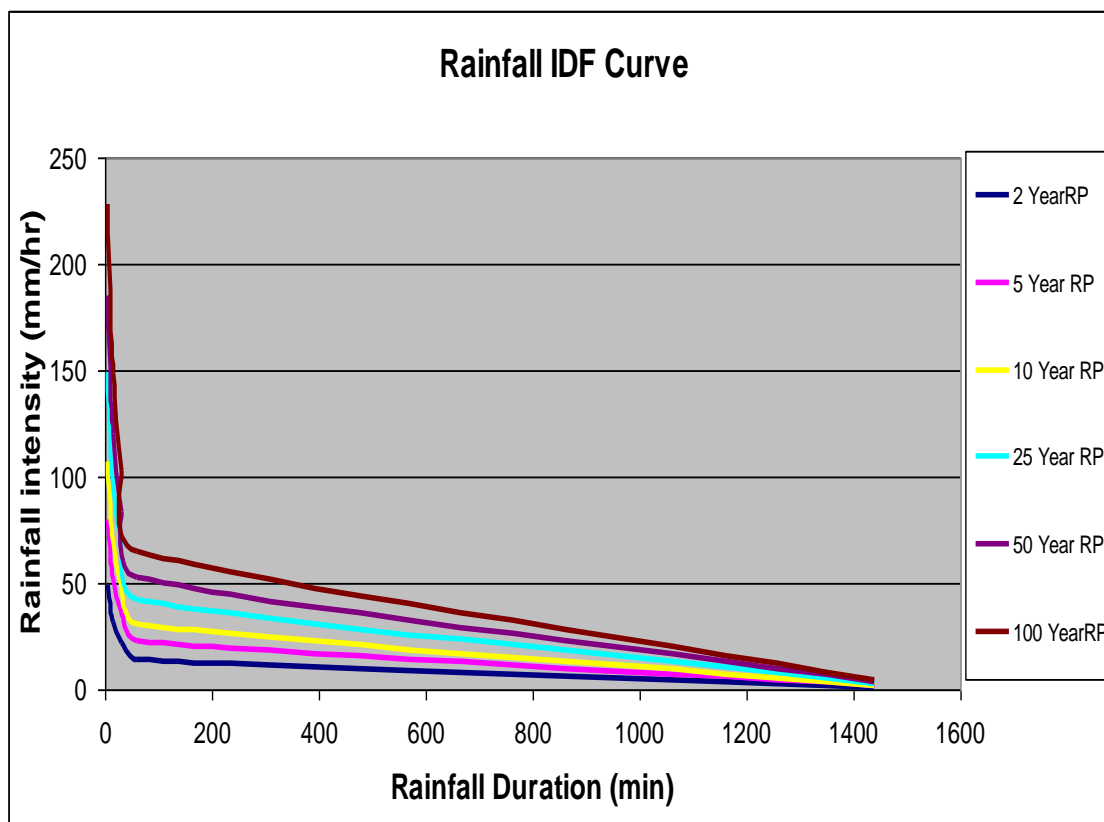


**Fig.(1) Intensity- Frequency- Duration Curves for Basrah City.**

Rainfall IDF empirical equation constants  $a$ ,  $b$ ,  $x$ , and  $y$  were calculated for different return period by least –square method as shown in Table (5). IDF empirical equation was formed by putting the value of  $a$ ,  $b$ ,  $x$ , and  $y$  in the mentioned equation format(1)-(2) for each return period separately as shown in Table (6).

**Table (5): Parameter values of rainfall IDF empirical equations for various return periods.**

Return period (year)	IDF empirical equation parameters			
	$a$	$b$	$x$	$y$
2	1416.41	31.4	205.59	0.715
5	2322.47	31.42	334.2	0.711
10	3103.61	31.48	449.78	0.715
25	4324.23	31.39	622.3	0.711
50	5368.45	31.37	781.63	0.715
100	6638.1	31.44	950.61	0.711

**Table (6):Rainfall (IDF) empirical equation for respective return period and their correlation coefficient(R).**

Return period (year)	$i=a/(b+td)$		$i=x*(td)^{-y}$	
	Equation	Correlation coefficient	Equation	Correlation coefficient
2	$1416.41/31.4+td$	0.988	$205.59*td^{-.715}$	.703
5	$2322.47/31.42+td$	0.988	$334.2*td^{-.711}$	.705
10	$3103.61/31.48+td$	0.989	$449.78*td^{-.715}$	.703
25	$4324.23/31.39+td$	0.988	$622.3*td^{-.711}$	.705
50	$5368.45/31.37+td$	0.988	$781.63*td^{-.715}$	.703
100	$6638.1/31.44+td$	0.988	$950.61*td^{-.711}$	.705

Correlation coefficient (R) was, also, calculated for each form of IDF empirical equation and their corresponding return period. It was observed in the study that the IDF empirical form  $[i=a/(b+td)]$  had the best fit rather than the equation form  $[i=x*(td)^{-y}]$  because it had R nearest to 1.

### **Conclusions:**

In this study short duration rainfall intensity –duration- frequency empirical equations were developed for Basrah city. Among the various available probability distribution functions Log- Pearson Type III distribution had the best approximation rainfall intensity for various return periods because it had the smallest  $x^2$  value which is 0.0372. The study showed that  $[i=a/b+td]$  was the best form of IDF empirical equation for Basrah city because it had a correlation coefficient R of 0.988 which is nearest to 1. These IDF equations will help to estimate the rainfall intensity for any specific return period in Basrah city in a short time and more easily. The study, also, showed that maximum intensities occur at short duration with large variations with return period, while with long duration there is no significant difference in intensities with return period and the maximum intensity occur at return period 100 years with duration of 5 minute while minimum intensity occur at return period 2 years with duration of 1440 minute.



**List of symbols:**

<u>symbol</u>	<u>definition</u>
$\chi^2$	chi-square goodness to fit
$O_i$	observed frequencies
$E_i$	expected frequencies
$i$	rainfall intensity(mm/hr)
$t_d$	rainfall duration (min)
$a, b, x, \text{ and } y$	fitting parameter
$F$	cumulative frequency
$T$	return period
$\mu$	mean
$\sigma$	standard deviation
$K_T$	frequency factor
$X_T$	The magnitude of a hydrologic event
$\Delta X_T$	the departure of the variant from the mean
$z$	standard normal variable
$\zeta$	location parameter
$\Gamma$	gamma function
$\varepsilon$	lower bound
$\beta$	sum of independent exponentially distribution

**References:**

Aron G., Wall D. J., White E. L. and Dunn C. N., Regional rainfall intensity-duration- frequency curves for Pennsylvania. Water Resources Bulletin. 23(3): 479-485,1987.

Bell, F.C., Generalized rainfall duration frequency relationships. Journal of Hydraulic Div., ASCE, 95(1), 311-327, 1969.

Bernard M.M.,Formulas for rainfall intensities of long duration, transactions, ASCE.96paper No.1801, pp592-624, 1932.

Brian S., Alaa Y., and Alshfey A., Alexandria Storm Water Management Study. Natio. Water Research Center, Unive. Of Alexandria, 2009.

Burlando P. and Rosso R., Scaling and multiscaling models of depth-duration-frequency curves for storm precipitation. Journal of Hydrology. 187(1-2): 45-64,1996.

Chen, C.L., Rainfall intensity-duration -frequency formulas, Journal of Hydraulic Engineering, ASCE, 109(12), 1603-1621, 1983.

Chow, V.T., Maidment, D.R. & Mays, L.W. . Applied Hydrology, McGraw-Hill Company, 1964.

Elsebaie, H., Ibrahim, Developing rainfall intensity–duration–frequency relationship for two regions in Saudi Arabia, Journal of King Saud University, engineering resource, 2010.

Hazen A., Storage to be provided in impounding reservoirs for municipal water supply. Trans. ASCE.77, 1308, 1914.

Hershfield, M., Davi, Estimating the Probable Maximum Precipitation, Journal of the Hydraulic Division, Proceeding of the ASCE, HY5, 99-116, 1961.

Kite G. W., Frequency and risk analysis in hydrology. Water Resources Publications, Fort Collins, CO. pp. 69-83, 1977.

Kothyari, U.C. and Grade, R.J. ,Rainfall intensity duration frequency formula for India, J. Hydr. Engrg., ASCE, 118(2), 323-336, 1992.

Koutsoyiannis, D., Manetas, A., A mathematical framework for studying rainfall intensity duration-frequency relationships, Journal of Hydrology, 206, 118–135, 1998.

Nhat,L.,Tachikawa,Y.,and Takara,k.,Establishment of Intensity-Duration-Frequency Curves for Precipitation in the Monsoon Area of Vietnam, annuals of Disas. Prev. Res. Inst.,Kyoto Univ., No.49B,2006.

Yevjevich V., Probability and statistics in hydrology. Water Resources Publications, Fort Collins, CO. pp. 149-158,1972.

## Flexural Behavior of Reactive Powder Concrete with Hybrid Section T-Beams

Lect. Dr.Rafid Saeed Atea

(Al-Furat Al-Awsat Technical University/Najaf Institute)

Rafid 1980@ yahoo.com

### ABSTRACT

Reactive powder concrete (RPC) is unique of the newest and greatest significant improvements in constructions field , it has usual excessive kindness happening current duration in the world owing toward its higher concrete properties , great ductility, durability, imperfect shrinkage penalties, great opposition to corrosion and abrasion. In this experimental investigation is carried out on the way to revision the flexural behavior of RPC with Hybrid Section T- Beams and the mechanical properties of this construction material. The experimental program included testing five beams to examine the things of steel fiber volumetric ratio, silica fume ratio, tensile steel ratio, hybrid section on flexural performance of RPC T-beams. The study was focused on determining the first crack load ( $P_{cr}$ ), ultimate flexural strength ( $P_u$ ), ultimate deflection ( $\Delta_u$ ), load-deflection behavior, letdown mode, strain supply across the depth of the beams and crack pattern at failure. The effects of steel fiber volumetric ratio and silica fume ratio were also considered in studying the mechanical properties of RPC mixes. Moreover, a study of hybrid beams exhibited that expending RPC happening web and normal concrete in flange efficiently enhances the enactment of T- beams in comparison with normal concrete T-beams and also studying hybrid beams exhibited that expending RPC happening flange and normal concrete in web efficiently enhances the enactment of T- beams in comparison with normal concrete T-beams.

**Keywords: Reactive powder, Steel Fiber, Silica Fume**

سلوك الانثناء لخرسانة المساحيق الفعالة للعتبات الهجينة بمقطع (T)

م.د. رافد سعيد عطية

جامعة الفرات الأوسط التقنية-المعهد التقني/ النجف

### الخلاصة

خرسانة المساحيق الفعالة هي واحدة من أحدث وأهم التطورات في تكنولوجيا الخرسانة، لقد أوليت اهتمام كبير في السنوات الأخيرة في العالم نظراً لخصائصها الميكانيكية الفائقة مثل: المقاومة العالية ، المطيلية العالية ، المتانة العالية ، الانكماش المحدود ، المقاومة العالية للتآكل والتعرية في هذا البحث تم إجراء تحري عملي لدراسة سلوك الانثناء لخرسانة المساحيق الفعالة للعتبات الهجينة بمقطع (T) و الخواص الميكانيكية لهذه المادة الجديدة. تضمن البرنامج التجريبي اختبار خمسة عتبات لتحري تأثير كل من النسبة الحجمية للألياف الحديدية ، نسبة أبخرة السليكا، المقطع الهجين و على سلوك الانثناء لعتبات خرسانة المساحيق الفعالة بمقطع (T). تركزت الدراسة على إيجاد حمل التشقق الأولي ، سعة الانثناء القصوى ، الهطول الأقصى ، سلوك الحمل-الهطول ، نمط الفشل ، توزيع الانفعال على مدى عمق العتبات وشكل التشقق عند الفشل . تأثير النسبة الحجمية للألياف الحديدية و نسبة أبخرة السليكا أيضاً اعتمدا في دراسة الخواص الميكانيكية لخلطات خرسانة المساحيق الفعالة. بالإضافة لذلك فقد بينت دراسة العتبات الهجينة أن

استخدام خرسانة المساحيق الفعالة في الوتر والخرسانة العادية في الشفة حسنت بشكل كفوء أداء العتبات بمقطع T بالمقارنة مع عتبة الخرسانة العادية، وأيضاً دراسة استخدام خرسانة المساحيق الفعالة في الشفة والخرسانة العادية في الوتر حسنت بشكل كفوء أداء العتبات بمقطع T بالمقارنة مع عتبة الخرسانة العادية.

## 1. INTRODUCTION

Reactive powder concrete (RPC) is unique of the informed and best significant improvements in concrete equipment, it has established excessive consideration in current years in the world owing toward its higher mechanical properties [1,2]. RPC is also recognized as ultra high enactment concrete (UHPC) allowing to its more structural presentation. It involves of great measure of cement, fine sand with particle size less than  $600\ \mu\text{m}$ , silica fume, fibers, low w/c ratio (less than 0.2), new generation of superplasticizers and on no account coarse aggregate[3]. RPC is quickly rising as an outstanding alternative to conventional concrete and even high strength concrete in many important structural submissions such as bridges, factories and power stations; therefore, there is increasing need to understanding the mechanical properties and structural behavior of this novel production material. Behavior of RPC beams is one of the fields which requires more studies because until this time there are quiet insufficient researches dealing with this field and there is surely absence of evidence about the analysis and design of RPC structural members. Therefore, this paper aims at studying experimentally and theoretically the flexural behavior of simply supported RPC T-beams under static load. In addition, some significant mechanical properties of RPC combination, are also experimentally recognized which institute data needed for the analysis and design of RPC structural members. Reactive powder concrete is a type of concrete which shows superior mechanical and durability properties, this goes to its elements (types and proportions), mixing efficiency, pressing after placing and curing regime. Each step of preparing RPC and each one of RPC components play key and significant part in getting high recital concrete[4]. In 2004, **Chan and Chu** [5] studied the conclusion of appearances in RPC, containing bond strength, pullout energy, etc. Various silica fume contents ranging from 0% to 40% were used in the mix proportions. Based on the results of bond strength and pullout energy, the optimal silica fume–cement ratio was found to be in between 20% and 30%, given the conditions of this experimental program. At the optimal silica fume dosage (30%), the pullout energy was increased by approximately 100%, whereas the bond strength was increased by 14%. The difference can be attributed to the dissimilar mechanisms of silica fume on supplement energy and on bond strength. In 2007, **Gao** [6] planned the influence of dynamic loads on the properties of plain RPC and fibers reinforced RPC. The test program included two types of case; concrete cylinder with dimension height and diameter ( $150\text{mm}\times 75\text{mm}$ ) and small beams with dimension depth, width and length ( $280\text{mm}\times 70\text{mm}\times 70\text{mm}$ ) with a span of 210mm. The addition of 1.5 % (by volume) of steel fiber significantly increased the flexure strength of RPC. However, there are no helpful belongings on solidity under quasi static and higher

rate loading. In 2008, **Hoang et al** [7] considered guidance of ultra high by using steel fibers enactment concrete (modified RPC, the investigation consequences exhibited that flexural strength and hardness of excessive enactment concrete is amended by adding of steel fibers. In 2010, **Prabha et al** [8] planned stress-strain properties of RPC under uniaxial compression. All the tests were approved out on concrete cylinder specimens of size (diameter=100 mm and height= 200mm) in the Universal Testing Machine. Two types of steel fibers ( $(L_f/d_f = 6/0.16$  and  $13/0.16)$  and various dosages of steel fibers (0%,1% and 2% for 13mm, while 1%,2% and 3% for 6mm and a arrangement of 1% of 6mm and 1% of 13 mm and to end a amalgamation of 1% of 6mm and 2% of 13mm) were used in RPC mix. The trials also showed that the elastic modulus of RPC mixes was found to be 21 % ( for 2%-6mm) to 24 % ( for 2%-13mm) higher than that of RPC without fibers. It was settled that the ratio of ultimate to peak strain was the highest for fibers permutation of 2% 13mm and 1%6mm (4.65) following by 2% 13mm (3.81) mix and 3% 6mm (3.73) mixes. The crack pattern confirmations realization of vertical cracks for lower percentages of small fibers reinforcement and diagonal cracks for higher percentages of fibers reinforcement. 3% of 6mm and 2% of 13mm seemed to be the optimal fibers contents for RPC as observed from the results gained in this revision. In 2010 **Hannawayya** [9] offered investigation to study the effects RPC on the concrete properties as a material as well as reviewing the flexural performance of RPC rectangular section beams. The investigational database involved investigating that conclusion of consequence steel fibers volumetric ratio ( $V_f$ ) and the content silica fume (SF) on some imperative properties of RPC such as compressive strength, uniaxial stress-strain relationship in solidity, splitting tensile strength and modulus of rupture. Supplementary investigational trials were also directed to training the result of  $V_f$ , SF and longitudinal steel bar ratio ( $\rho$ ) on the flexural behavior (in terms of load-deflection response, moment-curvature response, failure load and cracking pattern) of simply supported separately reinforced RPC beam having dimensions of  $140 \times 125 \times 1400$  mm under symmetrical two point load. This research offerings investigational revision on flexural behavior of simply supported RPC T-beams Hybrid Section under simple static load effect as well as studying some important mechanical properties of RPC. In this research, four beams were confirmed to exercise the consequence of steel fibers volumetric ratio ( $V_f$ ), silica fume ratio (SF), hybrid section on the flexural performance of singly reinforced RPC T-beams.

## 2. Materials:

### 2.1 Cement:

The castoff in this effort is Iraqi conventional Portland cement (Taasluja) type (I). It is stowed in impermeable plastic containers to evade exposure to altered atmospheric conditions. This cement is tested and checked allowing to the Iraqi Standard Specification (IOS 5:1984) [10]. Tables (1) and (2) show the chemical and physical properties of this cement. It imitates to the Iraqi specifications.

**Table (1): Chemical composition and main compounds of the cement**

Oxide composition	abbreviation	Content by weight (%)	Limit of Iraqi Specification No.5/1984 <sup>(10)</sup>
Lime	CaO	63.11	-
Silica	SiO <sub>2</sub>	20.66	-
Alumina	Al <sub>2</sub> O <sub>3</sub>	5.13	-
Iron oxide	Fe <sub>2</sub> O <sub>3</sub>	3.36	-
Magnesia	MgO	2.32	5.0 (max)
Sulfate	SO <sub>3</sub>	2.05	2.8 (max)
Loss on ignition	L.O.I.	2.39	4.0 (max)
Insoluble residue	I.R.	0.68	1.5 (max)
Lime saturation factor	L.S.F.	0.88	(0.66-1.02)%
<b>Main compounds (Bogue's equation)</b>			
Tricalcium Silicate	C <sub>3</sub> S	54.72	-
Dicalcium Silicate	C <sub>2</sub> S	18.25	-
Tricalcium Aluminate	C <sub>3</sub> A	8.05	-
Tetracalcium aluminoferrite	C <sub>4</sub> AF	10.21	-

**Table (2) :Physical properties of cement used in this study\***

Physical Properties	Test Results	Limits of Iraqi Specification No.5/ 1984[10]
Specific surface area(Blaine method),(m <sup>2</sup> /kg)	320	230 (Min.)
Setting time (vicat's apparatus)		
Initial setting time (hrs: Min.)	1 : 50	0:45 (Min.)
Final setting time (hrs : min.)	3: 40	10:00 (Max.)
Compressive strength (MPa)		
3 days	27.2	15 (min)
7 days	37.4	23 (min)
Soundness (Autoclave method),%	0.22	0.8(max)

\* Chemical and Physical tests analysis have been tested in the materials laboratory of the college engineering , University of Kufa



## 2.2 Fine Aggregate:

There are contain two types of fine aggregate are castoff in this revision:

1. For typical concrete combinations of this revision used typical sand from Al-Zubair region in Basrah city was used. The maximum size of this type (4.75mm) with pointed subdivision form and smooth. The arranging of this sort is revealed in Table (3). The consequences specified that the fine aggregate grading was within the supplies of the Iraqi description No.45/1984 (11). Table (4) shows the specific gravity, sulfate content, and absorption of fine aggregate.
2. For RPC is castoff very fine sand with maximum size (600 $\mu$ m). The classifying of fine aggregate revealed in table (6) Specification No.45/1984[11]. Table (6) expressions the physical possessions of the castoff fine aggregate .

**Table (3): Grading of fine aggregate used for normal concrete compared with the requirements of No.45/1984[11]**

Sieve Size IQ.S.23(mm)	Cumulative Passing %	Limits of No.45/1984[11]	
10(mm)	100	Zone(3)	Zone(4)
4.75	97	90-100	95-100
2.36	92	85-100	95-100
1.18	88	75-100	90-100
0.60	71	60-79	80-100
0.30	30	12-40	15-50
0.15	10	0-10	0-15

**Table (4): Physical properties of fine aggregate\***

Physical Properties	Test Result	Limit of Iraqi Specification No. 45/1984[11]
Specific gravity	2.7	-
Sulfate content%	0.09%	0.5% (Max)

**\*The tests have been performed in the materials test laboratory of the college engineering, University of Kufa**



**Table (5) :Grading of very fine sand**

<i>Sieve Size(mm)</i>	<b>Cumulative Passing %</b>	<b>Limits of B.S. 882/1992 Limit of grading Zone(F)[11]</b>
<b>4.75</b>	<b>100</b>	<b>100</b>
<b>2.36</b>	<b>100</b>	<b>80-100</b>
<b>1.18</b>	<b>100</b>	<b>70-100</b>
<b>0.60</b>	<b>100</b>	<b>55-100</b>
<b>0.30</b>	<b>47</b>	<b>5-70</b>
<b>0.15</b>	<b>9</b>	<b>-----</b>

**Table (6): Physical and chemical properties of very fine sand**

<b>Physical Properties</b>	<b>Test Result</b>	<b>Limit of Iraqi Specification No. 45/1984[11]</b>
<b>Specific gravity</b>	<b>2.65</b>	<b>-----</b>
<b>Sulfate content%</b>	<b>0.07</b>	<b>0.5(Max.)</b>

### 2.3 Coarse Aggregate:

typical concrete, Smooth type maximum size 14mm attained from Sanam mountain region in Basrah city was castoff as coarse aggregate. Table (7) confirmations grading of coarse aggregate which conforms to the Iraqi specification No.45/1984 [11]. Table (8) illustrates the specific gravity; sulfate content and absorption of coarse aggregate.

**Table (7) :Grading of coarse aggregate**

<b>Sieve Analysis (mm)</b>	<b>Cumulative Passing %</b>	<b>Limit of Iraqi Specification No. 45/1984[11]</b>
<b>20(mm)</b>		<b>100</b>
<b>14</b>	<b>100</b>	<b>90-100</b>
<b>10</b>	<b>87</b>	<b>50-85</b>
<b>5</b>	<b>16</b>	<b>0-10</b>
<b>2.36</b>	<b>2.2</b>	<b>-----</b>

**Table (8): Physical and chemical properties of coarse aggregate\***

Physical Properties	Test Result	Limit of Iraqi Specification No. 45/1984[11]
Specific gravity	2.67	-
Sulfate content	0.035%	≤ 0.1%

\*The tests have been performed in the materials test laboratory of the college engineering , University of Kufa

## 2.4 Silica Fume:

A gray densified silica fume was cast-off, which was introduced from Sika company. Silica fume is an awfully fine dust, its elements are periods minor than cement atoms, continuously cast-off in minor percentage all as incomplete replacement of cement or as an preservative (as cast-off in the current effort) to develop properties. Table (9), chemical is given conformations of silica fume castoff happening this research .The silica fume obeys to the supplies of ASTM C1240-04[12].

**Table (9): chemical properties of silica fume\***

Oxide composition	abbreviat ion	Oxide Content (%)	Limit of Specification Requirement (ASTM C 1240)[12]
Silica	SiO <sub>2</sub>	94.87	85.0 (Min.)
Alumina	Al <sub>2</sub> O <sub>3</sub>	1.18	-
Iron oxide	Fe <sub>2</sub> O <sub>3</sub>	0.09	-
Lime	CaO	0.23	-
Magnesia	MgO	0.02	-
Sulfate	SO <sub>3</sub>	0.25	-
Potassium oxide	K <sub>2</sub> O	0.48	-
Loss on ignition	L.O.I.	2.88	6.0(max)
Moisture content	-	0.48	3.0(max)

\*The tests have been performed in the materials test laboratory of the college engineering , University of Kufa

## 2.5 Superplasticizer (S.P.):

A great enactment concrete superplasticizer (entitled High Range Water Reduction Agent HRWA) established, which is recognized commercially as Glenium 51, is castoff in this revision. Glenium 51 is unrestricted from chlorides and obeys with ASTM C494 type a [13]. Table (10) shows the properties of Glenium 51.

**Table (10): Properties of Glenium 51\***


<b>Form</b>	<b>Viscous Liquid</b>
<b>Commercial name</b>	<b>Glenium 51</b>
<b>Chemical composition</b>	<b>Sulphonated melamine and naphthaline formaldehyde condensates</b>
<b>Subsidiary effect</b>	<b>Increased early and ultimate compressive strength</b>
<b>Form</b>	<b>Viscous liquid</b>
<b>Color</b>	<b>Light brown</b>
<b>Relative density</b>	<b>1.1 gm/cm<sup>3</sup> at 20 °C</b>
<b>pH</b>	<b>6.6</b>
<b>Viscosity</b>	<b>128 ± 30 cps @ 20° C</b>
<b>Transport</b>	<b>Not classified as dangerous</b>
<b>Labeling</b>	<b>No hazard label required</b>
<b>Chloride content</b>	<b>None</b>

**\*Supplied by the manufacturer**

## 2.6 Steel Fibers:

High enactment steel fibers were castoff in this investigation, Allowing to ASTM-A820-04 [14], this type of steel fibers is classified as (Type I). Its properties are listed in Table (11).

**Table (11): Properties of steel fiber\***

<b>Configuration</b>	<b>Property</b>	<b>Specification</b>
	<b>Description</b>	<b>Hooked</b>
	<b>Length</b>	<b>30 mm</b>
	<b>Diameter</b>	<b>0.375 mm</b>
	<b>Density</b>	<b>7800 kg/m<sup>3</sup></b>
	<b>Tensile strength</b>	<b>1800 MPa</b>
	<b>Modulus of elasticity</b>	<b>200GPa</b>
	<b>Aspect ratio(L<sub>f</sub>/D<sub>f</sub>)</b>	<b>80</b>

**\*Supplied by the manufacturer**

## 2.7 Water:

Conventional water is process without any additives

## 2.8 Steel Bars:

insignificant diameter (φ12mm) were castoff as tension reinforcement, while (φ6mm) warped steel bars were castoff as stirrups and (φ6mm) as oblique reinforcement of flange. The tensile experiments for all these bars are recorded in Table (12). from each nominal diameter are tested to define the average yield stress (f<sub>y</sub>) and the ultimate strength (f<sub>u</sub>). The investigation consequences of bars (φ12mm) satisfy ASTM A615 requirements [15].The test results are, as follows:

**Table (12) :Properties of steel bars**

<b>Diameter (steel bar) mm</b>	<b><math>f_y</math> (MPa)</b>	<b><math>f_u</math> (MPa)</b>	<b>Elongation %</b>
12	513	643	12
8	446	621	10
6	376	495	6.3

### 3. Concrete Mix Design:

Two forms of concrete mixtures were cast-off in this study:

#### 3.1 Typical Concrete Mix:

A typical concrete mixture involving of cement, fine aggregate, coarse aggregate, and water were cast-off to cast the normal and web in hybrid beams (Normal, PRC1, PRC2 and PRC3 ). Control sample in the form of cylinders and prisms were also cast from this mixture. The ( w/c) of this combination was 0.45 and the sizes of cement, fine aggregate and coarse aggregate were 1:1.5:3 (by weight) respectively.

#### 3.2 Reactive Powder Concrete Mixes:

Five RPC mixtures were castoff in this revision. Supplies quantities of all mix are recorded in table (13). Several mix proportions were tried to get maximum compressive strength conferring to ASTM C39[ 16] .The variables castoff in these mixes were the percentage of silica fume ratio (three percentages of silica fume as additive were used 15, 20 and 25%) and the volume ratio of steel fibers (three volume ratios were considered 0, 1 and 2%).

**Table (13) :Properties of the different types of RPC mixes**

<b>Mix*</b>	<b>Cement kg/m<sup>3</sup></b>	<b>Sand kg/m<sup>3</sup></b>	<b>Silica Fume* %</b>	<b>Silica Fume kg/m<sup>3</sup></b>	<b>w/cementitious</b>	<b>S.P. ** %</b>	<b>Steel Fiber*** %</b>	<b>Steel Fiber kg/m<sup>3</sup></b>
M0,25	1000	1000	25	250	0.2	1.7	0	0
M1,25	1000	1000	25	250	0.2	1.7	1	78
M2,25	1000	1000	25	250	0.2	1.7	2	156
M2,20	1000	1000	20	200	0.2	1.7	2	156
M2,15	1000	1000	15	150	0.2	1.7	2	156

♣ The letter M denotes Mix; the first number indicates the percentage of steel fiber content (V<sub>f</sub>) and the second number indicates the percentage of silica fume (SF).

\* Percent of cement weight.

\*\* S.P.: Superplasticizer, percent of binder (cement + silica fume) weight.

\*\*\* Percent of mix volume

### 3.3 Mixing Procedure:

RPC was varied by consuming a horizontal turning mixer with ( $0.1 \text{ m}^3$ ) ability obtainable in the structures laboratory, College of Engineering, Kufa University. Then the involvement process was stopped to shovel the mix by hand and then restarted for 3 additional minutes. This stage was recurrent in three cycles to assure the homogeneity of the combination. After the third cycle, steel fibers were all added by hand although involvement was integrated for 3 minutes. The total parting time was about 25-30 minutes. The normal concrete was mixed using the same mixer according to the conventional mixing of normal concrete.

### 3.4 Experimental Program:

In this research, four samples were established to revision the effect of (Vf), (SF) , hybrid section on the flexural conduct of singly reinforced RPC T-beams. The beams were separated as listed in table (14). The beams were considered to have suitable sizes that can be industrial, controlled and established as informal as likely. The minimal lengths of the confirmed beams were 1300mm in total distance and 160mm in depth. The web was completed with effective depth and 100mm width, the flange was prepared with 50mm thickness , 220mm flange width, clear span of 1200mm for all beams confirmed underneath exploit of two point loads, the space between two point loads was reserved constant at (400 mm).

Table (14): Beam details and concrete properties

Group No.	Parameter	Beam	V <sub>f</sub> %	SF %	Tensile reinf.	Concrete in section	Flange width(b <sub>f</sub> )(mm)
1	Changing in concrete of beam section	Normal	-	-	2 $\phi$ 12	Normal in all section	220
		RPC 1	2	25	2 $\phi$ 12	RPC in all section	220
		RPC 2	2	25	2 $\phi$ 12	RPC only in web	220
		RPC 3	2	25	2 $\phi$ 12	RPC only in flange	220

### 3.5 Hybrid Section

Two beams (RPC2 and RPC3) were castoff to explore inspiration incompletely using RPC on conduct T-beams equally contrast with completely RPC sample (RPC1) and typical sample (Normal), figure (1) shows details of cross-sectional .

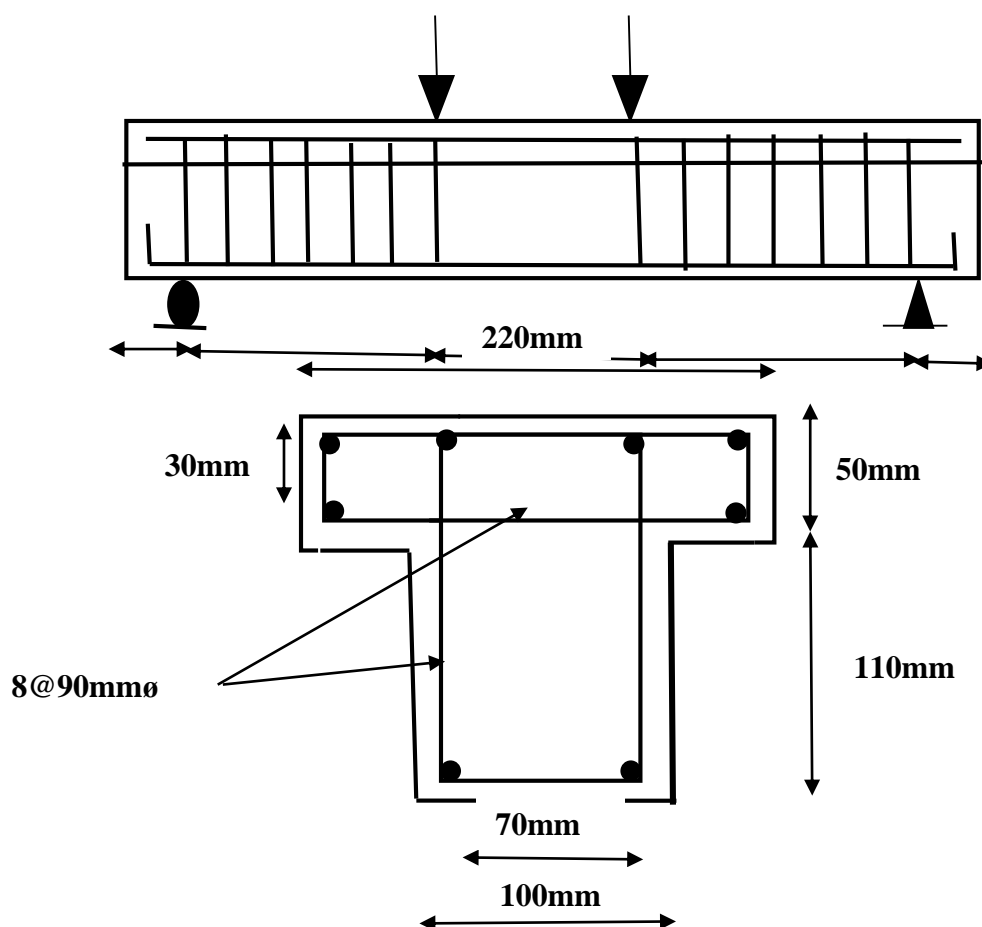


Figure (1) Details of cross-sectional dimensions and reinforcement of beams (Normal, RPC1, RPC2 and RPC3).

#### 4. Experimental Results and Discussion

The consequences of the investigational experiments approved out in this research to observe and assess the flexural performance of RPC with Hybrid Section T-Beams as well as revising the manual properties of RPC. Belongings of three constraints on the flexural behavior of RPC with Hybrid Section T- Beams, comprising: steel fiber volumetric ratio ( $V_f$ ), silica fume ratio (SF), hybrid section. The possessions were premeditated in expressions of load deflection curves, principal crack load, ultimate load, strain dissemination across the depth of the beam at dissimilar load stages, type of beam failure and crack form.

##### 4.1 Mechanical Properties of RPC :

Device cases were equipped commencing the same mixture of non fibrous and fibrous concrete for each column specimen. The details of the control specimens were as following: Cubes of 100 mm and cylinder 150× 300mm for compressive strength test of concrete( $f_c'$ ) were used conferring to ASTM C39-03[17], flexural strength test( $f_r$ ) (modulus of rupture) is approved out by consuming (100 x 100 x 500 mm) prisms, the experiment is supported out allowing to ASTM C78-02 [18], splitting tensile strength assessment( $f_t$ ) is achieved on a dimensions with diameter and height (150×300) mm concrete cylinder allowing to the ASTM C496-04[19],and with diameter and height (150×300) mm for concrete cylinders for dimension of static modulus of elasticity ( $E_c$ ) allowing to ASTM C469-02[20]. all the results shown in table(15).



**Table (15) :Results of Mechanical Properties of Hardened Concrete Tests**

<b>No.of mix</b>	<b>Mix type</b>	<b>Steel fiber Vf %</b>	<b>Silica fume SF %</b>	<b>(fc') (MPa)</b>	<b>(ft) (MPa)</b>	<b>(fr) (MPa)</b>	<b>(Ec) (MPa)</b>
<b>1</b>	<b>M0,25</b>	<b>0</b>	<b>25</b>	<b>92.52</b>	<b>6.71</b>	<b>6.3</b>	<b>37481</b>
<b>2</b>	<b>M1,25</b>	<b>1</b>	<b>25</b>	<b>113.53</b>	<b>11.95</b>	<b>14.7</b>	<b>42469</b>
<b>3</b>	<b>M2,25</b>	<b>2</b>	<b>25</b>	<b>124.95</b>	<b>16.29</b>	<b>19.0</b>	<b>45024</b>
<b>4</b>	<b>M2,20</b>	<b>2</b>	<b>20</b>	<b>120.45</b>	<b>15.24</b>	<b>18.1</b>	<b>44751</b>
<b>5</b>	<b>M2,15</b>	<b>2</b>	<b>15</b>	<b>114.33</b>	<b>14.86</b>	<b>17.4</b>	<b>44529</b>
<b>6</b>	<b>M-normal</b>	<b>-</b>	<b>-</b>	<b>27.04</b>	<b>2.88</b>	<b>3.5</b>	<b>25641</b>

#### **4.2 Effect of Concrete Type (Hybrid Section):**

To reading the talent of consuming typical concrete composed with RPC in the equivalent section to save part high cost of RPC and to achievement the benefits of the two materials in best technique, four beams were established.

Figure (2) shows the load-mid-span deflection of Normal, RPC1, RPC2, and RPC3.

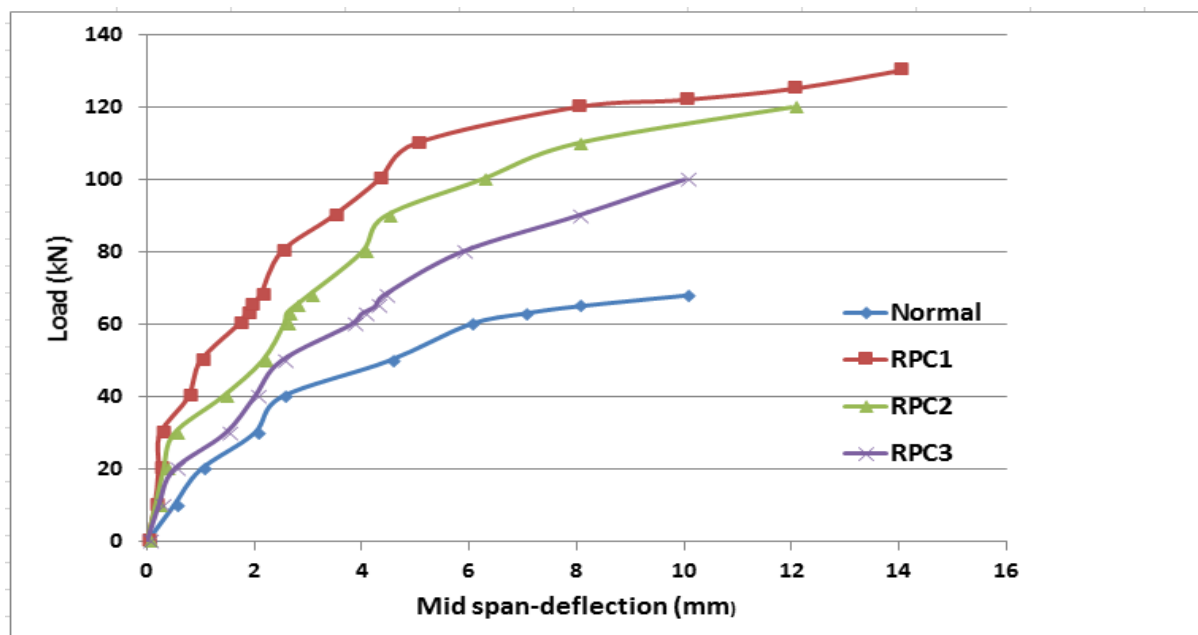


**Figure (2): Effect of hybrid section on load deflection curves of T-beams**

#### 4.3 Crack Patterns:

Generally cracks in concrete are formed at sections wherever the tensile stresses exist and exceed the definite tensile strength of concrete. For samples failing in flexure, cracks initiate at the tension fiber in the central region of the sample, thus all established beams of this revision due to creation of cracking at tension zone in middle third of the beam as shown in figure through (3) which show photographs of the crack patterns afterward the disappointment of the tested beams. The numeral alongside the crack designated the load when the crack entered the concrete upwards.

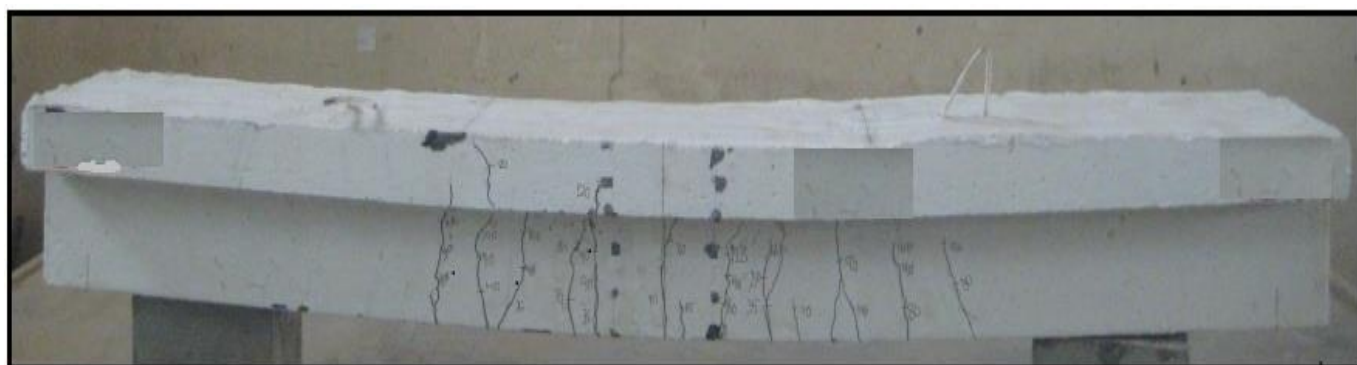


**Figure (3): Effect of hybrid section on Crack pattern of T-Beams**

#### 4.4 Strain Distribution:

The strains in the concrete at midspan section of the tested beams were unrushed at seven unlike stages above the depth every beam as revealed in figures (4) to (7).

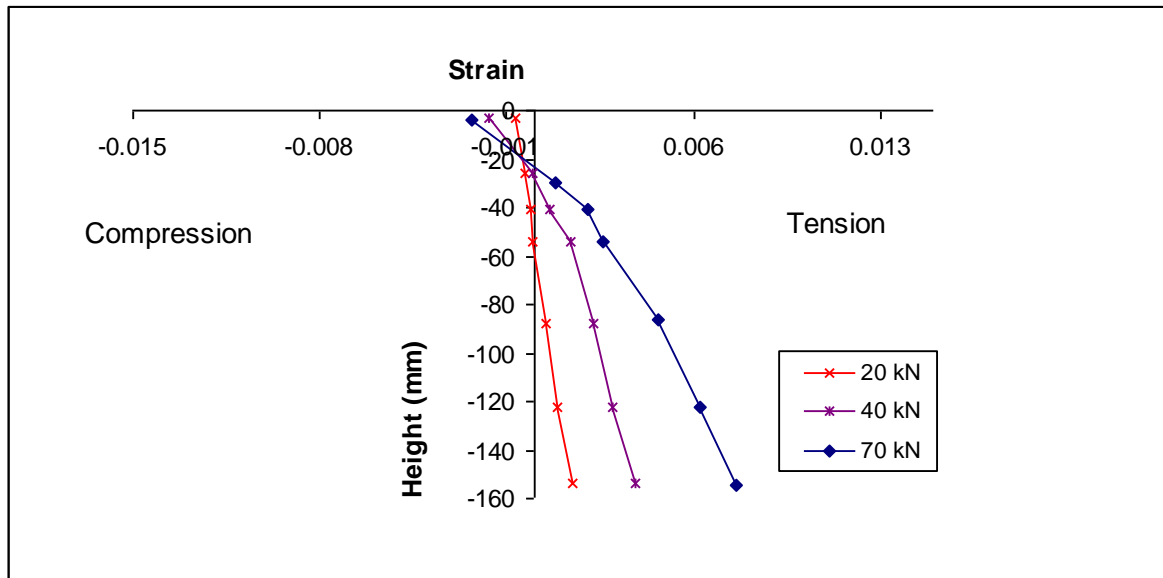


**Figure (4): Strain distribution at section midspan of beam (Normal)**

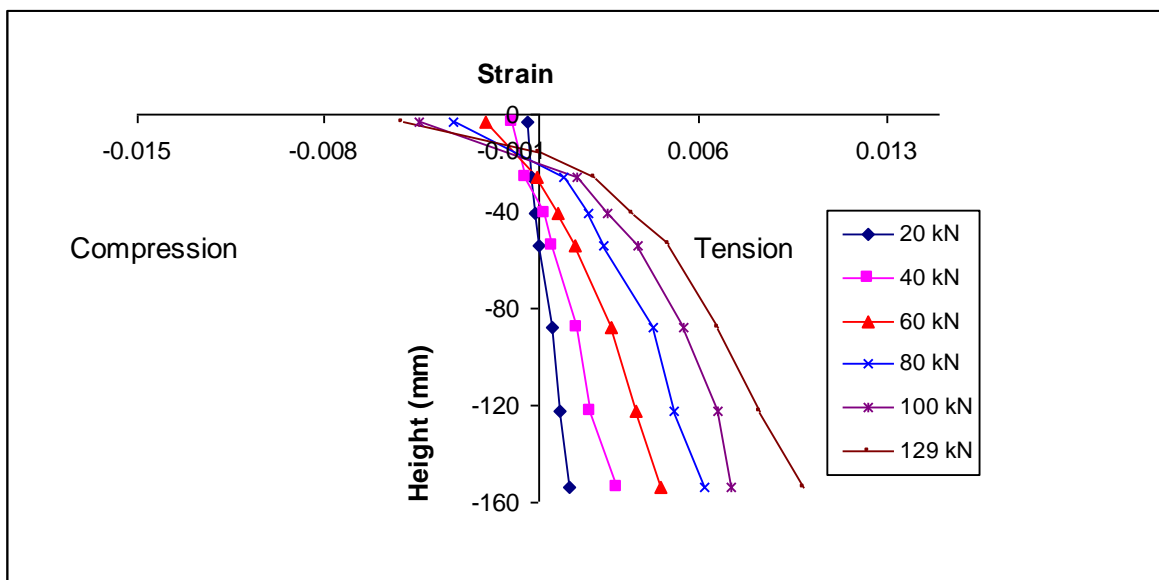


**Figure (5): Strain distribution at section midspan of beam (RPC1)**

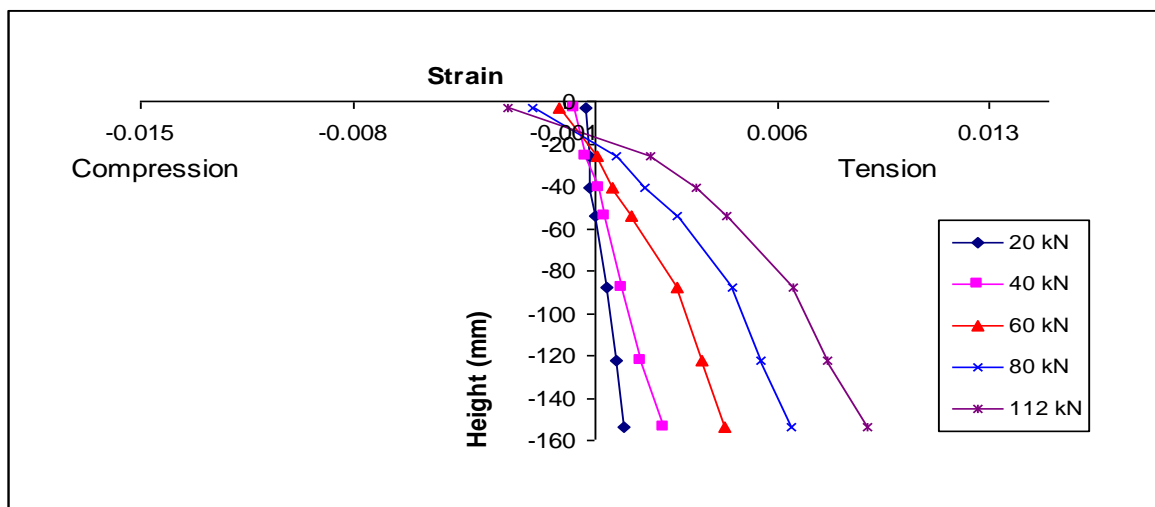


**Figure (6): Strain distribution at section midspan of beam (RPC2)**

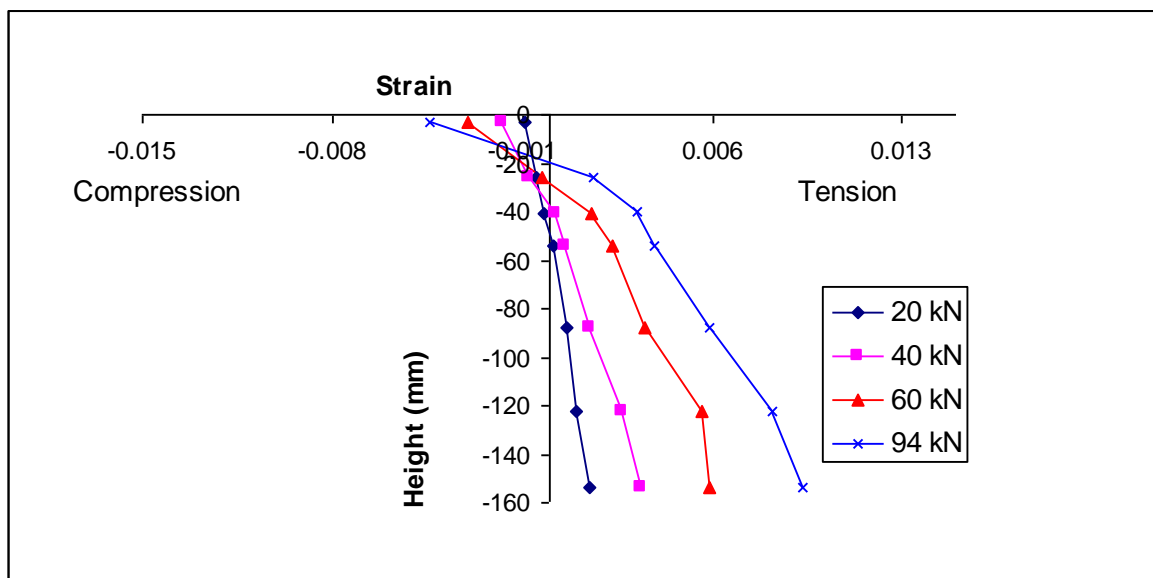


**Figure (7) :Strain distribution at section midspan of beam (RPC3)**

## 5. Conclusions Based on Experimental Work Results:

1. Influence of steel fiber volumetric ratio on the increase of ultimate deflection reveals that increasing steel fiber volumetric ratio to 2% makes RPC T-beams more ductile and capable of undergoing large deflections before attainment final load resonant ability. This possessions is exact significant structural supporters as it permits concrete to provide warning previously disappointment and avoids unexpected collapse.

2. Although the ultimate midspan deflection increases with increasing steel fiber volumetric ratio, the load-deflection curves of beams with (0, 1 and 2%) steel fiber volumetric ratio reveal that at a particular load level, the deflection decreases

with increasing steel fiber volumetric ratio at all stages of loading, due to increasing in stiffness.

3. The increases in first crack load and ultimate load for RPC T-beams with increasing steel fiber volumetric ratio belong to the reason that fibers across the initial flexural cracks restrict growth and extension of the cracks and transmit regularly tensile to the concrete nearby the cracks. This maintains the beam reliability all over the post-cracking steps, therefore the beam resist better load and exhibits more deflection previously disappointment. A larger ductility is achieved with a higher ratio of steel bars.

4. Silica fume with ratios from 15% to 25% has little consequence on the principal crack capacity, ultimate flexural and the midspan deflection of RPC T-beams. On the other hand, growing ratio from 15 to 25%, the first crack load, the ultimate flexural strength and the ultimate midspan deflection increase with percentages of 17, 10 and 15% respectively.

5. The part below load midspan-deflection curve of RPC T-beam increases with increasing steel fiber volumetric ratio and tensile steel ratio constant.

6. Main crack load, ultimate flexural strength and the ultimate midspan deflection with percentages increase of 22%, 31% and 12% respectively as compared with normal concrete T-beam, when using RPC in the flange with normal concrete in web for hybrid T-section beam show increase

7. Using RPC in the web with normal concrete in the flange for hybrid T-section beam show increase in the first crack load, ultimate flexural strength and the ultimate midspan deflection with percentages increase of 82%, 56% and 28% respectively as compared with normal concrete T-beam. Therefore, using RPC in the web does effectively enhance the performance of T-beams more than the case of RPC in flange.

8. Cracking of RPC beams with higher steel fiber volumetric ratios is associated with multiple cracking, while beams with lower steel fiber volumetric ratios are associated with localized cracking. Effect of silica fume on the crack pattern is not evident.

9. The strain distribution across the depth of the mid-span section of RPC beams is around line happening compression zone during the stuffing variety, while in the tension region, it is roughly linear at squat load levels and converts nonlinear at greater load levels owing to cracking. Also the presence of steel fibers leads to an growth in the final concrete strain values at together tension and compression zones but the influence is more pronounced in the tension zone. This can be

credited to the enhanced action of steel fibers in tension slightly than in compression and increasing in stiffness and modulus of elasticity.

10. The presence of steel fibers in RPC gives some improvement to its compressive strength. Increasing  $V_f$  from 0% to 1% and 2% resulted in an increase in compressive strength of the order 20% and 33% respectively. Although silica fume is a smaller amount operational; growing silica fume ratio starting 15% to 20% and 25 % increases the compressive strength of RPC by only 5% and 8.5% respectively.

11. Under compressive load the failure of nonfibrous RPC is of explosive and brittle nature, while the failure of RPC with steel fibers exhibits ductile behavior. Steel fibers result in more closely spaced cracks, reduces the crack width and improves resistance to deformation.

12. Steel fibers oblige a important consequence on tensile strength of concrete. As steel fibers proportion upsurges from 0% to 1% and 2%, the splitting tensile strength of RPC upsurges by 75% and 139% separately. Silica fume has a minor effect in growing the splitting tensile strength, as upsurges starting 15% , 20% then 25% increase by only 2.32% to 8.77% respectively.

13. Steel fibers have also a significant effect in increasing the modulus of rupture of RPC. As soon as steel fibers ratio rises starting 0% to 1% and 2% modulus of rupture of RPC rises by 129% to 198 % respectively. However silica fume appearances tiny consequence happening the modulus of rupture. As rises from 15% to 20% and 25 rises by only 4% and 9% respectively.

14. The strain distribution across the depth of the mid-span section of RPC beams is nearly direct in the compression region during the course of the charging variety, however happening the tension zone, it is nearly linear at short load levels and develops nonlinear at higher load levels owing to cracking. Also the presence of steel fibers leads to an rise in the ultimate concrete strain values at together tension and compression zones but the influence is more pronounced in the tension zone. This can be recognized to the enhanced action of steel fibers in tension reasonably than in compression.

## References

- 1- Richard, P. and Cheyrezy, M., “Reactive Powder Concrete with High Ductility and 200-800 MPa Compressive Strength”, ACI SP144-24, 1994, pp. 507-518.
- 2- Collepardi, S ., Coppola, L., Troli, R. and Collepardi, M., “Mechanical Properties of Modified Reactive Powder Concrete”, Proceedings fifth CANMET/ACI International conference on superplasticizers and the chemical admixtures in concrete, Rome. Italy. Farmington Hills, MI: ACI publication SP-173, 1997, pp. 1-21.
- 3- Richard, P. and Cheyrezy, M., “Composition of Reactive Powder Concrete”, Cement and Concrete Research, Vol. 25, No. 7, 1995, pp. 1501-1511.
- 4- Shaheen, Ehab. and Shrive, Nigel. G., “Optimization of Mechanical Properties and Durability of Reactive Powder Concrete”, ACI Materials Journal, November-December 2006, pp.444-451.
- 5- Gao, X.,”Mix Design and Impact Response of Fiber Reinforced and Plain Reactive Powder Concrete”, M.Sc. Thesis, School of Civil, Environment and Chemical Engineering, RMIT University, August 2007, 73p.
- 6- Hoang, K., H., Phat, H., B., Hien, L., V., D., “Influence of Types of Steel on Properties of Ultra High Performance Concrete”, The 3rd ACF International Conference-ACF/VCA, 2008, pp. 347-355.
- 7- Tai, Y., S.,” Uniaxial Compression Tests at Various Loading Rates for Reactive Powder Concrete “, Theoretical and Applied Fracture Mechanics, No. 52, 2009, pp. 14-21.
- 8- Prabha, S., L., Datta, J., K., Neelamegam, M., and Seshagiri Rao, M., V., “Study on Stress-Strain Properties of Reactive Powder Concrete under Uniaxial



Compression” , International Journal of Engineering Science and Technology, Vol.2(11) , 2010, pp. 6408-6416.

9- Hannawayya, S., P., Y., ”Behavior of Reactive Powder Concrete Beams in Bending”, Ph.D. Thesis, Building and Construction Engineering Department, University of Technology, Baghdad, 2010, 239p.

10.IraqiStandardsNo.5/1984,“Ordinary Portland cement” Ministry of Housing and Construction, Baghdad, 2004

11- Iraqi Standards No.45/1984, “Aggregate from Natural Sources for Concrete and Construction”, Ministry of Housing and Construction, Baghdad, 2004.

12- ASTM C1240-04, “Standard Specification for the Use of Silica Fume as a Mineral Admixture in Hydraulic Cement Concrete, Mortar and Grout”, Vol. 4.2, 2004, 6p.

13- ASTM C494/C494M-1999a, “Standard Specification for Chemical Admixtures for Concrete”, Vol. 4.2, 1999, 9p.

14- ASTM A 820/A 820M-04 “ Standard Specification for Steel Fiber for Fiber-Reinforced Concrete “ , 2004,pp.1-4.

15- ASTM A615/615M-05a, "Standard Specification for Deformed and Plain Carbon Structural Steel Bars for Concrete Reinforcement", Annual Book of ASTM Standards, Vol.01.02, 2005.

16- ASTM A615/615M-05a, "Standard Specification for Deformed and Plain Carbon Structural Steel Bars for Concrete Reinforcement", Annual Book of ASTM Standards, Vol.01.02, 2005.

17-.ASTM C39/C39M-2003, “Standard Test Method for Compressive Strength of Cylindrical Concrete Specimens”, Vol. 4.2, 2003, pp. 1-5 and B.S. 1881: Part

116: 1983, “Methods for Determination of Compressive Strength of Concrete Cubes”, January 1983, pp. 1-8.

18-.ASTM C78-02, “Standard Test Method for Flexural Strength of Concrete (Using Simple Beam with Third-point Loading)”, Vol. 4.2, (2002), pp. 1-3.

19-.ASTM C496/C496M-04, “Standard Test Method for Splitting Tensile Strength of Cylindrical Concrete Specimens”, Vol. 4.2, (2004), pp. 1-5.

20-.ASTM C469-02, “Standard Test Method for Static Modulus of Elasticity and Poisson's Ratio of Concrete in Compression”, Vol. 4.2, (2002), pp. 1-5

# AN EXPERIMENTAL INVESTIGATION FOR WATER FLOW ENHANCEMENT IN HORIZONTAL PIPES BY USING NANOPARTICLES

Hashim A. Hussein

Electromechanical Engineering Department -University of Technology- Bagdad-Iraq

E-mail: hashim171967@gmail.com, Mobile: 07904383422

## Abstract

This work has been devoted to investigate experimentally, the increase in range of horizontal discharge distance and velocity of water flow for pipes of fire-hoses and water jet propulsion systems in small ships. The enhancement method of water flow depends on increase the drag reduction and best uniform flow. One of the important practice techniques is adding a small amount of some materials, cheap and locally available added into water flow in a horizontal pipe. A simple experimental system is designed and constructed to investigate the increase in drag reduction. Nanoparticles (aluminum oxide – 30 nm diameters) and polyacrylamide (PAM) have been added alone and gain time together. Experimental calculations of average flow velocity, Reynolds number, and friction factor and percentage drag reduction are experimentally calculated under water heads of 75,100, 125,150,175 and 200 cm. The effects of concentration ratios of nanofluid ( $Al_2O_3$ ) on friction factor and drag reduction are studied and calculated. The present results showed that addition of  $Al_2O_3$  and PAM are caused reducing in friction factor, increase in range of horizontal discharge distance and the velocity of water flow. Also the results indicated that, drag reduction was 26% increased at addition of  $Al_2O_3$  and 39% at PAM while at mixing them together was 52 % as average for six heads were chosen. The results are represented graphically to explain the degrees of enhancement of increasing in drag reduction, flow velocity and the range of discharge distance for water in horizontal pipes. The originality of this work was addition materials of nanoparticles with polyacrylamide together.

**Keywords:** Fluid dynamics; Turbulent& laminar flow; Drag reduction; Nanofluids; Friction factor.

## تحقق عملي لتحسين جريان الماء في الانابيب الافقية باستخدام دقائق نانوية

### الخلاصة

اختص هذا العمل على التحقق العملي من امكانية زيادة مدى التدفق الافقي للماء وسرعة جريانه في الانابيب الافقية المستخدمة لخرطوم اطفاء الحرائق ومنظومات الدفع النفث للمياه في السفن الصغيرة. تركز طريقة التحسن المقترحة على تنظيم افضل للجريان وتحقيق زيادة في تقليل الاحتكاك. واحدة من اهم التقنيات العملية هي اضافة دقائق متناهية الصغر من بعض المواد الرخيصة والمتوفرة محليا الى جريان الماء في الانابيب الافقية. تم تصميم وبناء منظومة مبسطة للتحقق العملي من استخدام تلك الدقائق النانوية وتم اختيار دقائق اوكسيد الالمنيوم بقطر 30 نانومتر ودقائق من مادة بوليميرية تسمى (PAM) اضيفت كل مادة لوحدها مرة و مرة اخرى اضيفتا معا. عمليا تم حساب معدل سرعة الجريان ونسبة الزيادة في التدفق الافقي وعدد

رينولد ومعامل الاحتكاك والنسب المئوية لتقليل الاحتكاك تحت ارتفاعات 75, 100, 125, 150, 175 و 200 سم. تم حساب تأثيرات النسب الوزنية للدقائق النانوية لثنائي اوكسيد الالمنيوم على تقليل الاحتكاك وبقية المتغيرات الاخرى. نتائج العمل الحالي اثبتت عمليا تحقيق زيادة في مدى تدفق الماء افقيا وفي سرعة الجريان نتيجة لتقليل الاحتكاك وتنظيمه بصورة افضل باضافة الدقائق النانوية والبوليمرية الى الماء. كذلك بينت النتائج ان نسب الزيادة في تقليل معامل الاحتكاك كانت 26% عند اضافة دقائق ثنائي اوكسيد الالمنيوم و 39% عند اضافة المادة البوليمرية و 52% عند اضافة المادتين معا. تم تمثيل النتائج بيانيا لتوضيح نسب الزيادة في تقليل الاحتكاك وسرعة الجريان ومدى التدفق الافقي للماء في الانابيب الافقية. الاصلة في هذا العمل هو اضافة المواد النانوية والبوليمرية معا.

## 1. Introduction and literature survey

In an engineering practice the most flows are turbulent liquid flow, therefore, it is important needing to explain how turbulence in liquids flow effects on the rate of wall shear stress. Turbulent liquids flow is a very complex mechanism devoted by disturbances, the theoretical researches in turbulent liquid flow remains not enough to understanding these fluctuations. Turbulent liquid flow is described by random motion of liquid particles in directions transverse to the direction of the main liquid flow so that the liquid flow is unstable [1]. Turbulent liquid flow is described by a rapid disturbance of swirling areas of liquid, named eddies, during the water flow. These disturbances provide an additional mechanism for momentum and energy transfer. For laminar liquid flow, the particles of liquid flow in an orderly manner along path lines, and energy and momentum are transferred across streamlines by molecular diffusion while for turbulent liquid flow, the swirling eddy transport mass, energy, momentum, to other areas of flow more rapidly than molecular diffusion, greatly improving mass, momentum, and heat transfer, therefore, turbulent liquid flow is mainly devoted on the values of friction factors [2]. The turbulent liquid flow characteristic is strongly changed so that the study of nanofluids and polymeric drag reducing could help in gaining more knowledge about the turbulence itself. The application of addition of some nanofluids in water pipes that will minimize energy required for pumping and improve thermal properties of working fluid would allow one to save electrical energy needed to work of installations and reduce their operational costs [3]. One of the effective a possible improvement methods is the application of nanofluids and polymer materials with drag reducing. Because of the polymer materials are not expensive; the drag reduction has many practice applications, such as reduction of pumping energy requirements of oil pumping stations, increasing the speed and decreasing the fuel consumption of ships, extending the discharge distance of water from fire hoses. [4]. Turbulent eddies of liquid flow are generated at the pipe wall and move in to the center of the pipe. More energy is required to transport liquid at a given average flow velocity in turbulent liquid flow because not all of the energy goes toward overcoming viscous resistance to motion down the pipe. The velocity distribution can be considered independent of the axis - direction of water flow, and the water

flow is called to be fully developed, [5]. An application in reduction of energy losses in water pipelines has active intense research into reducing drag over big and small ships and has recently gained attention for enhancing efficiency in all heating and cooling systems, which heated water is generated at the area in a city center and pumped to the houses in the surrounding location. Addition of materials as nanofluid or polymer will causes a change in physical properties of liquid. Addition of small amount of these materials to a liquid flow leads to decrease the pressure drop. All types of additives, such as nanoparticles, solid spheres, fibers, bubbles, lead to drag reducing in the turbulent liquid flow. Because of the turbulent flow disturbances, changes in rate of shear stress can lead to profound alterations in the macroscopic characteristics of the flow (e.g., transition to turbulence, skin friction drag, turbulence energetic, and heat transfer). These flow changes consider mainly difference between non-Newtonian turbulence and Newtonian. An example of these differences is explained by the reducing in skin-friction drag (up to 80%) showed in turbulent liquid flows of polymers materials [2, 6].

**Sundar, et. al. (2010)** [7], calculated experimentally, the friction factor at different concentrations ratios for water flow in a tube. The physical properties such as the viscosity of nanofluid are calculated by many experiments at different concentrations ratios. **Kumar, et. al. (2012)** [8], performed a computational fluid dynamic experimental investigation of turbulent flow of heat transfer enhancement of a pipe. Mixing of very small sized nano particles to the liquid is one of the many important methods used for enhancing rate of heat convection in water flow in pipes. The practical problems such as high pressure loss, erosion of the material can be solving by addition small particles, which is a dispersion of nanosized particles in a base liquid. **Ali Mohammud, (2009)**, [9], studied that the additions of many polymer materials to water flow. He was proved that the polymer materials of (PAM, PEO, CMC1 and CMC2) are more suitable to be used for improving the discharge distance of water flow. He achieved an increasing in extending of distance of water up to 30 % with them. Some polymer materials used for reducing the drag friction such as,  $PAM > PEO > CMC1 > CMC2$ . **Naik, et. al. (2013)**, [10] studied the turbulent water flow with addition of copper oxide nanofluids with propylene glycol-water by volume ratio of (30:70). They provided to be the behavior of heat at the wall pipe uniform. Nanofluids concentrations ratios and the main parameters are investigated on the liquid flow in a circular pipe.

The present work aims to increase the range of horizontal discharge distance and velocity of water flow in pipes by using nanofluids ( $Al_2O_3$ ) and polymer material (PAM) together and study the effects of concentration ratio of nanofluid (0.1, 0.2, 0.3, 0.4 and 0.5 %) on the enhancement of percentage of drag reduction DR% and decreasing in the friction factor.

## 2. Theoretical part

The horizontal and vertical distances that are traveled by the jet during time (t) and velocity (u) as the following of set equations be the average velocity of the jet, then [11];

$$x_i = u_i \times t \quad (1)$$

$$y = \frac{1}{2} g t^2 \quad (2)$$

$$t = \sqrt{\frac{2y}{g}} \quad (3)$$

$$u_i = x_i \sqrt{\frac{g}{2y}} \quad (4)$$

To calculate the friction factor according to the Fanning equation, water flowing at a velocity (u) through a diameter of pipe (D) and length of pipe (L),  $f$  can be calculated from the following equations of friction factor [12] :-

$$f = \left( \frac{g h}{2 u^2} - 0.375 \right) \left( \frac{D}{L} \right) \quad (5)$$

$$f = \left( \frac{g h}{50 x^2} - 0.375 \right) \left( \frac{D}{L} \right) \quad (6)$$

$$f = 0.06447 \frac{h}{u^2} - 0.00123 \quad (7)$$

There is a relationship between friction factor and Remolds number (Re) for smooth pipes .The fiction factor can be achieved with turbulent water flow of Newtonian fluids in smooth cylindrical pipes related to Reynolds number (Re) a according to Blasius equation [13].

$$f = 0.0791 \text{ Re}^{-0.25} \quad (8)$$

While the equation that describes the relationship between ( $f$ ) and (Re) at the maximum drag reduction in turbulent liquid flow in pipes according to the following equation [14]:

$$f = 0.59 \text{ Re}^{-0.58} \quad (9)$$

After the values of average velocities are measured, Reynolds number (Re) can be calculated from the following Eq. [15]:-

$$\text{Re} = \frac{\rho u D}{\mu} = \frac{u D}{\nu} \quad (10)$$

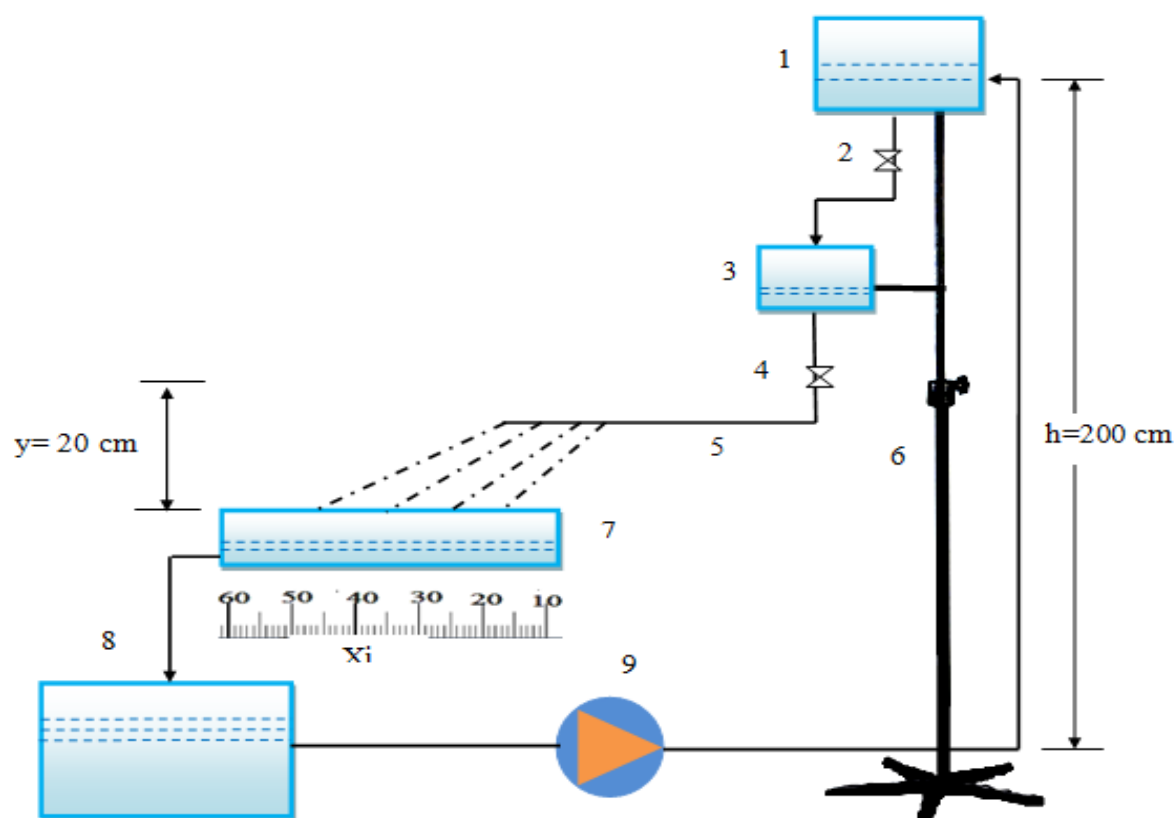
The percentage of drag reduction (%DR) can be calculated from the following Eq. [16]: -

$$\%DR = \frac{f_w - f_{np}}{f_w} \times 100 \quad (11)$$

### 3. vjxjExperimental part

#### 3.1 Experimental system description

The experimental system of this work which designed and constructed in Electromechanical-Eng. Dep.-University of Technology-Baghdad-Iraq for measurement of the discharge distance of water flow from the horizontal pipe. It consists of three reservoirs which are small containers that were used to supply water in order to maintain constant head throughout the experiment. The reservoir is connected to a pipe (16) cm with diameter of (1.2) cm which is connected to a valve and a slide conduit of (180) cm and with diameter of (1) cm. This, in turn, is connected by flexible pipe to a horizontal pipe (90) cm with diameter of (0.3) cm. The efflux from the horizontal pipe is allowed to fall freely a distance of (20) cm (y) into a trough, in such a way that the distance traveled horizontally, (x) is clearly measured.



[1-supplying container, 2-valve, 3 mixing container, 4- valve,5- rubber tube ,6- variable stand (head 75-200cm) ,7- trough (x measured),8- reservoir container, 9- pump,]

**Figure (1): Schematic diagram of design and construction of the system**

#### 3.2- Materials and methods

##### A- Nanofluid ( $Al_2O_3$ )

In the present work nanopowder of aluminum oxide-30 nm diameter, there are two step procedures for nanofluid preparation. Step one, is putting a small amount of nanopowder was weighted and suspended in reverse osmosis water. Step two, the mixture was continuously circulated through the ultrasonic device. Nanofluid has been prepared in the Laboratory of



Corrosion of the Materials Engineering - University of Technology. The summary steps of nanofluid preparation are shown in figure (2). The concentration ratios of five samples (0.1, 0.2, 0.3, 0.4 and 0.5) % were prepared.

### B- Polyacrylamide (PAM)

In this present work, polyacrylamide (PAM) have molecular weight ( $4 \times 10^6$  g/mol.), and concentration ratio (0.1% with 99% water), was selected according to their drag reducing properties as recorded by many researches. The homogenous solution preparation of PAM needs to 5 hr. with 75 rpm by Mechanical stirrer device (it start at 35 rpm and increased by 10 rpm for each two hours, then, the preparation of homogenous solution of PAM became ready to use . The reason for choosing PAM due to a very cheap and it uses in many applications such as fire- fighting water.

### 2.3-Measurment devices

Three devices are used in this work. First of these devices is to measure nanoparticles weights. The different weights of nanoparticle (0.1, 0.2, 0.3, 0.4, and 0.5) % have been measured using a sensitive balance named (Digital balance) Laboratory type, model number KD-TN, Power supply AC/DC, rated load (100 g) and accuracy is 0.0001g. Second device is Magnetic mixer which confuses the fluid (water + nanoparticles of  $Al_2O_3$  was added) .Magnetic mixer is laboratory device that uses magnetic field to mixing the fluids. The mixing time of water and  $Al_2O_3$  was 3 hrs. Third device is Ultrasonic homogenizer model type JY92-IIN has frequency (20-25 KHz), power 650w, mainframe weight (14kg) and packing size (534x295x435mm). The working time was 20 minute to disperse the particles in the water so that they become equally distributed.

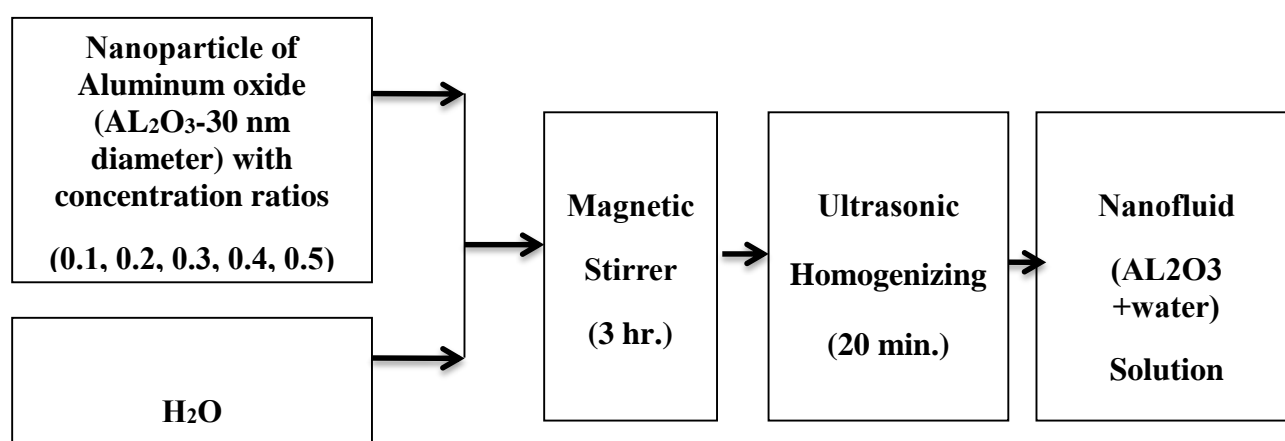


Figure (2): Summary of steps of preparation process of Nanofluid

## 4. EXPERIMENTAL MEASUREMENTS

As shown in figure (1), the distance (x) is measured for pure water flow and with additions of nanoparticle ( $Al_2O_3$ ) and PAM for different concentrations of  $Al_2O_3$  (0.1, 0.2, 0.3, 0.4 and 0.5) % and under different heads (75, 100, 125, 150, 175 and 200 cm) by many experimental tests. Then, the values of discharge distances (x) are used to calculate the average velocities (u)

according to the fundamental of fluid mechanics for free discharging of liquids through orifices and mouthpieces [11].

## 5. Results and discussion

### 5.1 Effect of additions of nanoparticles on the velocity of water.

It is generally believed that the discharge distance ( $x$ ) of the efflux falling freely from the horizontal tube is directly related to the liquid head above the discharge point ( $h$ ). Turbulence flow causes changes of momentum from core of pipe to liquid near to the pipe wall. Figures (3, 4 and 5) explain such variations with  $Al_2O_3$  and PAM. The values of increasing in these figures proved that the effect of small particles addition on extending the discharge distance ( $x$ ) and the velocity of water flow ( $u$ ) in horizontal pipe under heads of (75, 100, 125, 150, 175 and 200 cm) are very effective. The best increasing achieved in discharge distance and velocity of water flow at mixing  $Al_2O_3$  and PAM together. The result of the present work seems to be in good agreement with those observed by previous researchers. The different distances can achieve with a hose water jet for pure water (short jet distance) and for an addition of nanoparticles and polymers materials (long jet distance).

### 5.2 Effect of concentration ratios of nanofluid on the horizontal discharge distance

The variations of the discharge distance with nanofluid concentration under different liquid heads are shown in Figures (6 and 7) for  $Al_2O_3$ , the results indicate that %DR is considerably increased with increasing of nanofluid concentration so that %DR with  $Al_2O_3$  is considerably increased with increasing the concentration from (0.1 – 0.5) % under a liquid heads. The results explained that PAM is more efficient additive for drag reduction than nanofluid ( $Al_2O_3$ ).  $Al_2O_3$  interactions are considerably increased with increasing of its concentration and degree of turbulence which is directly related to the liquid head in the present work. Reduces the possibilities of shear degradation since the water was free falling by gravity without any applied force of pumping or rotating the water as in classical flow systems commonly used in such investigations.

### 5.3 Effect of concentration ratios of nanofluid on friction factor

Figures (8, 9, 10, 11 and 12) explain that the water flow entirely obey to Blasius equation. It is important to note that the behavior of the experimental data points of Nanofluid ( $Al_2O_3$ ) with concentration ratios of (0.1, 0.2, 0.3, 0.4, and 0.5) % is due to the higher %DR observed with  $Al_2O_3$  at these concentrations with different of water heads (75, 100, 125, 150, 175 and 200 cm). The behavior of these figures explains that, friction factor was decreased due to the increasing of concentration ratio of nanofluid and increasing of heads. Best increasing of DR% was at 0.3% concentration ratio.

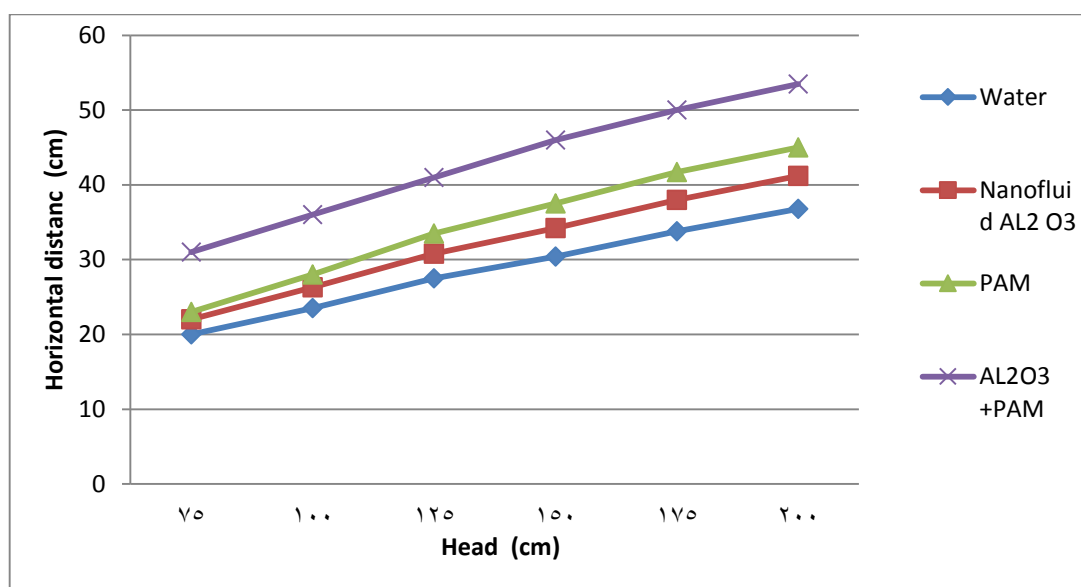


**Figure (3): Variation of discharge horizontal distance of water flow with nanofluid and PAM .**

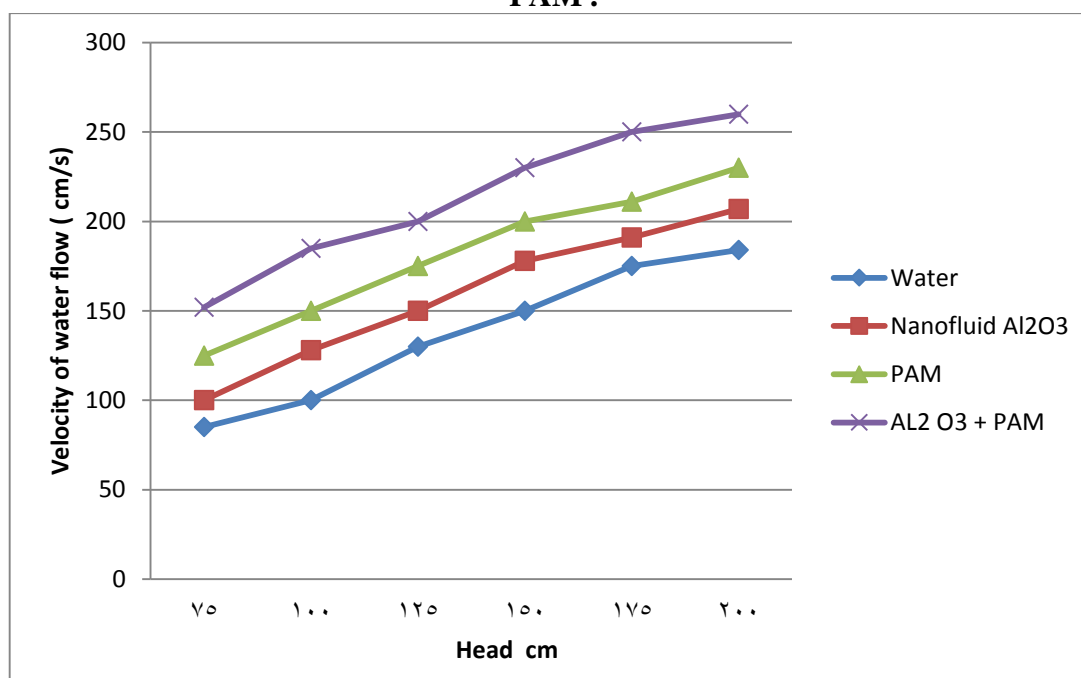


**Figure (4): Variation of velocity water flow with nanofluid and PAM and with mixing together.**

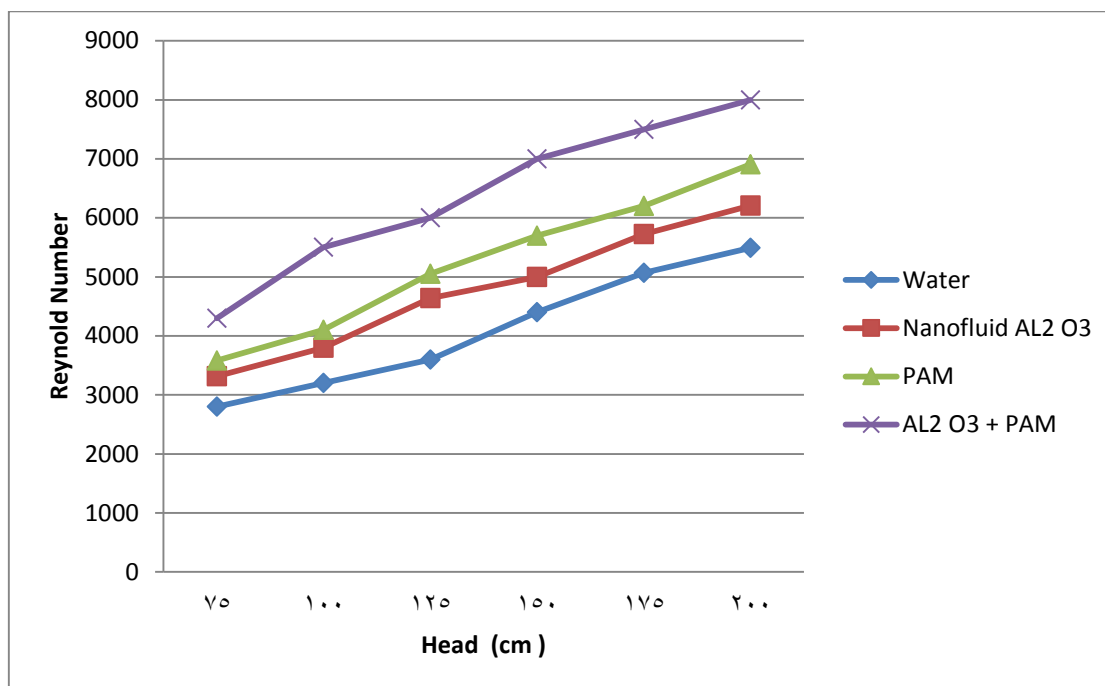


**Figure (5): Variation of Reynolds number of water flow with nanofluid and PAM and with them.**

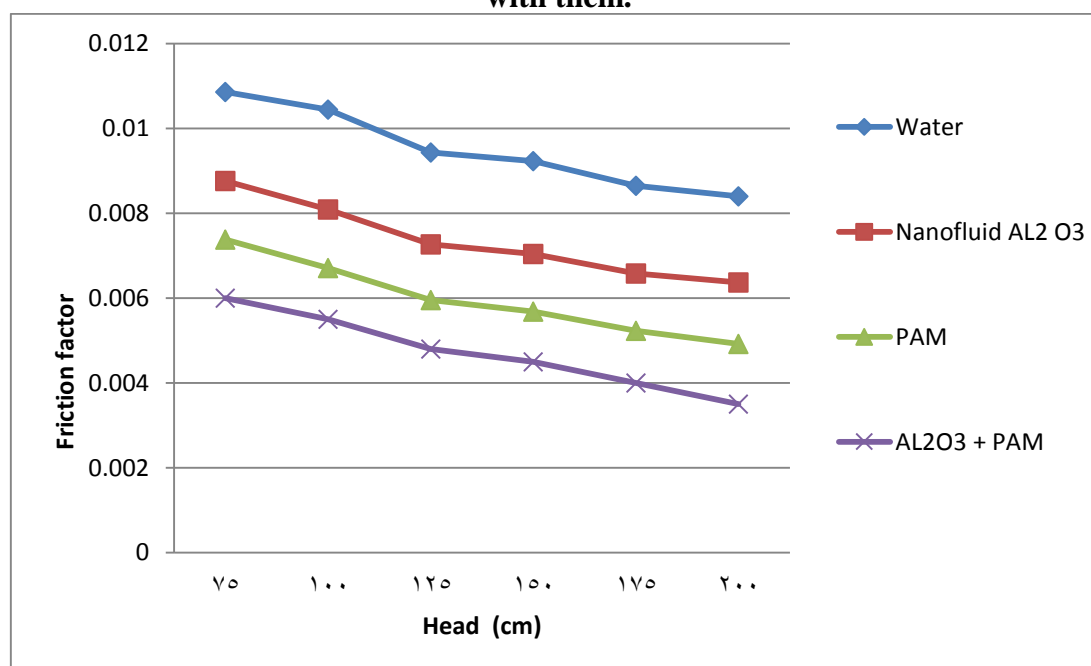


**Figure (6): Variation of friction factor of water flow with nanofluid and PAM**

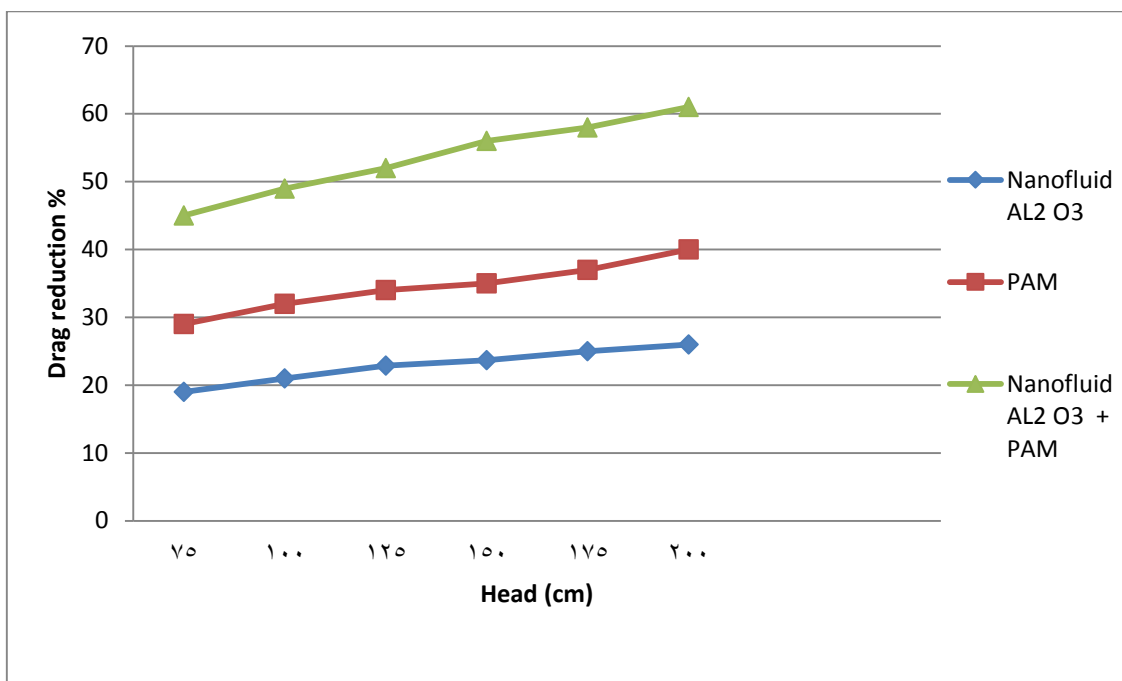


Figure (7): Variation of drag reduction of water flow in pipes with nanofluid and PAM.

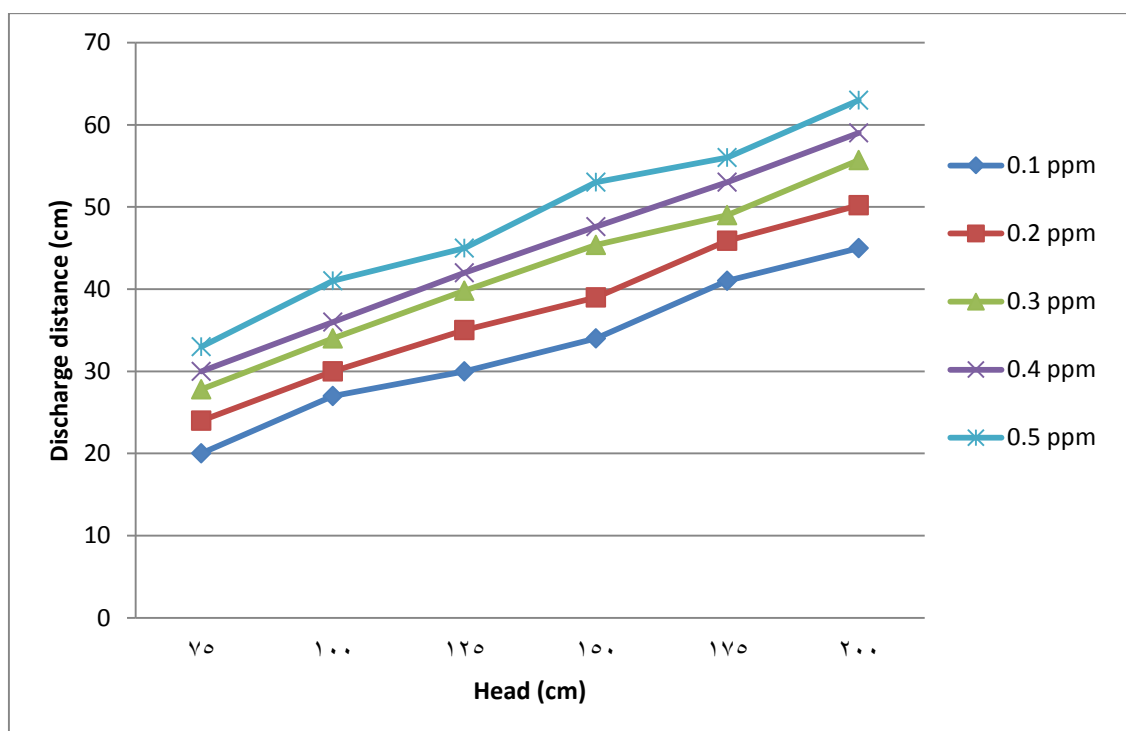


Figure (8): Effect of concentration ratio of nanofluid ( $\text{Al}_2\text{O}_3$ ) on the discharge horizontal distance of water flow in pipes

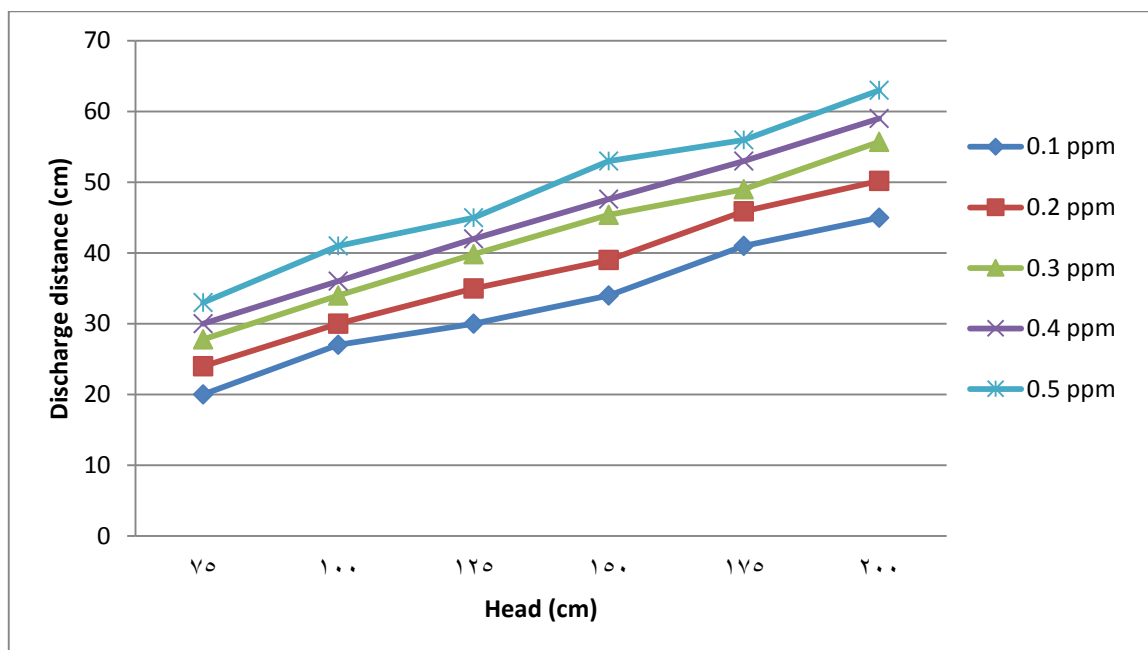


Figure (9): Effect of concentration ratio of nanofluid ( $\text{Al}_2\text{O}_3$ ) on the discharge horizontal distance of water flow in pipes

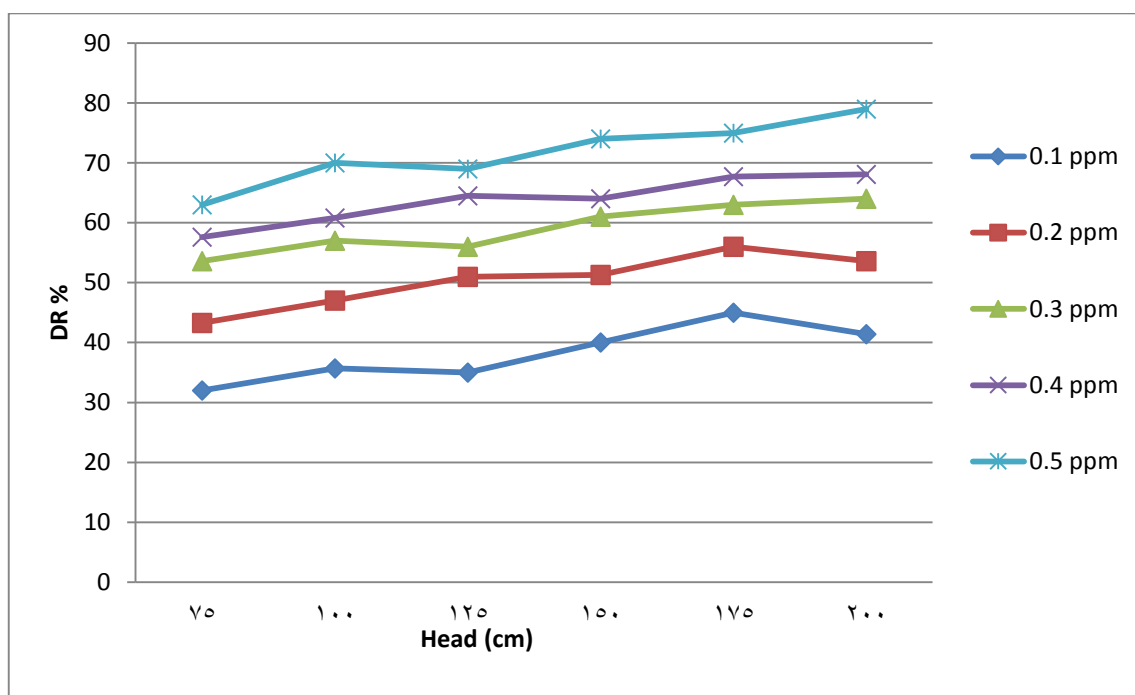
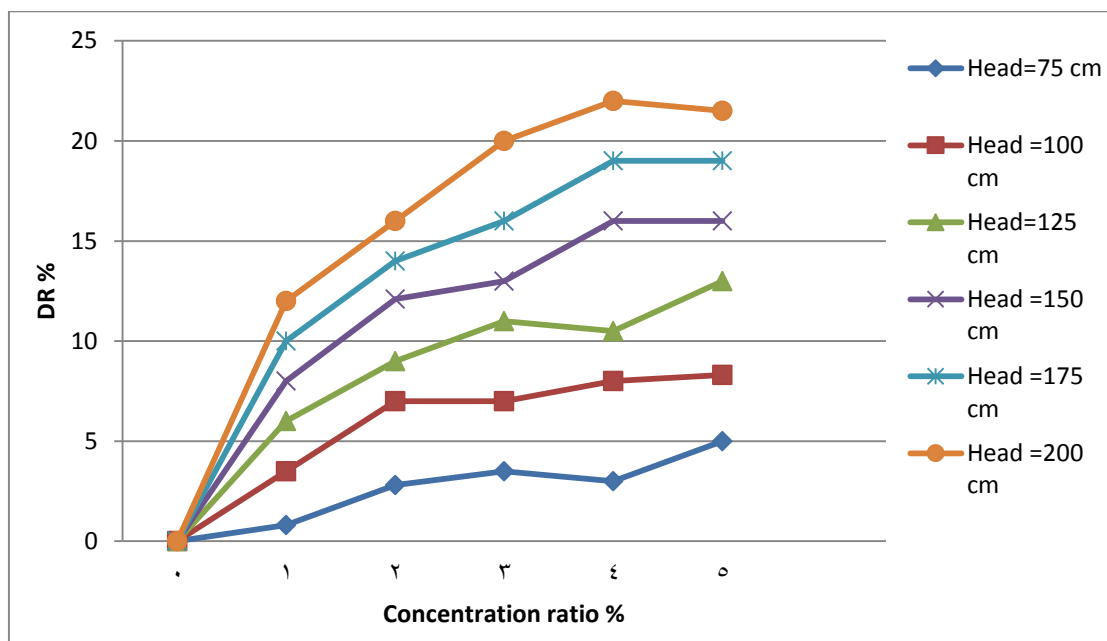
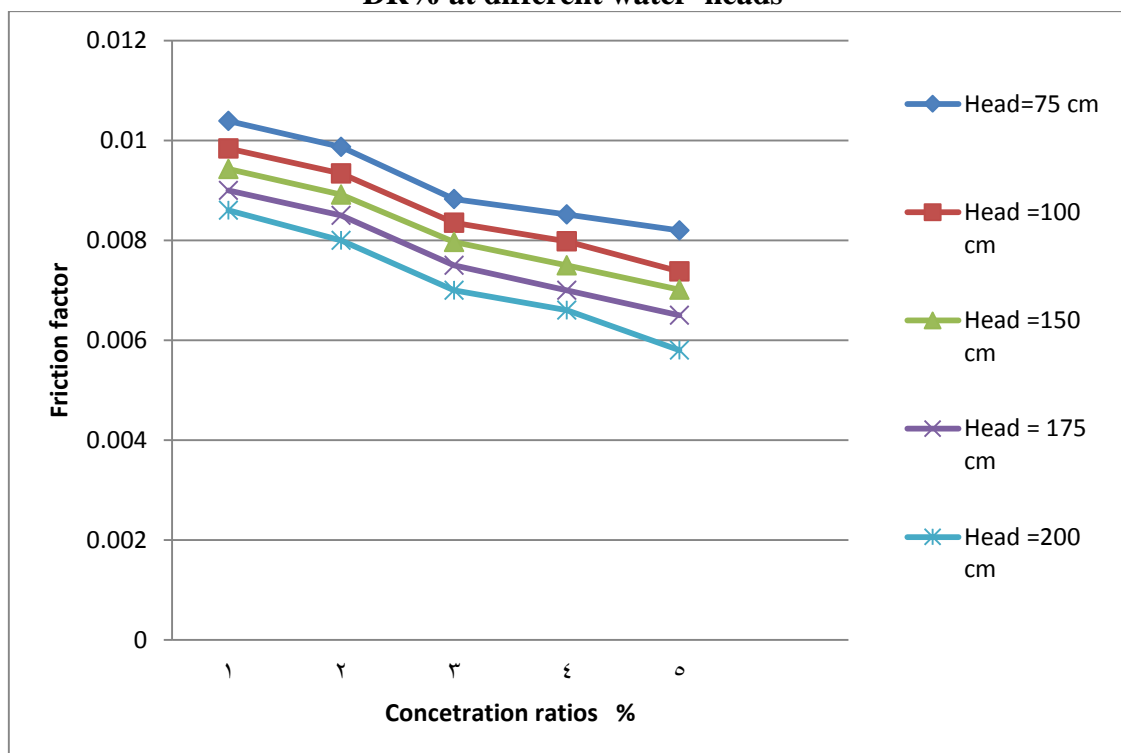


Figure (10): Effect of concentration ratio of nanofluid ( $\text{Al}_2\text{O}_3$ ) on the drug reduction DR% of water flow in pipes



**Figure (11): Effect of concentration ratio of nanofluid ( $\text{Al}_2\text{O}_3$ ) on the drug reduction DR% at different water heads**



**Figure (12): Effect of concentration ratio of nanofluid ( $\text{Al}_2\text{O}_3$ ) on the friction factor at different water heads**



## 6. CONCLUSIONS

This work concluded the following conclusions:-

- 1- Aluminum oxide  $Al_2O_3$  and Polyacrylamide PAM are efficient materials to use for increasing the velocity of water flow in long horizontal pipelines and horizontal distance (x) of water because % DR is increased.
- 2- PAM is more efficient than  $Al_2O_3$ . The percentage of DR noticed with PAM is higher than Aluminum oxide; this is due to the higher molecular weight of PAM compared to  $Al_2O_3$ .
- 3- The differences in % DR observed with  $Al_2O_3$  solutions are considerably increased with increasing concentration ratio which it is significantly decreased and slightly influenced by the liquid head.
- 4- The %DR is considerably increased with increasing of  $Al_2O_3$  concentration and liquid head for all tested additives. The friction factors measured with water entirely obey to Blasius equation.
- 5- Addition of aluminum oxide  $Al_2O_3$  and polyacrylamide PAM caused direct effect on the center line of velocity profile of water flow while it decreases the velocity profile near the wall pipe.
- 6- The value of eddy viscosity decreased when added aluminum oxide  $Al_2O_3$  and Polyacrylamide PAM together. The minimum value will be at the touching area of the pipe wall. Therefore, disturbance of the water flow in this region will be very small value when mixing them together and this give advantage of decreasing in the disturbance of water flow in this region.

## REFERENCES

- [1] Elders, N., Panahi Zadeh, F., & Elders, N. "Investigation of the usage of ethylene glycol - alumina oxide Nanofluid as a cooling fluid in the heat exchanger with two pipes", Journal of Mechanical Engineering Tutor, 11 (3), 75-84. 2011.
- [2] Cho, S.H., Tae, S.B., Zaheeruddin, M., "Effect of fluid velocity, temperature, and concentration of non-ionic surfactants on drag reduction", Energ. Conves Manage, 48, 913-918 (2007).
- [3] Abid, E.M; "Drag Reduction in Single and Two-Phase Turbulent Pipe Flow Using CMC Polymer", Ph.D. Thesis, University of Technology-Mechanical Engineering Dep., 2007.
- [4] Min, T.; Yoo, J. Y.; Choi, H. and Toseph, D. D.; "Drag Reduction by Polymer Additives in a Turbulent Channel Flow", J. Fluid Mech., 486, pp. 312-238, 2003.
- [5] Wen, D., & Ding, Y. "Experimental investigation into convective heat transfer of nanofluids at the entrance region under laminar flow conditions", International Journal of Heat and Mass Transfer, 47, 5181-5188, 2004.
- [6] Aguilar G., Gasljevic K., Matthys E. F., "Maximum friction and heat transfer reductions for drag-reducing surfactant solutions". Int. J. Heat Mass Transfer, 44, 2835-2843. 2001.
- [7] Syam Sundar, L., & K.V. Sharma, "Turbulent heat transfer and friction factor of  $Al_2O_3$  Nanofluid in circular tube with twisted tape inserts", International Journal of Heat and Mass Transfer, 53, 1409-1416, 2010.

- [8] Kumar, P., & R.Ganesan, "A CFD Study of Turbulent Convective Heat Transfer Enhancement in Circular Pipe flow", International Journal of Civil and Environmental Engineering, 6, 385- 392, 2012.
- [9] Ali Mohammad, "Extending the discharge distance of free falling water from horizontal tube by drag reduction", thesis of master degree in chemical engineering, (2009).
- [10] Naik, M.T., E.Vojkani, & G.Ravi, "Numerical Investigation of Turbulent Flow and Heat Transfer Characteristics of PGW-CuO Nanofluids", International Journal of Mining, Metallurgy & Mechanical Engineering (IJMMME), 1 (2), 141-145, 2013.
- [11] Ptasiński, P.K., Nieuwstadt, F.T.M., Van Den Brule, B.H.A.A., and Hulsén, M.A., "Experiments in Turbulent Pipe Flow with Polymer Additives at Maximum Drag Reduction, Flow", Turbulence and Combustion, 66, pp. 159-182, 2001.
- [12] Rodriguez, F., "Principles of Polymer Systems" 2<sup>nd</sup> edition, McGraw- Hill, New York, (1985).
- [13] Dosunmu, I.T.; Shah, S.N. "Turbulent flow behavior of surfactant solutions in straight pipes". J. Petroleum Sci. Eng. 124, 323–330, 2014.
- [14] Yang, J.W.; Park, H.; Chun, H.H.; Ceccio, S.L.; Perlin, M.; Lee, I. "Development and performance at high Reynolds number of a skin-friction reducing marine paint using polymer additives". Ocean Eng. 84, 183–193, 2014.
- [15] Tamano, S.; Ikarashi, H.; Morinishi, Y.; Taga, K. "Drag reduction and degradation of nonionic surfactant solutions with organic acid in turbulent pipe flow". J. Non-Newton. Fluid Mech., 2015.
- [16] Fu, Z.; Otsuki, T.; Motozawa, M.; Kurosawa, T.; Yu, B.; Kawaguchi, Y. "Experimental investigation of polymer diffusion in the drag-reduced turbulent channel flow of inhomogeneous solution". Int. J. Heat. Mass. Trans. 77, 860–873, 2014.

## NOMENCLATURE

D: Pipe diameter [cm]

g: Acceleration due to the gravity 981 [cm /s<sup>2</sup>].

h: Head [cm]

Re: Reynolds number [-]

u: Fluid velocity [cm /s ]

x: Horizontal discharge distance [cm]

y: Vertical distance [cm]

%DR: Percentage drag reduction

DR: Drag reduction

PAM: Polyacrylamide

$\rho$  : Fluid density [g/cm<sup>3</sup>]

$\mu$  : Dynamic viscosity [g/cm.s]

$\nu$  : Kinematic viscosity [cm<sup>2</sup> /s ]

$f$  : Fanning friction factor [-]

$f_w$  : Friction factor for water [-]

$f_{n.p.}$ : Friction factor for nanoparticle[-]

PAM: Polyacrylamide

PEO: Polyethylene oxide

CMC: Sodium carboxymethyl cellulose

CMC1: CMC with MW of  $4 \times 10^5$

CMC2: CMC with MW of  $1 \times 10^5$

# Dynamic Analysis of Absorption Column

Maryam Yousif Ghadhban

University of Technology /chemical engineering department, Iraq-Baghdad.

[Mariammeme2004@yahoo.com](mailto:Mariammeme2004@yahoo.com)

## ABSTRACT

The absorption column is one of the essential separation processes in industrial operation, so the need arises to control absorption column by process simulation and also to analyze system by method called frequency response using MATLAB8. This work dealt with gas-liquid (air-water) absorption packed column which is analyzed by bode plot and frequency response to determine the stability of the system with or without Proportional Controller (P), Proportional Integral Controller (PI) or Proportional Integral Derivatives Controller (PID). The frequency response gives the transient response information, by defining such frequency response quantities as gain margin and phase margin. This work presents dynamic analysis of absorption column which is single input/single output (SISO) using feedback control (P, PI and PID) with the parameters of Cohen-Coon, Ziegler Nichols and Internal Model control and compares between them.

**KEY WORD:** absorption, control, gas, liquid, column,

## التحليل الديناميكي لعمود الامتصاص

مريم يوسف غضبان

الجامعة التكنولوجية/قسم الهندسة الكيميائية

## الخلاصة

عمود الامتصاص هو واحد من عمليات الفصل الاساسية في الصناعات البتروكيمياوية، لذلك دعت الحاجة للسيطرة على عمود الامتصاص بواسطة عملية المحاكاة وايضا عن طريق تحليل النظام بطريقة تدعى استجابة التردد باستخدام برنامج MATLAB8. تم في هذا العمل استخدام عمود الامتصاص المحشو ذو نظام غاز-سائل (ماء - هواء) الذي حلل بواسطة طريقة ال (Bode) واستجابة التردد لحساب استقرارية النظام مع او بدون السيطرة. استجابة التردد تعطى معلومة الاستجابة العابرة بواسطة تعريف بعض كميات استجابة التردد مثل Phase Margin And Gain Margin. هذا العمل يقدم التحليل الديناميكي لعمود الامتصاص والذي هو احادي المدخل احادي المخرج (SISO) باستخدام سيطرة التغذية الراجعة (P, PI, PID) مع معاملات (Ziegler - Nichols, Cohen - Coon And Internal Model Control) والمقارنة بينهم.

## 1-INTRODUCTION:

Gas-liquid absorption columns are largely employed in chemical industry separation units. Absorption process nonlinearities and environment variations are such that a fixed parameter conventional feedback controller cannot adequately achieve satisfactory performance [1].

Absorption is a unit operation in which an air stream containing the component intended for removal is passed upward through a packed tower while a stream of water is passed downward through the tower [2]. Contact between these streams allows for mass transfer. Packing increases the internal surface area of the tower, thus increasing the opportunity for component transfer [3].

Gas liquid absorption is a heterogeneous process, which involves the transfer of a soluble component of a gas phase into a relatively non-volatile liquid absorbent as shown Franks in 1967 [4]. Coulson in 1996 prove that gas liquid absorption could be employed in purification of waste gases [5]. There are two types of absorption, first type is the chemical absorption, in which the liquid solvent reacts with the gas stream and remains in solution. Second type is the physical absorption, in which the solute in the gas is more soluble in the liquid solvent and, therefore, the solute is transferred to the liquid. Chemical is usually preferred

over physical because the equilibrium for chemical absorption is much more favorable for the separation. However, physical absorption is important since it can be applied when chemical absorption is not possible [6].

Absorption equipment generally includes: stirred vessels, packed beds, and bubble columns. One of the most common and rapidly developing systems used to carry out the absorption process on an industrial scale is the packed tower. A packed tower is essentially a piece of pipe set on its end and filled with inert material or tower packing [7]. Generally, the packed tower operates in countercurrent flow, where the liquid enters the system through the top and wets the surfaces of the packing, and the gas stream mixed with the effluent enters the bottom. As the liquid and the gas are contacted with one another, the components of the effluent can be absorbed into the liquid. Gas absorption in a countercurrent flow packed tower is dictated by the equilibrium conditions between the contaminant gas and the absorbing liquid. The overall controlling mechanisms are ruled by the solubility of the gas in the liquid and by any reactions that may be caused to occur in the liquid with the reacting chemical [8]. Diffusion is used to move the gas to the liquid surface and the overall gas/liquid equilibrium controls the design of the tower. Since the gas is absorbed at the liquid surface, the more liquid to gas interactions that can be caused to occur, the closer the exiting streams will approach equilibrium [7].

The conventional method of process control is to use the feedback control loop with a controller. The control actions depend upon the control models present and at what values of gain and time constants of the model are set. A feedback system gives satisfactory control for a wide range of processes, and design of feedback loop does not demand any knowledge of the dynamic behavior of the process. Feedback can modify the natural dynamics of a system. For instance, using feedback, one can improve the damping of an under damped system, or stabilize an unstable operating condition, such as balancing an inverted pendulum. Open-loop or feed-forward approaches cannot do this. For flow control applications, an example is keeping a laminar flow stable beyond its usual transition point. Classical control refers to techniques that are in the frequency domain (as opposed to state-space representations, which are in the time-domain), and often are valid only for linear, single-input, single-output systems. Thus, in this section, we assume that the input  $f$  and output  $y$  are scalars, denoted  $f$  and  $y$ , respectively [9].

The corresponding methods are often graphical, as they were developed before digital computers made matrix computations relatively easy, and they involve using tools such as Bode plots, Nyquist plots, and root-locus diagrams to predict behavior of a closed-loop system. The most common type of classical controller, Proportional-Integral-Derivative (PID) feedback [9].

A proportional–integral–derivative controller (PID controller) is a generic [control loop feedback mechanism \(controller\)](#) widely used in industrial [control systems](#). A PID controller calculates an "error" value as the difference between a measured [process variable](#) and a desired [set point](#). The controller attempts to minimize the error by adjusting the process control inputs. In the absence of knowledge of the underlying process, a PID controller is the optimal controller. However, for best performance, the PID parameters used in the calculation must be [tuned](#) according to the nature of the system – while the design is generic, the parameters depend on the specific system. PI Controller (proportional-integral controller) is a feedback controller which drives the [plant](#) to be controlled with a weighted sum of the error (difference between the output and desired [set-point](#)) and the integral of that value. It is a special case of the common [PID controller](#) in which the derivative (D) of the error is not used [10].

The control system performance can be improved by combining the [feedback](#) (or closed-loop) control of a PID controller with [feed-forward](#) (or open-loop) control. Knowledge about the system (such as the desired acceleration and inertia) can be fed forward and combined with

the PID output to improve the overall system performance. The feed-forward value alone can often provide the major portion of the controller output [11]. The PID controller can be used primarily to respond to whatever difference or *error* remains between the set point (SP) and the actual value of the process variable (PV). Since the feed-forward output is not affected by the process feedback, it can never cause the control system to oscillate, thus improving the system response and stability. Feedback is a mechanism, process or signal that is looped back to control a [system](#) within itself. Such a loop is called a feedback loop [12]. In systems containing an input and output, feeding back part of the output so as to increase the input is *positive feedback*; feeding back part of the output in such a way as to partially oppose the input is *negative feedback*. Feedback is also a synonym for:

- Feedback signal - the information about the initial event that is the basis for subsequent modification of the event
- Feedback loop - the causal path that leads from the initial generation of the feedback signal to the subsequent modification of the event
- Audio feedback - the special kind of positive feedback that occurs when a loop exists between an audio input and output.

Set point is the target value that an automatic control system, for example [PID controller](#), will aim to reach [13, 14].

The computer plays an important role in the design of modern control systems. Fortunately there is computer and software that remove the hard work from the task. With desktop computer, performance analysis, design, and simulation can be made with one program, with the ability to simulate a design rapidly, easily make changes and immediately test a new design. A computer model of the system behavior may be utilized to investigate various designs of a planned system without actually building the system itself [12, 15].

Several linear control applications for absorption columns are found in the literature. **Minorsky, in 1922** worked on automatic controllers for steering ships and showed how stability could be determined from the differential equations describing the system. **Danckwerts, in 1951 and 1954** consider the liquid surface to be composed of a large number of small elements each of which is exposed to the gas phase for an interval of time after which they are replaced by fresh elements arising from the bulk of the liquid [16, 17]. **Moor, in 1970** has worked with a scalar space model, using the analytic solution of the modeling equation to predict the value of the state one delay time ahead. This analytical predictor was developed primarily for sampled data systems and hence included in its structure corrections for effect of sampling and zero-order hold [18]. **Najim and Ruiz in 1995** presented first principles modeling and a long-range predictive control of an absorption packed column. This equipment was used to decrease the concentration of CO<sub>2</sub> in a gas mixture below a desired value. A solution of diethanolamine (DEA) was used as the absorbent. The flow rate of the absorbent and the concentration of CO<sub>2</sub> were selected, respectively, as manipulated and controlled variables. An extended horizon control policy, based on the minimization of a quadratic criterion function of the input and output tracking errors, was used for the feedback control. The simulation studies highlighted the applicability of this adaptive control algorithm to packed columns [19]. **Palú et al in 2004** studied the application of a linear dynamic matrix control (DMC) to a staged absorption column [1]. **Meleiro et al in 2005** used neural networks for the control of the fermentation step of an alcohol production process. The internal model of the nonlinear predictive controller was represented by two Functional Link Networks (FLN). This structure presented the advantages of fast training and guaranteed convergence. The performance of the proposed controller was evaluated for servo and regulatory problems, and in both cases, it showed satisfactory results [20]. **Najim K., in 2007** describes the model and solution of the constrained optimal control problem associated with a packed absorption column. The control problem is solved



using a learning automaton operating in a random environment. On the basis of physical and chemical laws, a model has been developed. It consists of three hyperbolic partial non-linear differential equations. A solution of diethanolamine (the absorbent) is used to absorb the  $\text{CO}_2$  contained in a gas mixture. The primary manipulated variables are the flow rate of the absorbent and the concentration of  $\text{CO}_2$  in the gas mixture. The control objective is to maintain the concentration of  $\text{CO}_2$  close to a desired value, subject to control limit restriction, in order to avoid the flooding of the column. It leads to a stochastic programming problem, the solution of which is closely associated with the behavior of an automaton in a random environment corresponding to the column. Detailed computer simulation results which demonstrate the performance of this automaton controller are presented [21].

The aim of the present work is Design the required controller (P, PI and PTD) to improve process response and using (P, PI and PID) as a conventional control methods with tuning methods (Cohen-Coon, Ziegler Nichols)

## **2- THEORATICAL CONTROL ON THE ABSORPTION OF AIR-WATER SYSTEM:**

In this work, a gas-liquid absorption packed column operating under a continuous mode for the absorption of air-water system. Gas absorption is usually carried out in vertical counter current packed column. The packed column is arranged to operate individually.

The liquid solvent is fed at the top of the column and is distributed over the surface of the packing either by nozzle or distribution plates. Pressure tapping is provided at the base, center and top of the column to determine pressure drops across the column. Sampling points are also provided for the gas at the same three points. The liquid outlet stream and feed solution are also equipped with sampling point. Suitable manometer measurement is included. Water/solvent is taken from a sump tank, and pumped to the column via a calibrated flow meter. Air/solute is supplied and monitored from a small compressor.

The effluent gas leaves the top of the column and is intended to be exhausted to atmosphere outside the laboratory building. The apparatus is designed to absorb air into an aqueous solution flowing down the column. Gas analysis is provided for this system shown in Figure 1 below [16]. The apparatus used in the experiments consists of a glass packed cylindrical tower filled with packing material.

The packing material used was a 3/8" glass Raschig ring randomly packed into a three inch diameter by six foot high section. A Raschig ring is simply a hollow cylinder that has an outer diameter equal to its height. The liquid and gas streams are designed to flow counter-currently past each other to obtain the greatest absorption rate. The liquid (tap water) enters the column from the top and exits out the bottom, while the gas (air) enters the bottom of the column and exits through the top. Each inlet stream has two flow meters; one mechanical and the other an electrical transmitter [14].

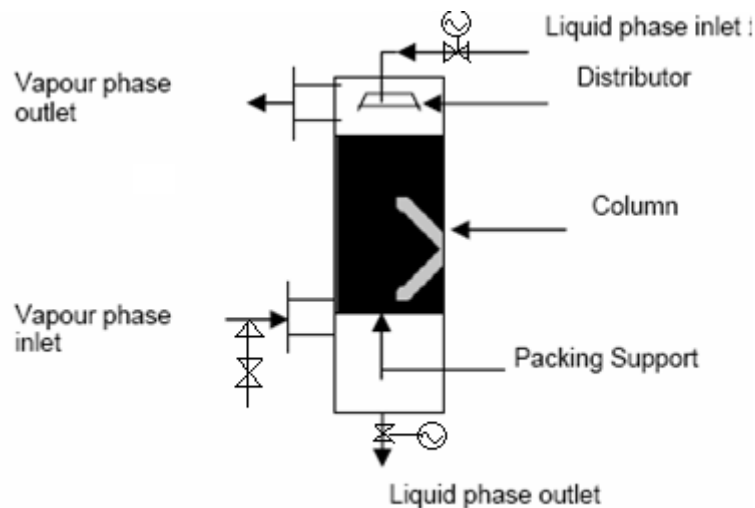


Figure (1) Gas absorption column

### **P CONTROLLER:**

In this type of control the output of proportional controller changes only if the error signals changes. Since a load change requires a new control valve position, the controller must end up with a new error signal; this means that proportion controller usually gives a steady state error off set. The magnitude of the offset depends on the size of the load disturbance and on the controller gain, that means the bigger gain, the smaller the offset as the gain is made bigger, however, the process becomes under damped and eventually at still higher gain, the loop will go unstable, acting like an on/off.

$$P \propto E(t) \quad \dots (1)$$

Where p is proportional controller;

Moreover,  $E(t)$  is the error which depends on time:

$$P = G_c E(t) + P_s \quad \dots (2)$$

$$G_c = K_c \dots (3)$$

$$P - P_s = K_c E(t) \dots (4)$$

$$P(s) = K_c E(s) \dots (5)$$

$$\frac{P(s)}{E(s)} = K_c = G_c(s) \dots (6)$$

Therefore, the transfer function of proportional controller is  $G_c = K_c \dots (7)$

In the frequency response, proportional controller merely multiplies the magnitude of system at every frequency by constant  $kc$ . On bode plot, this means proportional controller raises the log magnitude curve by  $20 \log(kc)$  dB but has no effect on the phase angle curve [13].

### **PI Controller**

Proportional-integral controller is a feedback controller which drives the plant to be controlled with a weighted sum of the error (difference between the output and desired set-point) and the integral of that value. It is a special case of the common PID controller in which the derivative (D) of the error is not used.

The integral action eliminates steady state error. The smaller  $\tau_i$  then the faster the error is reduced, but the system becomes more under damped as  $\tau_i$  is reduced, if it is made too small, the loop becomes unstable.

$$P = K_c E(t) + \frac{K_c}{\tau_i} \int_0^t E(t) dt + P_s \quad \dots (8)$$

$\tau_i$  is the integral time constant



$$P - P_S = K_c E(t) + \frac{K_c}{\tau_I} \int_0^t E(t) \partial t \quad \dots (9)$$

$$P_S = K_c E(s) + \frac{K_c E(t)}{\tau_I s} \quad \dots (10)$$

Therefore, the transfer function of proportional integral controller is:

$$G(S) = K_c \left( 1 + \frac{1}{\tau_I S} \right) \dots \quad (11)$$

In bode plot, at low frequency a proportional integral controller amplifies magnitudes and contributes -90 of phase angle lag. This loss of phase angle is undesirable from a dynamic standpoint since it moves the  $Gm$   $Gcpolar$  plot closer to the (-1,0)point [12].

### Advantages and disadvantages

- The integral term in a PI controller causes the steady-state error to reduce to zero, which is not the case for proportional-only control in general.
- The lack of derivative action may make the system more steady in the steady state in the case of noisy data. This is because derivative action is more sensitive to higher-frequency terms in the inputs.
- Without derivative action, a PI-controlled system is less responsive to real (non-noise) and relatively fast alterations in state and so the system will be slower to reach setpoint and slower to respond to perturbations than a well-tuned PID system may be

### PID Controller:

A **proportional–integral–derivative controller (PID controller)** is a generic [control loopfeedback mechanism](#) ([controller](#)) widely used in industrial [control systems](#) – a PID is the most commonly used feedback controller. A PID controller calculates an "error" value as the difference between a measured [process variable](#) and a desired [setpoint](#). The controller attempts to minimize the error by adjusting the process control inputs. In the absence of knowledge of the underlying process, a PID controller is the optimal controller [22]. However, for best performance, the PID parameters used in the calculation must be [tuned](#) according to the nature of the system – while the design is generic, the parameters depend on the specific system.

The derivative action helps to compensate for lags in the loop.

$$P = K_c E(t) + \frac{K_c}{\tau_I} \int_0^t E(t) \partial t + K_c \tau_d \frac{\partial E(t)}{\partial t} + P(s) \dots (12)$$

$$P - P(s) = K_c E(t) + \frac{K_c}{\tau_I} \int_0^t E(t) \partial t + K_c \tau_d \frac{\partial E(t)}{\partial t} \quad \dots (13)$$

$$P(s) = K_c E(S) + \frac{K_c}{\tau_I S} E(S) + K_c \tau_d S E(s) \quad \dots (14)$$

$$\frac{P(S)}{E(S)} = K_c + \frac{K_c}{\tau_I S} + K_c + \tau_d S \dots (15)$$

$$G(S) = K_c \left( 1 + \frac{1}{\tau_I S} + \tau_d S \right) \dots (16)$$

Two methods are used to find  $K_c$ ,  $\tau_I$  and  $\tau_d$  [13].

### **Ziegler-Nichols Tuning**

The **Ziegler–Nichols tuning method** is a heuristic method of tuning a PID controller. It was developed by John G. Ziegler and Nathaniel B. Nichols. It is performed by setting the I and D gains to zero. The "P" gain is then increased (from zero) until it reaches the **ultimate gain**  $K_u$ , at which the output of the control loop oscillates with a constant amplitude.  $K_u$  and the oscillation period  $T_u$  are used to set the P, I, and D gains depending on the type of controller used. The period of the resulting oscillation is called the ultimate period,  $P_u$  (minutes per cycle). The Ziegler-Nichols settings are then calculated below for the three types of controllers. Notice that a lower gain is used when integration is included in the controller (PI) and that the addition of derivatives permits a higher gain and faster rest [9].

### **Cohen-Coon Tuning**

The Cohen-Coon method of controller tuning corrects the slow, steady-state response given by the Ziegler-Nichols method when there is a large dead time (process delay) relative to the open loop time constant; a large process delay is necessary to make this method practical because otherwise unreasonably large controller gains will be predicted. This method is only used for first-order models with time delay, due to the fact that the controller does not instantaneously respond to the disturbance (the step disturbance is progressive instead of instantaneous).

The Cohen-Coon method is classified as an 'offline' method for tuning, meaning that a step change can be introduced to the input once it is at steady-state. Then the output can be measured based on the time constant and the time delay and this response can be used to evaluate the initial control parameters.

The advantages of this method it is used for systems with time delay and its quicker closed loop response time. But the disadvantages it can only be used for first order models including large process delays, Offline method and approximation's for the  $K_c$ ,  $\tau_i$ , and  $\tau_d$  values might not be entirely accurate for different systems [11].

### **Internal Model Control (IMC)**

One of the most popular control strategies in industrial process control is the Internal Model Control (IMC) strategy, because of its simple structure, fine disturbance rejection capabilities and robustness. This control strategy can be used for both linear and non-linear systems. The IMC design is lucid for the following reasons

- 1- It separates the tracking problem from the regulation problem.
- 2- The design of the controller is relatively straightforward.

The IMC strategy is especially suitable for the design and implementation of the open-loop stable systems and many industrial processes happen to be intrinsically open-loop stable. A more elegant approach is internal model control (IMC). The premise of IMC is that in reality, we only have an approximation of the actual process. Even if we have the correct model, we may not have accurate measurements of the process parameters. Thus the imperfect model should be factored as part of the controller design. In the block diagram implementing IMC (Fig. 2), our conventional controller  $G_c$  consists of the (theoretical) model controller  $G_c^*$  and the approximate function  $\tilde{G}_p$  [23]

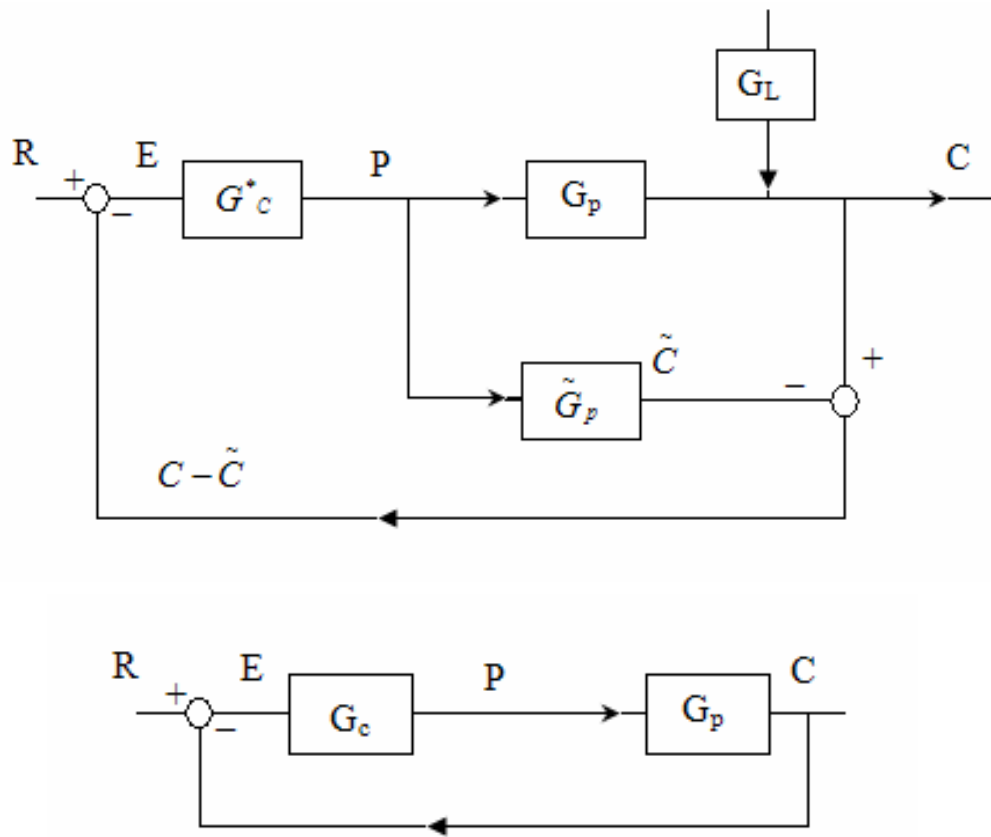


**Figure (2)** A system with IMC (upper panel) as compared with a conventional system

Firstly the closed-loop functions for the system must be derived based on the block diagram, the error is

$$E + R - (C - \tilde{C}) \dots (17)$$

And the model controller output is

$$P = G_c^* E = G_c^* (R - C + \tilde{C}) \dots (18)$$

If substitute  $\tilde{C} = \tilde{G}_p P$ , then

$$P = G_c^* (R - C + \tilde{G}_p P) \dots (19)$$

rearrange to obtain

$$P = \frac{G_c^*}{1 - G_c^* \tilde{G}_p} \dots (20)$$

The gist of this step is to show the relationship between the conventional controller function  $G_c$  and the other functions:

$$G_c = \frac{\tilde{G}_c}{1 - G_c^* \tilde{G}_p} \dots (21)$$

This is an equation that will be used to retrieve the corresponding PID controller gains. For now, we substitute Eq.(21) in an equation around the process,

$$C = G_L L + G_p P = G_L L + \frac{G_p G_c^*}{1 - G_c^* \tilde{G}_p} \dots (22)$$

From this step, we derive the closed-loop equation

$$C = \left[ \frac{(1 - G_c^* \tilde{G}_p) G_L}{1 + G_c^* (G_p - \tilde{G}_p)} \right] L + \left[ \frac{G_p G_c^*}{1 + G_c^* (G_p - \tilde{G}_p)} \right] R \dots (23)$$

The terms in the brackets are the two closed-loop transfer function. As always, they have the same denominator---the closed---loop characteristic polynomial. There is still one unfinished business. We do not know how to choose  $G_C^*$  yet. Before we make this decision, we may recall that the poles of  $G_C$  are "inherited" from the zeros of  $G_P$ . If  $G_P$  has positive zeros, it will lead to a  $G_C$  function with positive poles. To avoid that, we "split" the approximate function as a product of two parts:

$$G_P \approx G_{P+} G_{P-} \dots (24)$$

With  $G_{P+}$  containing all the positive zeros, if present. The controller will be designed on the basis of  $G_{P-}$  only. Now define the model controller function is defined as

$$G_C^* = \frac{1}{G_{P-}} \left[ \frac{1}{\tau_c s + 1} \right]^r, \text{ where } r = 1, 2, \text{ etc } \dots (25)$$

$\tau_c$  equal two-thirds the value of dead time

$\tau_c$  is the closed-loop time constant and our *only* tuning parameter. The first order function raised to an integer power of  $r$  is used to ensure that the controller is physically realizable.

Repeat the derivation of a controller function for a system with a first order process with dead time using IMC.

By modeling our process as a first order function with time delay, and expecting experimental errors or uncertainties, our measured or approximate model function is

$$G_P \approx \frac{K_P e^{-t_d s}}{\tau_P s + 1} \dots (26)$$

The first order Padé approximation is used for the dead time and the positive zero term is isolated as in Eq.(24)

$$G_P \approx \frac{K_P}{(\tau_P s + 1) \left( \frac{t_d}{2} s + 1 \right)} \left( -\frac{t_d}{2} s + 1 \right) = G_{P-} G_{P+} \dots (27)$$

Where

$$G_{P+} = \left( -\frac{t_d}{2} s + 1 \right) \dots (28)$$

If we choose  $r=1$ , eq.(3.6.9) gives

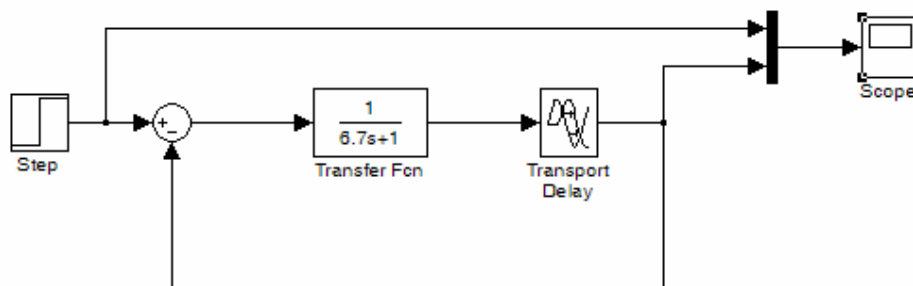
$$G_C^* = \frac{(\tau_P s + 1) \left( \frac{t_d}{2} s + 1 \right)}{K_P} \frac{1}{(\tau_c s + 1)} \dots (29)$$

Substitution of Eq. (27) into Eq. ((20)), and after some algebraic work, will lead to the tuning parameters of an ideal PID controller :

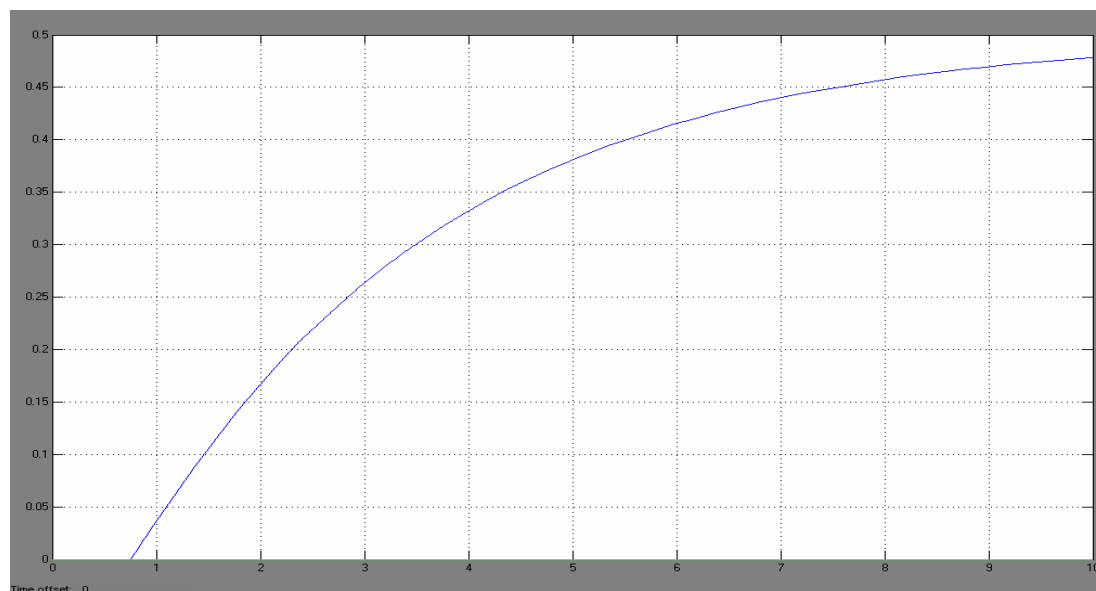
$$K_c = \frac{1}{K_P} \frac{\left( 2 \frac{\tau_P}{t_d} + 1 \right)}{\left( 2 \frac{\tau_c}{t_d} + 1 \right)} ; \tau_1 = \tau_P + \frac{t_d}{2} ; \tau_d = \frac{\tau_P}{2 \frac{\tau_P}{t_d} + 1} \dots (30)$$

### 3- RESULTAND DISCUSSION

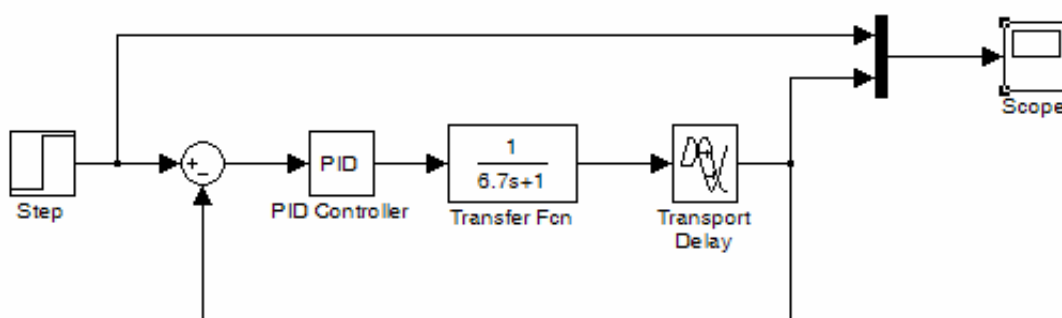
The process simulations are represented and explain in these figures. Before running the process simulation controllers we must test it without controllers. Figure3 and 4 represents the block and step response respectively of absorption column without any controller.



**Figure (3)** Block diagram of absorption column without controller



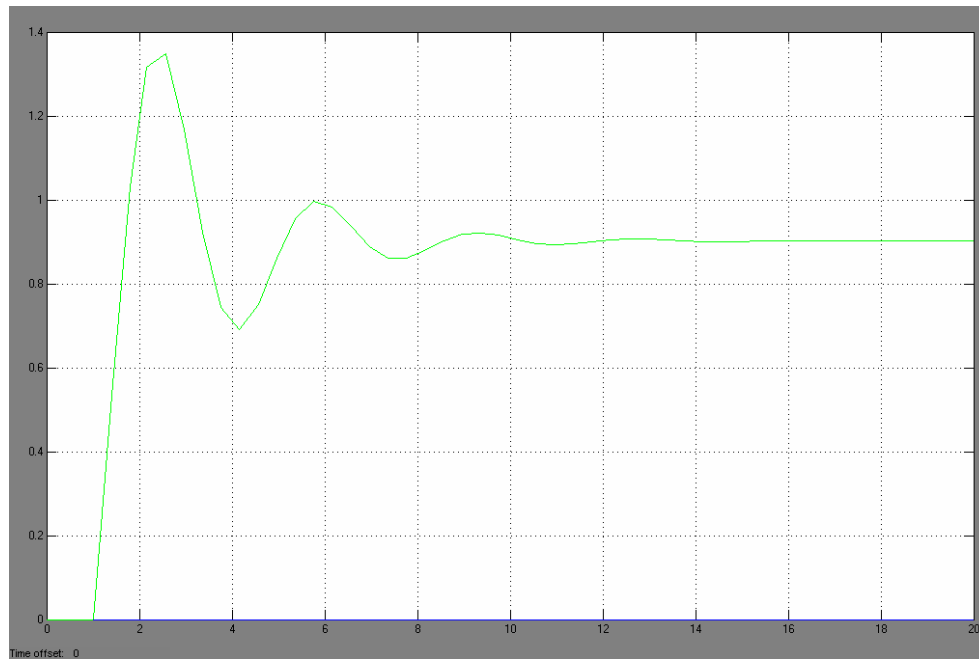
**Figure (4)** Response of absorption column without controller



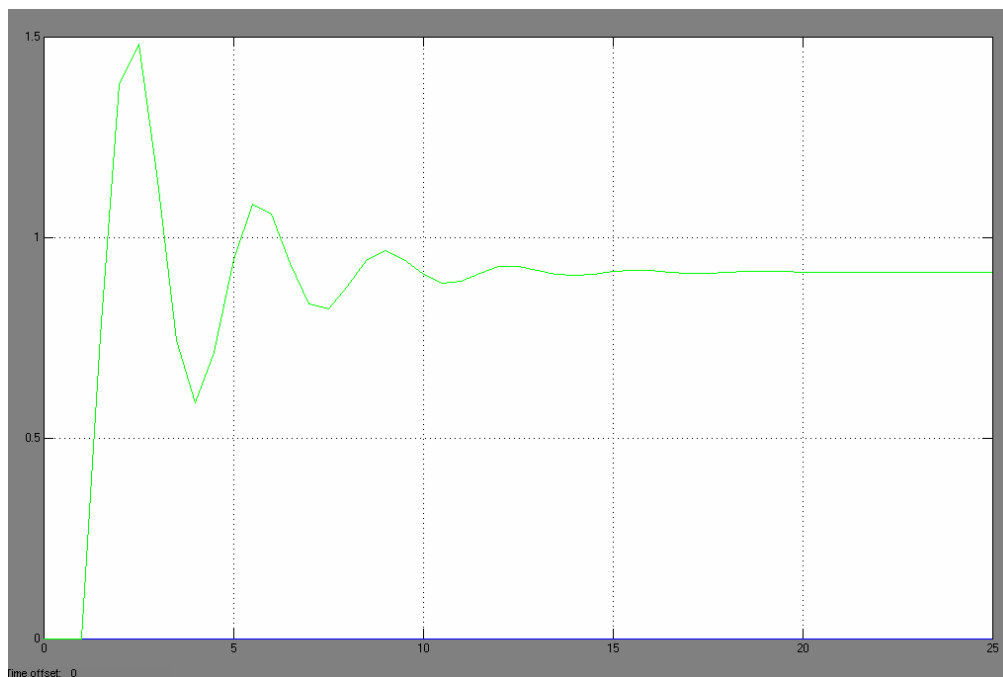
**Figure (5)** Block diagram with controller

Figure 4 shows the step change of system without controller, while figure 5 shown the system with controller. Comparison is made between P, PI and PID for each method used in this work via response to see which is the best value of controller setting that gives the best steady state value of control variable. When the P controller is applied to the Cohen-Coon tuning and Ziegler-Nichols tuning as represented in figure 6 and 7 which shows that when only the

proportional action were applied, the control system is able to arrest the rise of the controlled variable and ultimately bring it to rest at a new steady-state value. The difference between this new steady-state value and the original value is called offset. The offset value of these figures is 2.5%.



**Figure (6)** Response of control variable using P controller with Cohen-Coon tuning



**Figure (7)** Response of control variable using P controller with Ziegler-Nichols tuning

In the PI controller when it is applied to the Cohen-Coon tuning, Ziegler-Nichols tuning and internal model control as shown in figure 8, 9 and 10. Figure (8) shows the too much oscillation so the system in Internal Model Control with PI controller is unstable. On the other hand in Figures (9) and (10) applying the proportional-integral will eliminate the offset and the controlled variable ultimately returns to the original value.

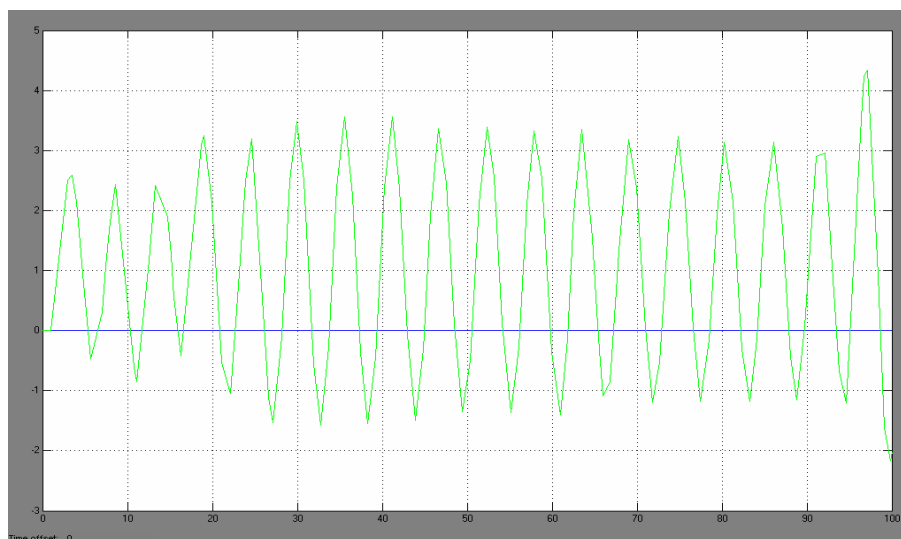


**Figure (8)** Response of control variable using PI controller with Internal Model Control tuning

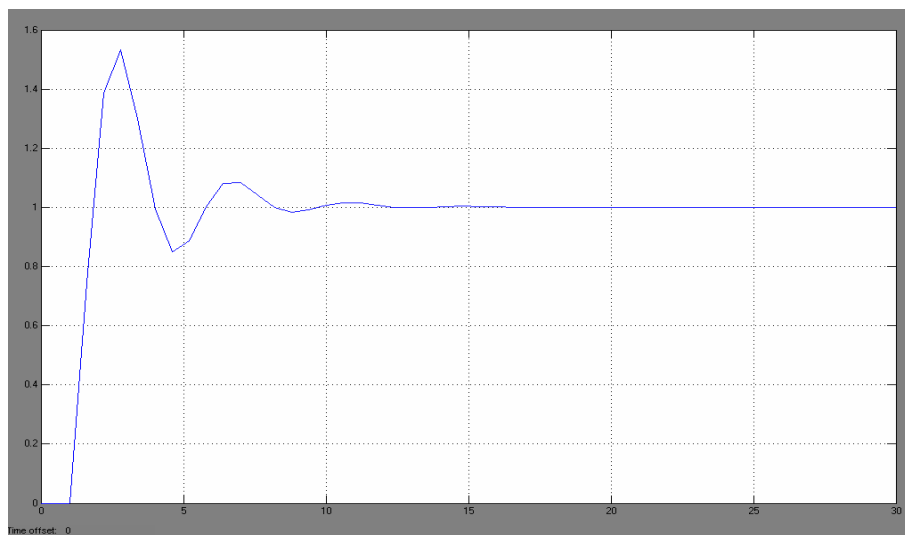


**Figure (9)** Response of control variable using PI controller with Cohen-Coon tuning

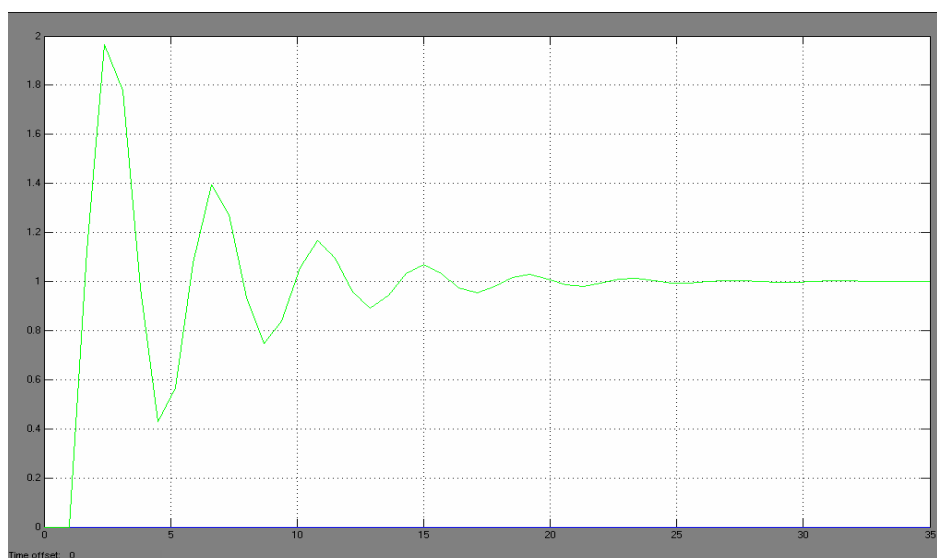


**Figure (10)** Response of control variable using PI controller with Ziegler-Nichols tuning

When the PID controller is applied to the Cohen-Coon tuning, Ziegler-Nichols tuning and Internal model control we get the following diagrams:



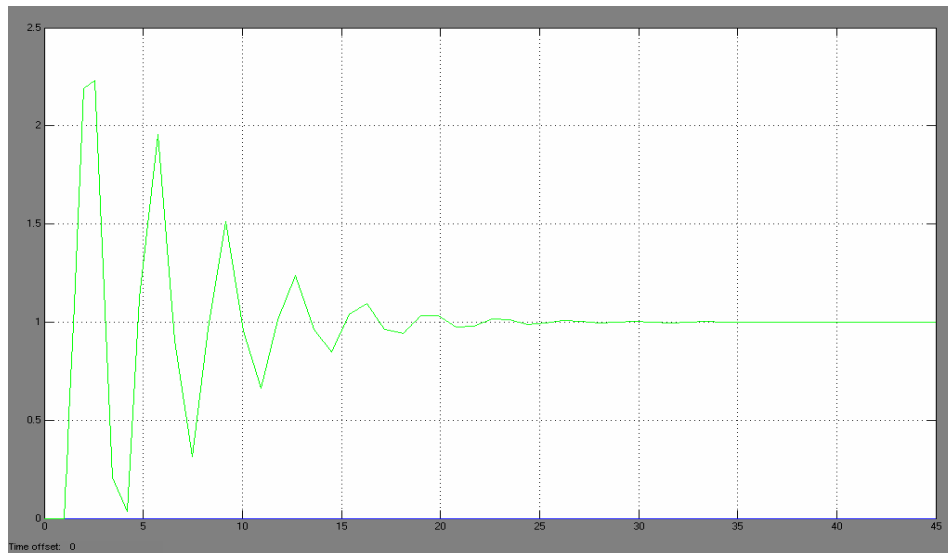


**Figure (11)** Response of control variable using PID controller with Internal Model Control tuning

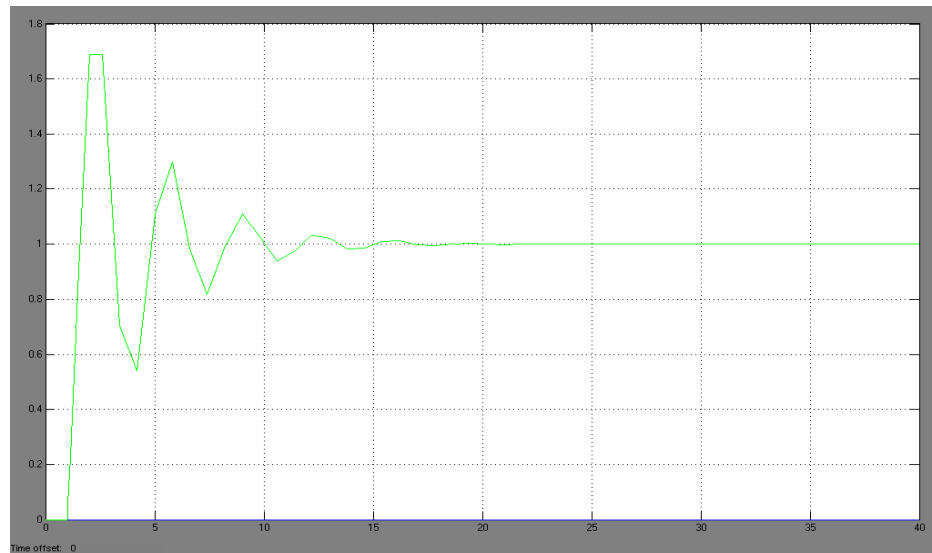


**Figure (12)** Response of control variable using PID controller with Cohen-Coon tuning

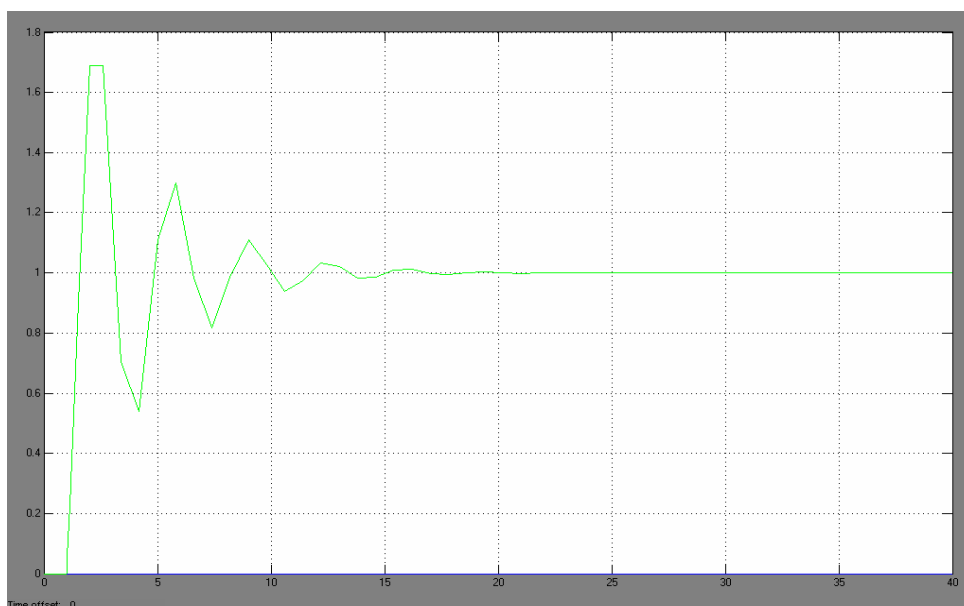


**Figure (13)** Response of control variable using PID controller with Ziegler-Nichols tuning

Figure (11) shows that the oscillation in Internal Model Control with PID controller is more than that of Cohen-Coon tuning and Ziegler-Nichols tuning. On the other hand Figures (12) and (13) show that when the proportional-integral is applied, it will eliminate the offset and the controlled variable ultimately returns to the original value, so they are stable. The all times responses for all figures from (6) to (13) are presented in Table (1) below

**Table 1: Times Responses**

Method	Controller	Settling time(sec.)	Rise time (sec.)	Steady state
Cohen-Coon	P	5.70	0.56	0.905
	PI	9.20	0.589	1
	PID	2.32	0.267	1
Ziegler-Nichols	P	6.65	0.979	0.916
	PI	6.35	0.539	1
	PID	—	N/A	Inf.
Internal Model Control	—	—	—	—
	PI	21.8	3.42	0.334
	PID	—	N/A	N/A

In Table 1 it can be noticed that the Cohen-Coon tuning with PID controller is the best method for reaching stability in the open loop system compared with other methods using other kinds of controllers, this is because the Cohen-Coon tuning with PID controller has the lowest settling time and rise time of all the others.

#### **4- CONCLUSIONS**

The present work was carried out to study the “real time” process simulation in process control and process control for different control strategies. The time response which includes settling time, rise time and steady state show that Cohen-Coon method in PID controller has the lowest settling and rise time with steady state equal to one. This means that the Cohen-Coon method is the best to get stability. To improve process response we must use P, PI and PID controller and compare between them.

The response Figure for the system without controller is unstable but when controller is used the system is more stable. From these figures it can be seen clearly that Cohen-Coon tuning with PI controller is more stable and the controlled variable ultimately returns to the original value.

**5- NOTATION:**

$A$	Cross sectional area of the column $m^2$
$A$	The packing area per volume $m^{-1}$
$C$	State Space -
$E$	Experimental error -
$F$	Feed Rate $Kmol/s$
$ G_{(jw)} $	Magnitude of the open loop system -
$G_{(jw)}$	The open loop transfer function -
$G^*$	Theoretical transfer function -
$G_c$	Transfer Function of Controller -
$G_m$	the Molar Flow rates of The Gas and Liquid $Kmol/s$
$\sim G_p$	Approximate transfer function -
$H$	Henry's law constant -
$K_c$	Controller Gain -
$K_G$	Mass transfer coefficient of gas phase -
$K_s$	Steady State Gain -
$L_m$	The Molar Flow rates of The Gas and Liquid $Kmol/s$
$P$	Total pressure which is constant $N m^{-2}$
$r$	Integer power -
$s$	Laplace Form -

**Greek Letters**

$\tau$	Time constant s
$\tau_D$	Derivative time s
$\tau_I$	Integral time s

**Subscripts**

$i$	Number of component
$j$	Number of component

**Abbreviations**

ADC	Analog to digital converter
DAC	Digital to analog converter
MIMO	Multi-input/Multi-output
ODE's	Ordinary differential equation
P	Proportional controller
PI	Proportional integral controller
PID	Proportional integral derivatives controller

**6- REFERENCE:**

- 1- Palú, F., Fileti, A. M. F., Pereira, J. A F. R. (2004) Controlepreditivo de colunas de absorção com o método de controlepormatrizzdinâmica. .Paper presented at XV Brazilian Congress of Chemical Engineering (COBEQ), CD-ROM, in portuguese.
- 2- Moses A. and Elizabeth J., 2008, "Modelling of a Gas Absorption Column for CO<sub>2</sub>-NaOH System under Unsteady-State Regime". Leonardo Electronic Journal of Practices and Technologies, Issue 12, pp. 105-114.
- 3- McCabe W.L., Smith J.C., Unit Operations of Chemical Engineering, 5<sup>th</sup> Ed. McGraw-Hill Book Co, Singapore, 1993, pp. 681-729.
- 4- Franks R.G.E. 1967. Mathematical Modeling In Chemical Engineering. John Wiley and Sons, Inc., New York, NY, USA, pp. 4-6.
- 5- Coulson J.M., Richardson J.E., 1996, Chemical Engineering, volume Two, 4th edition, Butterworth-Heinman., London, , pp. 530-550.
- 6- Jenson V. G., Jeffereys G. V., Mathematical Methods in Chemical Engineering, U.S Ed., Academic Press Inc. (London) Ltd., London, 1991, pp.25-70.
- 7- Cussler, E. L., 1997, Absorption. Diffusion: Mass Transfer in Fluid Systems (2nd ed. pp. 245-264). USA: Cambridge University Press.
- 8- Kohl, A. L. and Neilsen R., 1997, "Gas Purification". 5<sup>th</sup> ed. USA: Gulf Professional Publishing.
- 9- Tobia I.F. , 1997, "On-Line Control of Multicomponent Distillation Column", Ph.D, Thesis, University of Technology, Iraq
- 10- Bennett, Stuart, 1993, "A history of control engineering". 1930-1955. IET. [pp. 48. ISBN 9-780863412998](#)
- 11- Lelic, Muhiden, PID Controllers in the Nineties, Corning Inc. 1999. [http://www.ece.rutgers.edu/~gajic/IEEET\\_alk.pdf](http://www.ece.rutgers.edu/~gajic/IEEET_alk.pdf)
- 12- Katsuhiko Ogata, 2002,"Modern Control Engineering" 4<sup>th</sup> edition, Prentice Hill, New Jersey.
- 13- Luyben M. L. and Luyben W. L. , 1997; "Essential Of Process Control", McGraw-Hill, New York
- 14- Cullen E.J. Davidson J.F. (1957),: Absorption Of Gases In liquid Jets, Trans. Faraday Soc. 53 113.
- 15- Norman S. N, 2000; "Control System Engineering", 3rd edition, Johan Wiley and Sons., Inc
- 16- Danckwerts P.V. and Kennedy A.M., 1954, Kinetics of liquid-film processes in gas absorption, Trans. Inst. Chem. Eng. 32 S49.
- 17- Danckwerts P.V., (1951), Significance of liquid-film coefficients in gas absorption, Ind. Eng. Chem. 43 1460.
- 18- Moore C. F., Smith C.L. , 1970, Instrument Control, 43, 1, 70.
- 19- Najim, K., Ruiz, V. (1995), Long-range predictive control of an absorption packed column. Appl. Math. Modelling. 19, 39-45.
- 20- Meleiro, L. A. da C., Costa, A. C. da, Maciel, R. Filho (2005), Non-linear multivariable control of an alcoholic fermentation process using functional link networks, Brazilian Archives of Biology and Technology, 48, 7-18.
- 21- Najim K. , 2007, "Modeling And Self-Adjusting Control Of An Absorption Column", Adaptive Control And Signal Processing,5(5), pp. 335-345
- 22- King C.J. , 1971, "Separation Processes," McGraw-Hill, New York.
- 23- Davorin K., Anita K. K. and Mirko M., 2009,"Internal Model Control".Wseas Transactions On Environment AndDevelopment.Issue 4, Volume 5, pp.361-370.



ISSN 2075-9746

مجلة جامعة ذي قار

# للعلوم الهندسية

مجلة علمية محكمة  
تصدر عن،  
كلية الهندسة  
جامعة ذي قار

رقم الإيداع في دار الكتب والوثائق / بغداد ١٥٥٣ لسنة ٢٠١١

# مجلة جامعة ذي قار للعلوم الهندسية

ISSN 2075-9746

مجلة علمية محكمة تصدر عن كلية الهندسة

رئيس هيئة التحرير

الأستاذ المساعد الدكتور كاظم كريم محسن

مدير التحرير

الأستاذ المساعد الدكتور مشتاق إسماعيل حسن

هيئة التحرير

الأستاذ المساعد الدكتور حسين كامل جايل

الأستاذ المساعد الدكتور رسول ريسان شاكر

الأستاذ المساعد الدكتور رافد معلك حنون

الهيئة الاستشارية

جامعة ذي قار

جامعة برادلي

الجامعة التكنولوجية

جامعة البصرة

الجامعة التكنولوجية

جامعة النهريين

جامعة بغداد

جامعة البصرة

جامعة كربلاء

جامعة بابل

الأستاذ الدكتور نبيل كاظم عبد الصاحب

الأستاذ الدكتور أحمد محمود فخر

الأستاذ الدكتور عدنان عباس السماوي

الأستاذ الدكتور صالح إسماعيل نجم

الأستاذ الدكتور جلال محمد جليل

الأستاذ الدكتور رعد سامي فياض

الأستاذ الدكتور قاسم محمد دوس

الأستاذ الدكتور تركي يونس عبد الله

الأستاذ الدكتور صباح رسول داخل

الأستاذ الدكتور عادل عباس علوان

التصميم والطباعة

محمد كشيش مهدي

## تعليمات النشر في المجلة

مجلة جامعة ذي قار للعلوم الهندسية مجلة علمية محكمة تقبل الأبحاث من داخل و خارج العراق باللغتين العربية و الإنكليزية في جميع مجلات العلوم الهندسية والتي لم تنشر سابقا في أية مجلة علمية أو وقائع مؤتمر علمي، على أن تراعى الشروط الآتية:

١. تقدم ثلاث نسخ من البحث بإحدى اللغتين العربية أو الإنكليزية مع العنوان والمستخلص باللغة الأخرى مطبوعة على وجه واحد من ورق A4 بإستخدام برنامج Microsoft Word مع قرص CD.
٢. يجب أن لا يزيد عدد صفحات البحث عن (١٥) صفحة.
٣. يقدم الباحث طلبا تحريريا إلى السيد رئيس تحرير المجلة يطلب فيه نشر بحثه في المجلة و يرفق مع الطلب إستمارة التعهد الخاصة التي تشير إلى عدم نشر البحث أو تقديمه إلى أية جهة أخرى، و يذكر الباحث عنوانه الكامل و البريد الإلكتروني و رقم الهاتف لتسهيل مراسلته و الإتصال به.
٤. يتحمل الباحث مسؤولية كاملة عن محتويات بحثه.
٥. تخضع الأبحاث إلى تقويم علمي من قبل خبراء من ذوي الكفاءة و الاختصاص.
٦. يتم إشعار الباحث بنتيجة تقويم بحثه.
٧. يدفع الباحث من داخل العراق أجور التقويم و النشر و مقدارها (٥٠٠٠٠) فقط خمسون ألف دينار للمدرس فما دون و (٧٥٠٠٠) فقط خمسة و سبعون ألف دينار للأستاذ المساعد و (١٠٠٠٠٠) فقط مائة ألف دينار للأستاذ، غير قابلة للرد لقاء وصل استلام رسمي إلى حسابات المجلة حسب تعليمات وزارة التعليم العالي و البحث العلمي. أما من خارج العراق فيدفع الباحث (١٠٠) دولار دفعة واحدة.
٨. لا يرد أصل البحث المرسل إلى المجلة سواء نشر أم لم ينشر.
٩. يزود الباحث بنسخة واحدة مجانا من العدد المنشور فيه بحثه.
١٠. تعليمات طباعة الأبحاث:
  - ❖ حاشية الورق : تترك مسافة من جميع الجهات بمقدار ٢,٥ سم.
  - ❖ نمط الخط : Times New Roman
  - ❖ عنوان البحث : حروف كبيرة حجم ١٦ غامق.
  - ❖ أسم الباحث أو الباحثين : يكتب تحت عنوان البحث ، حجم ١٤ غامق وتذكر عناوين الوظائف الحالية والبريد الإلكتروني أسفل أسم الباحث وفي وسط الصفحة ، حجم ١٠ غامق.
  - ❖ العناوين الرئيسية : حجم ١٤ غامق بعد الحاشية اليمنى للأبحاث المطبوعة باللغة العربية وبعد الحاشية اليسرى للأبحاث الإنكليزية.
  - ❖ العناوين الفرعية : حجم ١٤ غامق وتكون بداية كل كلمة حرف كبير ، وموضوعة بعد الحاشية اليمنى للأبحاث المطبوعة باللغة العربية وبعد الحاشية اليسرى للأبحاث المطبوعة باللغة الإنكليزية ، ويترك سطر فارغ قبل وبعد العنوان.
  - ❖ النص : يكتب بالحروف الصغيرة حجم ١٢ عادي والتباعد بين السطور بمقدار ١,٥ سطر.
  - ❖ المعادلات : تكتب المعادلات بأستخدام محرر المعادلات Microsoft Equation وترقم بالأقواس الى الجهة اليمنى ويترك سطر واحد فارغ قبل وبعد المعادلة. ويشار إلى المعادلة كما يأتي : المعادلة (x) حيث x تعني رقم المعادلة.
  - ❖ الجداول : تعطى الجداول أرقام متسلسلة وعناوين واضحة تكتب فوق الجدول وسط السطر وبحجم ١٢ غامق.
  - ❖ الأشكال : تعطى الأشكال أرقام متسلسلة وعناوين واضحة تكتب أسفل الشكل وسط السطر وبحجم ١٢ غامق ، مع مراعاة أستخدام أساليب الرسم الحديثة.
  - ❖ المراجع : يشار الى المراجع بالأرقام حسب ظهورها في متن البحث ويوضع الرقم بين أقواس مربعة وتراعى الشروط الآتية عند كتابة المراجع.
  - ❖ الدوريات : اللقب يتبع بفراغ ، الحرف الأول للأسم ، الحرف الأول لأسم الأب ، السنة ، " عنوان البحث " ، جهة النشر ، رقم المجلد والعدد ، الصفحات.
  - ❖ الكتب : اللقب يتبع بفراغ ، الحرف الأول للأسم ، الحرف الأول لأسم الأب ، السنة ، " عنوان الكتاب " ، الطبعة ، مكان النشر ، دار النشر.
  - ❖ الرسائل والأطاريح : اللقب يتبع بفراغ ، الحرف الأول للأسم ، الحرف الأول لأسم الأب ، السنة ، " عنوان الرسالة أو الأطروحة " ، الجامعة.

## ملاحظة:

- ✓ في حالة وجود أكثر من باحث أو مؤلف في المراجع توضع فارزة بين أسم وآخر ويكرر نفس الترتيب في كتابة الأسماء الأخرى.
- ✓ المستخلص : يجب أن يبتدئ البحث بمستخلص بنفس لغة البحث يتبعه مستخلص ثانٍ باللغة الأخرى على أن لا يزيد عدد الكلمات في كل واحد منهما عن ٢٠٠ كلمة.
- ✓ الكلمات الرئيسية: يجب أن تتبع المستخلص، خمس إلى عشرة كلمات رئيسية ذات علاقة بالموضوع الرئيس للبحث مكتوبة بحروف صغيرة حجم ١٢ غامق.
- ✓ الرموز : يجب أن ترتب الرموز أبجدياً وتوضع بعد قائمة المراجع.
- ✓ الأرقام : تستخدم الأرقام الإنكليزية إذا كان متن البحث مكتوب باللغة العربية والأرقام العربية إذا كان متن البحث مكتوب باللغة الإنكليزية.

## المراسلات

مجلة جامعة ذي قار للعلوم الهندسية – كلية الهندسة – جامعة ذي قار – محافظة ذي قار – جمهورية العراق

E-mail:thiqarej@gmail.com